

**PARTICLES AS STABILIZERS AND WETTING MODIFIERS IN
COLLOIDAL MULTIPHASE SYSTEMS**

A Dissertation
Presented to
The Academic Faculty

by

Yi Zhang

In Partial Fulfillment
of the Requirements for the Degree
Doctor of Philosophy in the
School of Chemical & Biomolecular Engineering

Georgia Institute of Technology
August, 2016

COPYRIGHT 2016 BY YI ZHANG

PARTICLES AS STABILIZERS AND WETTING MODIFIERS IN COLLOIDAL MULTIPHASE SYSTEMS

Approved by:

Dr. Sven H. Behrens, Advisor
School of Chemical & Biomolecular
Engineering
Georgia Institute of Technology

Dr. J. Carson Meredith, Advisor
School of Chemical & Biomolecular
Engineering
Georgia Institute of Technology

Dr. Elsa Reichmanis
School of Chemical & Biomolecular
Engineering
Georgia Institute of Technology

Dr. Yulin Deng
School of Chemical & Biomolecular
Engineering
Georgia Institute of Technology

Dr. Alberto Fernandez-Nieves
School of Physics
Georgia Institute of Technology

Date Approved: April 15th, 2016

To my family for their love and support

ACKNOWLEDGEMENTS

Words cannot adequately express my gratitude to the supports from many people throughout my Ph.D. study at Georgia Tech. I would like to give my special appreciation to my thesis advisors Dr. Sven H. Behrens and Dr. J. Carson Meredith, who are knowledgeable, inspiring, motivating, encouraging, and always supportive. I cannot express how lucky I feel to have both of them as my advisors. I also would like to thank my thesis committee members, Dr. Elsa Reichmanis, Dr. Yulin Deng, and Dr. Alberto Fernandez-Nieves for their comments, suggestions, and time on my thesis work.

I am very grateful to my past lab mates, Dr. Shanhong Xu, Dr. Hongzhi Wang, Dr. Jie Wu, Dr. Oluwatimilehin Fadiran, Dr. Natalie Girouard, Dr. Joohyung Lee, and Dr. Abiola Shitta for imparting their knowledge and skills to me and training me for the use of equipments; I also would like to thank my current lab mates, Dr. Haisheng Lin, Joanna Tsao, Songcheng Wang, Xiaotang Du, Donglee Shin, Zihao Qu, Chinmay Satam, and Maritza Mujica for their help and being such great colleagues.

Special thanks also to help from undergraduates: Jiarun Zhou, Ruiyang Zhao, Stephane Tcheimou, Greg Benz, and David Schilpp.

I would also like to thank my best friends Qingpeng Wang, Lingyang Niu, Zhicheng Shen, Haibo Liu, Bo Qin, Guanglin Xu, Chengwei Deng, and Xu Du.

Finally, I would like to thank my family for their love and unconditional support always. Without their love and support, this work cannot have been possible. Especially, I would like to thank my wife and lovely daughter, who are always the sweetest part of my life.

TABLE OF CONTENTS

	Page
ACKNOWLEDGEMENTS	iv
LIST OF TABLES	viii
LIST OF FIGURES	ix
LIST OF SYMBOLS	xviii
LIST OF ABBREVIATIONS	xix
SUMMARY	xx
<u>CHAPTER</u>	
1 Introduction	1
1.1 Colloidal systems	1
1.2 Particles at fluid-fluid interfaces	2
1.3 Foams and Pickering foams	5
1.4 Capillary suspension	7
1.5 Wetting in colloidal multiphase systems	8
1.6 Thesis motivations and objectives	12
1.7 Thesis outline	13
1.8 References	14
2 Capillary foams: a small amount of oil makes big difference	19
2.1 Introduction	19
2.2 Materials and Methods	20
2.3 Results and Discussion	24
2.4 Conclusions	29
2.5 References	30

3	Stabilization mechanism of capillary foams	32
3.1	Introduction	32
3.2	Materials and Methods	33
3.3	Results and Discussion	41
3.4	Conclusions	49
3.5	References	50
4	Capillary foams: formation stages and effects of process parameters	51
4.1	Introduction	51
4.2	Materials and Methods	52
4.3	Results and Discussion	54
4.4	Conclusions	64
4.5	References	65
5	Capillary foams: stabilization and functionalization of porous liquids and solids	69
5.1	Introduction	69
5.2	Materials and Methods	72
5.3	Results and Discussion	76
5.4	Conclusions	87
5.5	References	88
6	Bubble meets droplet: particle-assisted reconfiguration of wetting morphologies in colloidal multiphase systems	91
6.1	Introduction	91
6.2	Materials and Methods	93
6.3	Results and Discussion	98
6.4	Conclusions	119
6.5	References	120

7	Interfacial activities of isotropic particles at fluid-fluid interfaces	126
7.1	Introduction	126
7.2	Materials and Methods	128
7.3	Results and Discussion	132
7.4	Conclusions	146
7.5	References	147
8	Conclusions and future work	152
8.1	Conclusions	152
8.2	Future work	154
8.3	References	157

LIST OF TABLES

	Page
Table 1.1: Examples of colloidal systems.	1
Table 2.1: Surface and interfacial tensions of fluids used in this study. Equilibrium interfacial tension data of TMPTMA were obtained from reference 12. The equilibrium surface and interfacial tensions were used to calculate the interfacial energy change and effective spreading coefficient, where a, o, w represent the air, oil, water phase respectively. γ' is the equilibrium surface/interfacial tension and γ is the surface/interfacial tension of pure liquids.	23
Table 3.1: Comparison between experimental observations and theoretical estimates for foams from a variety of particle and fluids combinations. θ_{awp} and θ_{owp} are particle contact angles at air-water interface and oil-water interface respectively. S_{eff} is the effective spreading coefficient. The cellulose and aluminum oxide particles are not included here because it is challenging to measure contact angles for these irregularly shaped particles.	44
Table 4.1: Hydrodynamic radius and wettability of silica particles coated with various extends of methylsilyl groups. Contact angle data of 100% SiOH particles were obtained from reference 28.	53
Table 4.2: Surface and interfacial tensions of oils used in this study. Interfacial tension data of TMPTMA were obtained from reference 29. Here, γ is the equilibrium surface/interfacial tension, where a, o, w denotes the air, oil, and water phase. S is the spreading coefficient.	53
Table 7.1: Hydrodynamic radius and wettability of silica particles coated with various extends of methylsilyl groups. Contact angle data of 100% SiOH silica particles were obtained from reference 35.	130
Table 7.2: Packing density and contact angle of EC particles in the TMPTMA-water interfaces.	141
Table 7.3: Theoretically predicted and experimentally measured effective interfacial tension of particles in fluid-fluid interfaces.	143
Table 7.4: Theoretically predicted and experimentally measured packing density of particles in fluid-fluid interfaces.	145

LIST OF FIGURES

	Page
Figure 1.1: Cartoon showing adsorption of solid particles to a fluid-fluid interface. Adsorption of a particle from the phase 2 to the interface replaces the phase 1-2 contact area with particle-phase 1 contact area.	3
Figure 1.2: Materials from particle adsorption at fluid-fluid interfaces. (a) Cartoons showing oil-in-water emulsion, water-in-oil emulsion, foam and liquid marble. ¹⁴ SEM images of (b) bijels ²⁰ and (c) colloidosomes. ¹¹ Images reproduced from references 14, 20, and 11.	4
Figure 1.3: Scheme of breakdown process in foams.	5
Figure 1.4: Scheme for foam bubble stabilized by adsorption of surfactants (left) and particles (right).	6
Figure 1.5: Capillary suspension. ^{42,43} (a) The transition from fluid-like behavior to gel-like behavior with the addition of small amounts of water to a suspension of hydrophobically modified calcium carbonate. (b) Schematic illustration of pendular state. (c) Schematic illustration of the capillary state. (d) Particle-decorated droplets of a Pickering emulsion formed at much higher volume fraction of the secondary liquid. Images reproduced from references 42 and 43.	8
Figure 1.6: Possible wetting configurations of a water droplet on a homogeneous solid substrate.	9
Figure 1.7: Possible wetting configurations for three immiscible fluids.	10
Figure 2.1: SEM images of the particles used in this study. (a) Modified silica (Aerosil 200), mean diameter: 619.15 nm. (b) Modified cellulose powder, mean diameter: 33.90 μm . (c) PVC Vinnolit SA/1062/7, mean diameter: 29.59 μm . (d) Aluminum oxide particles, mean diameter: 5.27 μm . (e) Glass (Spherglass 5000), mean diameter: 4.44 μm . (f) Polyethylene particles, mean diameter: 9.65 μm . (g) Monodisperse silica spheres (SS03N), diameter: 0.96 μm . (h) PVC Vinnolit P70F, mean diameter: 0.93 μm .	21
Figure 2.2: Particle size distributions.	22
Figure 2.3: Stable foams requiring both particles and a secondary liquid. (a) Attempts of producing foams via frothing in the presence of PVC (Vinnolit SA 1062/7) particles only (14.16 wt%), and of both particles and a secondary liquid combined (14.16 wt% total, including 0.5 wt% of the secondary liquid). (b) Photographs of the same samples after 24 hours or 1 month.	25

Figure 2.4: Experimental observations of foam stability where a variety of particles and fluid combinations were tested. The particles tested cover a range of particle size, shapes and wettability. 26

Figure 2.5: Combined adsorption of particles and secondary fluid at bubble surfaces of a capillary foam. (a-c) SEM images of a dried capillary foam formed by addition of gas bubbles and 1 wt% TMPTMA as the secondary fluid to suspensions of PE or PVC Vinnolit 1062/7 or glass particles in water with a solids loading of 10 vol.%. The secondary fluid was first solidified by photo-polymerization, and then the water was removed by drying. (d-f) Close-up of particles and polymerized secondary fluid surrounding a gas bubble. (h-j) Network of particles and polymerized secondary fluid bridges in the aqueous suspension bulk. (k-m) Confocal microscope image of the wet capillary foam with the secondary fluid TMPTMA labelled by Nile red. 27

Figure 2.6: Network formation without foam stabilization. (a) Failed attempt of producing capillary foam from a silica particle suspension (2 wt.%) in the presence of secondary fluid TMPTMA (3 wt.%, with respect to the amount of bulk phase water). (b-c) SEM images of a dried silica particles suspension. The secondary fluid was solidified by photo-polymerization prior to water removal. 28

Figure 2.7: Attempts of producing foams via frothing in the presence of secondary liquids only (14.16 wt. %). 29

Figure 3.1: Schematic representation of a PDMS replica with trapped particle. (a) Contact angle smaller than 90° . (b) Contact angle larger than 90° . 34

Figure 3.2: Schematic illustration of capillary foams. (a) In capillary foams, suspension particles and the secondary liquid jointly adsorb at the interface of gas bubbles. The decorated bubbles are further entrapped in a network of excess particles in the primary liquid bridged by a secondary liquid. (b) Particles adsorbing preferentially at an interface of the secondary liquid can mediate the spreading of a secondary liquid film around the gas bubbles, in direct analogy to the “particle-assisted wetting” of a macroscopic air-water interface by a drop of oil. Depending on their wetting properties, the particles can adsorb at oil-water interface (i) or the oil-air interface (ii) (or both). 42

Figure 3.3: The effective oil spreading coefficient S_{eff} (a) and the equilibrium particle contact angle (b) at the air-water interface for Pickering foams and at the oil-water interface for capillary foams from a variety of particle/oil combinations. Full marks are used for systems that produce stable foam heads upon frothing, open markers denote patently unstable systems, and the half-open marker (“semi-stable”) is for systems developing only a very small, albeit durable, foam head and a large sediment of particles not participating in bubble stabilization. The standard spreading coefficient S_o of paraffin oil, DINP and TMPTMA are -10.17 mN/m, 5.74 mN/m and -0.11 mN/m respectively. 46

Figure 3.4: SEM image of PVC particles trapped in the PDMS replica of a macroscopic air-water interface (a) and of several oil-water interfaces (b-d) using the gel trapping technique. The visible part of particle originally resided in the water phase. 47

Figure 3.5: Experimental observation of the particle location at the interface. (a) SEM image of the mixed layers of TMPTMA and particles formed on an air-water interface. (b) SEM image of PVC particles trapped on the PDMS replica of oil-water interface using the gel trapping technique. The visible part of particle has been immersed in the water phase. 48

Figure 4.1: Structure of capillary foams. The system contains a continuous water phase, a gas phase, an oil phase, as well as particles. The agitation of the mixture results in a space-spanning network of particles in water (ii) connected by bridges of oil phase (iii), with air bubbles embedded in the network (iv) via a joint adsorption of particles and a thin oil film. 55

Figure 4.2: Formation stages of capillary foams. Photographs and corresponding microscope images of PVC particle suspension in the presence of 1 wt% (a) TMPTMA, (b) Paraffin oil, and (c) Silicone oil during several stages of frothing. Scar bars are 110 μm . (d) Schematic illustration of suspension morphologies during formation of capillary foams. 56

Figure 4.3: Possible formation stages of capillary foams. (a) Particle dispersion. (b) Mixture of generated air bubbles, oil droplets, and particles in water. (c) Particle-coated bubbles. (d) Spanning particle networks in a capillary suspension. (e) Oil-coated bubbles. (f) Capillary foams. 58

Figure 4.4: Photograph of capillary foams stabilized with different concentrations of PVC particles. The photograph was taken at (a) 0 minute and (b) 5 months after preparation. 59

Figure 4.5: Effects of particle hydrophobicity on the formation of Pickering and capillary foams. (a) Photographs of foams prepared by using particles with various hydrophobicity. (b) Initial foam volume as a function of particle wettability. 61

Figure 4.6: Effects of oil types and fractions on the formation and stability of capillary foams. Capillary foams prepared with 10 wt% PVC particles in the presence of 1 wt% (a) Paraffin oil, (c) TMPTMA, and (e) Silicone oil. (b, d, f) Appearances of foams after 5 months. The equilibrium spreading coefficients S_o of paraffin oil, TMPTMA, and silicone oil are -10.17 mN/m , -0.11 mN/m , and 9.85 mN/m , respectively. 63

Figure 5.1: Multi-phase colloidal systems prepared from particle dispersions. (a) Particle suspensions are the starting point. (b) Suspension mixing with a large amount of secondary liquid can result in “Pickering emulsion” drops of oil-in-water or water-in-oil stabilized with hydrophilic or hydrophobic particles, respectively. (c) Mixing with a small amount of secondary liquid can result in the formation of a capillary suspension in which particles are connected by bridges of secondary liquid (either forming “pendular” menisci between particle pairs or the center of “capillary” agglomerates, depending on which liquid wets the particles preferentially). (d), (e) Suspension mixing with a gas phase can lead to “armored bubbles” (particle- stabilized bubbles that connect, at high concentration, forming a “Pickering foam”), to “liquid marbles” (particle stabilized droplets in air), depending on the particle wettability. (f) In capillary foams, suspension particles and the secondary liquid jointly adsorb at the interface of the gas bubbles with the primary liquid. The decorated bubbles are further entrapped in a network of excess particles in the primary liquid bridged by a secondary liquid. (g) Particles adsorbing preferentially at the interface of the secondary liquid can mediate the spread of the secondary liquid film around the gas bubbles, which is directly analogous to the “particle-assisted wetting” of a macroscopic air-water interface by a drop of oil. Depending on their wetting properties, the particles can adsorb at the oil-water interface (i) or the oil-air interface (ii). 70

Figure 5.2: Processing steps for the preparation of load-bearing, lightweight porous solids. 73

Figure 5.3: Capillary foams were prepared through multiple routes. (a) 10 wt% PE particles suspensions. (b) Mechanical frothing of suspension produced a Pickering foam. (c) Suspension mixing with 2 wt% oil (TMPTMA) resulted in the formation of a capillary suspension. Capillary foams were prepared by (d) mixing 2 wt% oil (TMPTMA) to a Pickering foam (e) introducing 2 wt% oil (TMPTMA) and air bubbles simultaneously to a particles suspension (f) introducing air bubble to a capillary suspension. TMPTMA was treated with Al_2O_3 to remove inhibitor, and enriched with 5 wt % of the photoinitiator benzoin isobutyl ether. (g) SEM image of dried capillary suspension in (c). The particles were bridged by the minority oil phase. (h-j) SEM images of corresponding dried foam in (d), (e), and (f), respectively. Both particles and a thin oil film adsorbed on the bubble surface. For dried capillary suspension and foam, the secondary liquid was first solidified by photopolymerization, and then the water was removed by drying. 77

Figure 5.4: Mold casting of capillary foams. (a) The prepared capillary foams with 25.2 vol% PVC 1062/7 particle concentration and 2.92 wt% TMPTMA were molded into containers of various shapes by hand. (b) Capillary foams were cured under UV light and then dried in the oven. 79

Figure 5.5: Functional load-bearing, lightweight porous materials from capillary foams. (a) Photograph of 11 lbs weight on a cured and dried foam with a density of 0.24 g/cm^3 and porosity of 82.97 %. The foams were prepared from PVC (Vinnolit SA 1062/7) particles with a solid content of 21 vol % and 1.5 wt% TMPTMA by a hand mixer (Rival 5-Speed Hand Mixer) running at the maximum speed. (b) Variation in porosity with the amount of secondary fluid phase for prepared porous solids from capillary foam. 80

Figure 5.6: Photographs and spectra of colored foams formed by traditional foaming methods. (a) Photographs of foams stabilized by 0.05 wt% SDS surfactant and colored by 0.003 wt % allura red (left) or FD&C blue NO.1 (right) dye. (b) Transmittance spectra of bulk liquid suspension of the foam in (a). (c) Reflectance spectra of foam area of the foam in (a). (d) Photographs of foams stabilized by 7.41 wt% PE particles and colored by 0.0028 wt % allura red (right) or FD&C blue NO. 1 (left). (e) Transmittance spectra of bulk suspension of the corresponding foams stabilized by PE particles in (d). (f) Reflectance spectra of foam area of the corresponding foams stabilized by PE particles in (d). 83

Figure 5.7: Schematic of the formation of colored capillary foam. The dye is dissolved in the secondary fluid. During the foaming process, dyes adsorb onto the bubble surfaces, and they are bridged by particles in the region between bubbles. 84

Figure 5.8: Intensely colored capillary foam. (a,c) Photographs and confocal microscope images of colored foams stabilized by 2 wt% dye solution (0.37 mg of Nile red was dissolved in 0.5 g TMPTMA) and 7.41 wt% PE or PVC 1062/7 particles. Inserts in (a) and (c) are confocal microscopic images of the particle network among the bubbles. The additional zoom factors for the inserts are 1.61 and 3.05, respectively. (b) Transmittance spectra of bulk suspension of the corresponding capillary foam. (d) Reflectance spectra of foam area of the corresponding capillary foams. 85

Figure 5.9: Images of dried color foams. (a) Dried capillary foams stabilized by the synergistic action of 18.5 vol% PVC 1062/7 particles and 4 wt% TMPTMA (1.5 mg of Nile red was dissolved in 2g TMPTMA). (b) Dried capillary foams formed from the synergistic action of 10 vol % PVC 1062/7 particles and 5 wt% TMPTMA (10.2 mg of oil blue N was dissolved in 2 g TMPTMA). (c) Reflectance spectra of the corresponding dried foams in (a) and (b). (d) Dried Pickering foam stabilized by 7.41 wt% PE particles and colored by 0.003 wt % allura red (left) or FD&C blue NO.1 (right). 86

Figure 6.1: SEM images and size distributions of particles used in this study. SEM image of (a) HP 55 and (b) EC particles. Scale bars are 200 nm. Intensity-weighted particles size distribution of (c) HP 55 and (d) EC particles obtained from dynamic light scattering by inversion of the scattering intensity autocorrelation function. The Z-average sizes of the EC and HP55 particles are 102.3 nm and 137.4 nm, respectively. The corresponding coefficients of variation are 13% and 10%, respectively. 96

Figure 6.2: (a) A single air bubble was generated and then transferred into the square capillary. (b) A single oil droplet was dispensed directly into the square capillary through the second tapered round tube. (c) The generated bubble and oil droplet were kept in the device to allow particles to adsorb on the bubble and oil droplet surfaces. (d) The bubble and oil droplet were brought into contact by slightly tilting the capillary and exploiting the bubble's buoyancy. (e) The wetting configuration was examined optically in the glass capillary. 97

Figure 6.3: Possible wetting morphologies of an air bubble and an oil droplet in water and schematic illustration of equilibrium contact angle at the three-phase contact line. Here $S_o = \gamma_{aw} - (\gamma_{ao} + \gamma_{ow})$, where a, o, w denote the air, oil, and water phase respectively. 100

Figure 6.4: Particles promote the bubble wetting. First row: experimental observations of an air bubble and a hexadecane droplet brought into contact in a water medium containing (a) no particles, (b) 0.2 wt% EC particles, and (c) 0.2 wt% HP 55 particles. Scale bars are 500 μm . Second row: the dynamic effective surface and interfacial tension of an air-hexadecane-water system in which the water phase contains (d) no particles, (e) 0.2 wt% EC particles, and (f) 0.2 wt% HP 55 particles. Third row: the dynamic effective spreading coefficient of an air-hexadecane-water system in which the water phase contains (g) no particles, (h) 0.2 wt% EC particles, and (i) 0.2 wt% HP 55 particles. The yellow band indicates the complete wetting regime as predicted based on the of positive effective spreading coefficient ($S'_o > 0$), the grey band indicates the partial wetting regime expected for a negative effective spreading coefficient ($S'_o < 0$). 101

Figure 6.5: Formation of hexadecane oil lens at the macroscopic air-water interface. (a) A top view of hexadecane at the air-water interface where water phase contains 0.2 wt% EC particles. (b,c) Side views of oil lens in (a) using a CCD camera. 104

Figure 6.6: Particles promote the bubble de-wetting. Experimental observations of an air bubble and a TPGDA droplet brought into contact in a water phase containing (a) no particles, (b) 0.2 wt% EC particles, and (c) 0.2 wt% HP 55 particles. Scale bars are 500 μm . The dynamic effective surface and interfacial tension of an air-TPGDA-water system in which the water phase contains (d) no particles, (e) 0.2 wt% EC particles, and (f) 0.2 wt% HP 55 particles. The dynamic effective spreading coefficient of an air-TPGDA-water system in which the water phase contains (g) no particles, (h) 0.2 wt% EC particles, and (i) 0.2 wt% HP 55 particles. The yellow and grey background indicates the different wetting regimes as in Figure 6.4. 105

Figure 6.7: Wetting behaviors as a function of particle concentrations. (a) Wetting morphologies and corresponding effective spreading coefficients of air-hexadecane-water system by gradually changing concentrations of the HP 55 particles. (b) Wetting morphologies and corresponding effective spreading coefficients of air-TPGDA-water system by gradually changing concentrations of the EC particles. Scale bars are 500 μm . 107

Figure 6.8: The adsorption of appropriate particles in the interfaces leads to the tuning of the wetting configuration. (a) Confocal microscope images of a close-up of hexadecane-water interface when an air bubble and a hexadecane droplet were brought into contact in a water medium containing 0.2 wt% Nile red-labeled HP 55 particles. Confocal microscope images of a close-up of (b) air-water interface and (c) hexadecane-water interface when an air bubble and a hexadecane droplet were brought into contact in a water medium containing 0.4 wt% Nile red-labeled EC particles. Scale bars are 100 μm . (d, e, f) The fluorescence intensity profiles along a line across the confocal images in parts a, b, and c, respectively. 109

Figure 6.9: In-situ transition of the wetting morphology as particles diffuse to the interfaces. (a) Schematic illustration of the experimental procedure: an air bubble and an oil droplet are brought into contact in a particle-free water phase inside an open microfluidic glass channel, which is then placed in a particle suspension containing 0.4 wt% EC or 0.2 wt% HP 55 particles. (b) Wetting morphology transition for air-hexadecane-water system as HP 55 particles diffuse. (c) Wetting morphology transition for air-TPGDA-water system as EC particles diffuse. Scale bars are 500 μm . 110

Figure 6.10: Transient wetting behavior. An air bubble and a hexadecane oil droplet were brought into contact in a particle-free water phase inside an open microfluidic glass channel, which was then placed in a particle suspension containing 0.2 wt% EC particles. Wetting morphology transition for air-hexadecane-water system as EC particles diffuse. Scale bar is 500 μm . 113

Figure 6.11: (a) The dynamic effective surface and interfacial tensions and (b) the corresponding dynamic effective spreading coefficient of an air-hexadecane-water system in which the water phase contains 0.2 wt% EC particles. (c,d) Close-up of figures in (a) and (b) in the first 350 seconds, respectively. 113

Figure 6.12: (a) Dynamic surface tension of supernatant of EC particles (red points) in comparison to the dynamic surface tension of ultrapure DI water (black points). (b) Dynamic surface tension of supernatant of HP 55 particles (red points) in comparison to the dynamic surface tension of ultrapure DI water (black points). 0.1 M hydrochloric acid was added before centrifugation to ensure the formation of particle aggregates and achieve good separation. 115

Figure 6.13: The Contact angle of a particle on the air-oil interface. (a) Graphical illustration that particle contact angle at the air-oil interface can be correlated to the oil droplet contact angle on a flat surface. Contact angles of hexadecane droplet on (b) EC-coated flat surface and (c) HP 55-coated flat surface, respectively. Contact angle of TPDGA droplet on (d) EC-coated flat surface and (e) HP 55-coated flat surface, respectively. 117

Figure 6.14: EC particles are not collected in the hexadecane-air interface. (a) Experimental observation of an air bubble and a hexadecane droplet brought into contact in a water phase containing 0.4 wt% Nile red labeled-EC particles. Scale bar is 500 μm . (b) Confocal microscope image of a close-up of hexadecane-air interface. Scale bar is 100 μm . 118

Figure 7.1: Interfacial activity of hydrophilic silica particles (100% SiOH) in the air-water interface. (a) Surface tension over time for 1 wt% hydrophilic silica particles in the air-water interface. (b) Steady state surface tension obtained at $t=1800$ s for various particle concentrations. Water was used as the drop phase in which silica particles were dispersed. 133

Figure 7.2: Interfacial activity of hydrophobic silica particles (32% SiOH) in the air-water interface. (a) Surface tension over time for 1 wt% hydrophobic silica particles at the air-water interface. (b) Steady state surface tension obtained at $t=1800$ s for hydrophobic silica particles with various particle concentrations. (c) Surface tension over time for 1 wt% hydrophobic silica particles at the air-water interface in the presence of 50 mM NaCl. (d) Steady state surface tension obtained at $t=1800$ s for hydrophobic silica particles with various particle concentrations in the presence of 50 mM NaCl. Water was used as the drop phase in which silica particles were dispersed. 135

Figure 7.3: Evidence that salt and particles do not introduce significant surface-active impurities. (a) Dynamic surface tension of 1 M NaCl. (b) Dynamic surface tension of supernatant of 32% SiOH silica. 136

Figure 7.4: Interfacial activity of silica particles in the hexadecane oil-water interface. (a) Steady state hexadecane-water interfacial tension obtained at $t=1800$ s for hydrophilic silica particles (100% SiOH) with various particle concentrations. (b) Steady state hexadecane-water interfacial tension obtained at $t=1800$ s for hydrophobic silica particles (32% SiOH) with various particle concentrations. 137

Figure 7.5: Measurements of contact angle and packing density of particles in fluid-fluid interfaces. (a) Image of a TMPTMA drop on a flat EC particle thin film placed inside the water medium. (b) Experimental setup for the measurement of the particle packing density in the TMPTMA-water interface. (c, d, e, f) SEM images of trapped EC particles at different locations on a polymerized TMPTMA droplet. Scale bars are 200 nm. 141

Figure 7.6: Comparison between theoretically predicted and experimentally measured effective interfacial tension. 143

Figure 7.7: Comparison between theoretically predicted and experimentally measured packing density. 145

Figure 8.1: Capillary emulsions. The system contains a continuous water phase, an oil phase, another immiscible oil phase, as well as particles. The agitation of the mixture results in a space-spanning network of particles in water (ii) connected by bridges of oil phase (iii), with another immiscible oil droplets embedded in the network (iv) via a joint adsorption of particles and a thin oil film. 155

LIST OF SYMBOLS

γ	Surface/Interfacial tension
A	Area
R	Radius
θ	Contact angle
G	Interfacial energy
S	Spreading coefficient
n_p	Number of particles
ϕ	Packing density
ε	Porosity
ρ	Density

LIST OF ABBREVIATIONS

SEM	Scanning electron microscopy
PDMS	Polydimethylsiloxane
TMPTMA	Trimethylolpropane trimethacrylate
PVC	Polyvinyl chloride
DINP	Diisononyl phthalate
SiOH	Residual hydroxyl groups on silica surface
EC	Ethyl cellulose
HP	Hypromellose phthalate
TPGDA	Tripropylene glycol diacrylate

SUMMARY

Common colloidal systems such as particle suspensions, foams, and emulsions are simply fine dispersions of one phase in another. More complex systems containing multiple dispersed fluids (gas bubbles and liquid droplets or droplets of different immiscible liquids) also occur naturally and even play increasingly important roles in industrial applications such as cosmetics, pharmaceutical formulations, water purification, or food processing. Their various applications depend on both their stability and their intrinsic wetting morphology. As the traditional choice for stabilizers and wetting modifiers, surfactants are widely used in many of these processes. However, surfactants cannot generally fully prevent the aging of a colloidal system because they frequently fluctuate in and out of an interface. Furthermore, surfactants suffer from drawbacks such as chemical degradation under harsh application conditions, environmental pollution, and difficult recovery. Colloidal particles of appropriate wettability at a two-phase interface can absorb and stabilize the interface and do not possess most of the problems common to surfactants. Therefore, my doctoral research focuses on using colloidal particles, instead of surfactants, as novel stabilizers and wetting modifiers in colloidal multiphase systems.

As part of my doctoral research on particles as stabilizers in a colloidal multiphase system, we discovered a new class of foam materials, capillary foams, which are obtained by frothing a particle suspension in the presence of a small amount of oil. In capillary foams, spanning particle networks are formed in which particles are connected by oil bridges with strong capillary forces. In addition, particles and a thin oil film jointly

adsorb on bubble surfaces, contributing the stabilization of gas bubbles. Capillary foams were prepared with a diverse set of particle/liquid combinations to demonstrate the generality of the phenomenon. The observed foam stability correlates with the particle affinity for the liquid interface formed by spreading the minority liquid at the bubble surface.

We also studied the formation stages of capillary foams and reported that particle networks are formed first and then air bubbles are entrapped in capillary foams. In addition, we investigated the influence of the particle concentration, particle wettability, and oil types on the preparation of capillary foams. It was shown that capillary foams can be prepared alternatively by either introducing air or oil simultaneously to a particle suspension, by frothing a capillary suspension, or by mixing oil into Pickering foam. To illustrate some of the application potential, we demonstrated the preparation of intensely colored foams that are notoriously difficult to achieve with traditional methods, and the preparation of load-bearing porous solids.

In addition to serving as co-stabilizers, it has been discovered that colloidal particles can be used as efficient wetting modifiers. The wetting configuration of an air bubble by an oil droplet in water medium was used as a model system due to its presence in a wide variety of industrial processes. This work demonstrated that particles can be used both to promote “bubble wetting” and induce the complete bubble engulfment by an oil drop, or to trigger progressive “bubble de-wetting”, i.e. substantially reduce the oil-bubble contact area. A mechanistic understanding of this reconfiguration process is obtained by measuring the effective dynamic surface and interfacial tensions obtained by

axisymmetric drop shape analysis. The tunability is attributed to changes in interfacial energy caused by the adsorption of particles at fluid-fluid interfaces.

Finally, despite many studies about the adsorption of particles in the interface, there has been a long ongoing debate on whether isotropic particles adsorbed in an interface can reduce the interfacial tension. The interfacial activity of isotropic silica nanoparticles for air-water and hexadecane-water interfaces was analyzed through pendant drop tensiometry. Our measurements show that isotropic particles can change interfacial tensions provided that they have a strong affinity to an interface by virtue of their wettability and that no energy barriers to adsorption prevent them from reaching the interface. A simple thermodynamic model was used to estimate the effective interfacial tension accounting for particle adsorption; its predictions are consistent with experimental data presented. We suggest that dynamic interfacial tension measurements, when combined with information about the particles' wetting properties, provide a convenient and accurate way to assess the packing density of particles in fluid-fluid interfaces. These results will help understand and control the assembly of isotropic nanoparticles at fluid-fluid interfaces which is relevant to applications ranging from surfactant-free formulations and food technology to oil recovery.

CHAPTER 1

INTRODUCTION

1.1 Colloidal systems

Common colloidal systems are simply fine dispersions of one phase in another,^{1,2} in which the size of dispersed phase is in the range from a few nanometers to about 10,000 nanometers in diameter. The dispersed and continuous phases could include gas, liquid, or solid (Table 1.1). These systems can consist of solid particles in a liquid or gas, such as solid particles suspended in air, which we call an aerosol, or solid particles suspended in water, which we call a suspension (Table 1.1). A colloidal system can also be composed of one fluid suspended in another fluid, for instance liquid droplets suspended in air (mist), liquid droplets suspended in another liquid (emulsion), and gas bubbles suspended in water (foam) (Table 1.1). Colloidal systems are ubiquitous in everyday life and present in many industrial applications including coating, ceramics, foods, cosmetics, and pharmaceutical formulations.^{1,2}

Table 1.1 Examples of colloidal systems.

Dispersed Phase	Continuous Phase	Examples
Liquid	Gas	steam, mist, fog
Solid	Gas	aerosols, smoke
Liquid	Liquid	emulsions
Solid	Liquid	dispersions, suspensions
Gas	Liquid/solid	foams

More complex colloidal systems containing multiple dispersed fluids (gas bubbles and liquid droplets or droplets of different immiscible liquids) also occur naturally and even play increasingly important roles in industrial applications such as cosmetics, pharmaceutical formulations, water purification, or food processing.

For many colloidal systems, achieving long-term stability is desirable but often difficult. In addition, the utility of colloids in various applications depend on both colloidal stability and the intrinsic wetting morphology, such as in the encapsulation,³ and controlled defoaming,⁴ and separation of oily wastewater through froth flotation.⁵ As the traditional choice for stabilizers and wetting modifiers, surfactants are widely used in many of these processes.² However, surfactants cannot fully prevent the aging of a colloidal multiphase system because they frequently adsorb and desorb from the interface. In addition, surfactants suffer from drawbacks such as chemical degradation under harsh application conditions and their accumulation can be harmful to the environment.

1.2 Particles at fluid-fluid interfaces

It has been known for a hundred years that colloid particles with appropriate wetting properties can attach strongly to interfaces between two immiscible fluids (e.g., water, oil or air).^{6,7} The driving force for this strong interfacial attachment is a reduction in interfacial area, and therefore, the interfacial energy. The reduction energy of particle adsorption (the free energy change upon particle adsorption to the interface) is given by:^{8,9}

$$\Delta G_{ad,12} = -\pi R^2 \gamma_{12} (1 - \cos \theta_{12})^2$$

where γ_{12} denotes the surface (interfacial) tension, θ_{12} is the contact angle of a single particle at the interface measured through phase 2, and R is the particle radius (Figure 1.1).

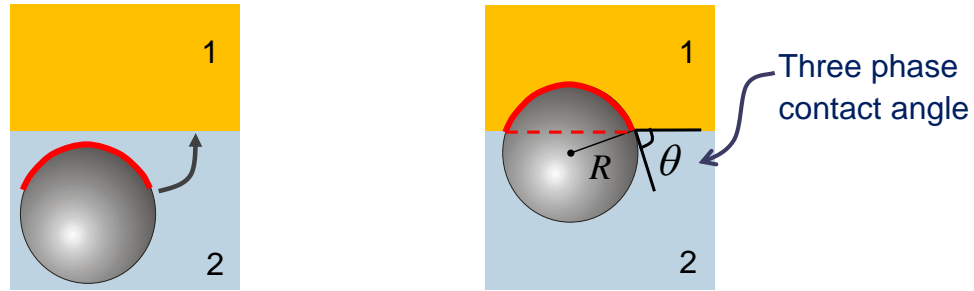


Figure 1.1 Cartoon showing adsorption of solid particles to a fluid-fluid interface. Adsorption of a particle from phase 2 to the interface replaces some of the phase 1-2 contact area with particle-phase 1 contact area.

For particles with appropriate wettability at an interface, the reduction energy of particle adsorption to the interface is much larger than the thermal energy, which indicates that, once the particle is attached to the interface, thermal fluctuations cannot make it detach from the interface.

Particle adsorption at fluid-fluid interfaces plays an important role in various technological processes. For example, it can be used in froth flotation processes to separate particles in the mining industry and papermaking process.¹⁰ In addition, given the flexibility of both chemistry and morphology of particles and unique property of fluid-fluid interfaces, adsorption of particles in an interface provides many opportunities to prepare functional materials with well-defined properties and functionality. A familiar example is the colloidosome produced by assembly of colloidal particles at the water-oil interface.¹¹ They are semi-permeable microcapsules with many advantages such as bio-

compatibility, controlled size and permeability, and mechanical sturdiness.¹¹ Interfacial adsorption of colloidal particles in air-water interface has been used to stabilize foams¹² or liquid marbles,^{13,14} which have potential applications in foods, personal care products, cosmetics, and pharmaceuticals. Particles can also adsorb in the oil-water interface to prepare ultra-stable emulsions. The unique stabilization behavior of particles in the oil-water interface has enabled the development of applications in drug delivery,^{15,16} enhanced oil recovery^{17,18} and catalysis.¹⁹

More recently, a new class of soft materials, biocontinuous interfacially jammed emulsion jells (bijels), was prepared by arresting spinodal decomposition of a partially miscible fluid by using colloidal particles with specific wetting properties.²⁰ The resultant materials with unique microstructures can be used in catalysis, energy storage, separations, and tissue engineering.²¹

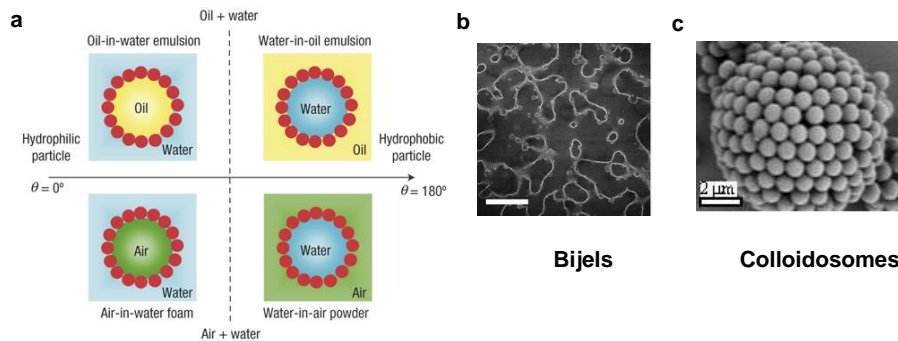


Figure 1.2 Materials from particle adsorption at fluid-fluid interfaces. (a) Cartoons showing oil-in-water emulsion, water-in-oil emulsion, foam and liquid marble.¹⁴ SEM images of (b) bijels²⁰ and (c) colloidosomes.¹¹ Images reproduced from references 14, 20, and 11.

1.3 Foams and Pickering foams

Aqueous foams are concentrated dispersions of gas bubbles in a continuous liquid phase. They can be found in our personal life; they also play important roles in many industrial processes, such as enhanced oil recovery, froth flotation, cosmetics, and food processing.^{1,2} Good foam stability is desirable for some of these applications.²² However, all foams are thermodynamically unstable systems due to the large interfacial energy associated with air-water interfaces.²³ In this case, foam stabilizers, such as surfactants, polymers or proteins²⁴, are added to kinetically stabilize the foams by slowing down the drainage, coalescence and coarsening of foams.

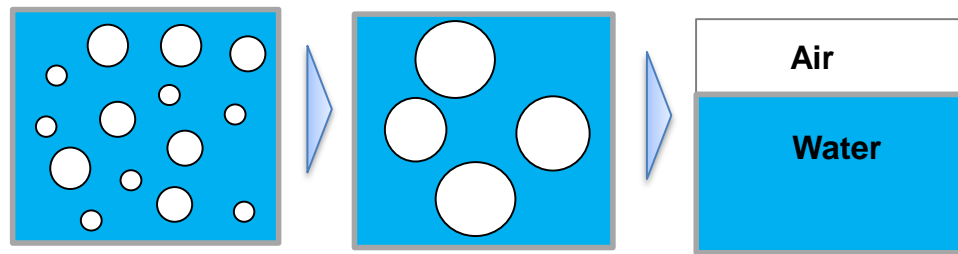


Figure 1.3 Scheme of breakdown process in foams.

Foams can also be stabilized by adsorbing colloidal particles; and the resulting foams, often referred to as “Pickering foams”, can achieve superior long-term stability.²⁵⁻
³¹ The transfer of particles with appropriate wettability from the liquid bulk to the gas-liquid interface tends to lower the interfacial energy so significantly that the particle attachment is practically irreversible.^{32,33} As a consequence, any coalescence (merging) of particle covered bubbles results in an increase of the interfacial particle concentration. Once a sufficiently high interfacial coverage is reached, further coalescence is effectively inhibited and the resulting foam can be stable for many months.³⁴ In addition to long-

term stability, certain hazardous, allergenic surfactants could be avoided and replaced by environmentally friendly, biorenewable, or even food-grade particles for the applications in surfactant-free cosmetics, food technology, and pharmaceutical formulation.^{35,36} More recently, they have become popular as precursors and templates for the assembly of novel materials, including microcapsules and lightweight materials.³⁷ Finally, particles offer many options to prepare stimulus-responsive foams for the controlled formation and destabilization of foams.³⁸⁻⁴⁰

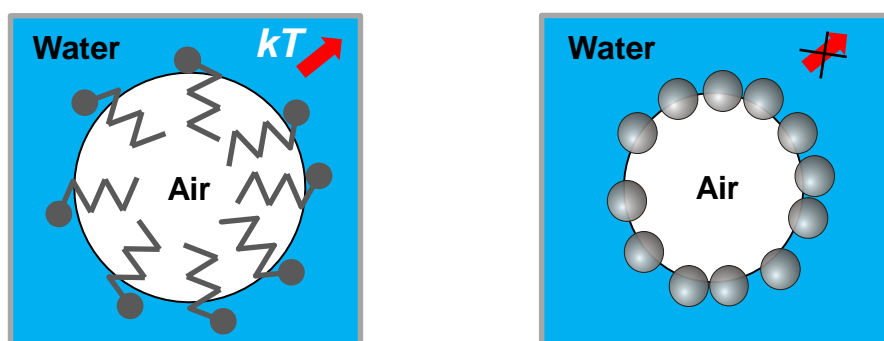


Figure 1.4 Scheme for foam bubble stabilized by adsorption of surfactants (left) and particles (right).

While the breadth of potential applications for Pickering foams keeps growing, the types of available particles to make stable Pickering foams are limited. This is because the attachment of particles at the air-water interface requires particles have desired wettability. Often, however, many commercial available particles, such as silica, aluminum oxide, and polymer particles, are too hydrophilic or hydrophobic to bind to the air-water interface and serve as efficient foam stabilizers. In that case particle-stabilized foams can only be achieved by substituting a different type of particle or by adjusting the

particle wettability via surface modification,⁴¹ which usually involves chemicals and solvents and is thus expensive, time-consuming, and environmentally unfriendly.

1.4 Capillary suspension

In 2011 it was reported that the addition of a small amount (0.05-10 wt.%) of an immiscible secondary liquid to a particle suspension can transform it from a viscous fluid into an elastic gel, in which particles at a relatively low volume fraction form a system-spanning network, held together by the strong capillary forces associated with small liquid bridges between the particles, giving the suspension solid-like properties (Figure 1.5a).^{42,43} Two different types of liquid bridges and particle network states were distinguished : the scenario in which particles are preferentially wetted by the bridging secondary liquid is referred to as the pendular state (Figure 1.5b), whereas the scenario of preferential particle wetting by the continuous phase (primary liquid) is referred to as the capillary state (Figure 1.5c). Liquid bridges in the pendular state tend to connect two particles per bridge and promote the formation of chain-like networks, whereas a typical bridge in the capillary state connects more than two particles. The term capillary suspension has been used to summarily describe “suspensions formed through the addition of a secondary fluid to a classical particle suspension”, which includes suspensions in both the pendular and capillary states.

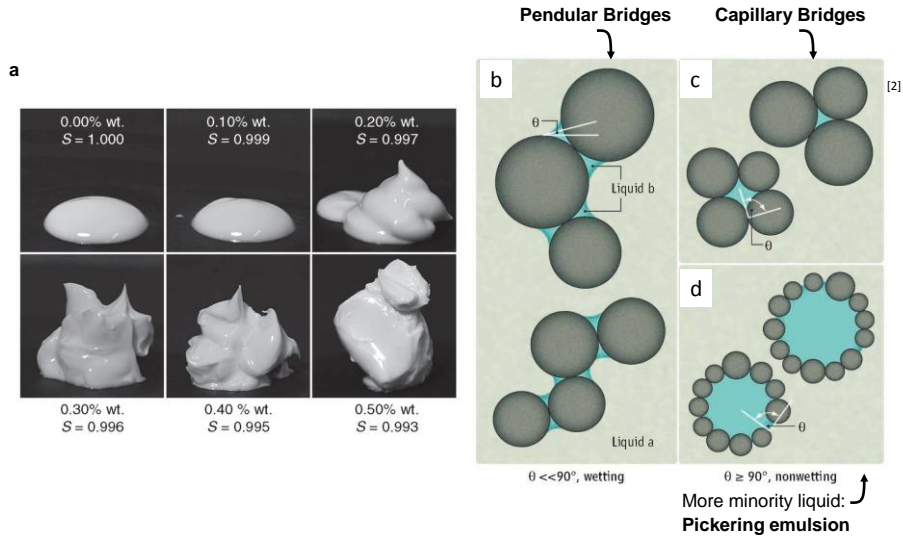


Figure 1.5 Capillary suspension.^{42,43} (a) The transition from fluid-like behavior to gel-like behavior with the addition of small amounts of water to a suspension of hydrophobically modified calcium carbonate. (b) Schematic illustration of pendular state. (c) Schematic illustration of the capillary state. (d) Particle-decorated droplets of a Pickering emulsion formed at much higher volume fraction of the secondary liquid. Images reproduced from references 42 and 43.

1.5 Wetting in colloidal multiphase systems

Wetting phenomena are ubiquitous both in nature and in various industrial processes and products.^{1,2,44,45} When a liquid droplet is put in contact with a flat homogenous solid surface, three distinct wetting configurations may be found: complete wetting, partial wetting, and non-wetting. While the wetting of a solid surface has been intensively studied, the wetting morphologies resulting from the encounter of two immiscible fluid droplets within a fluid medium have received less attention.

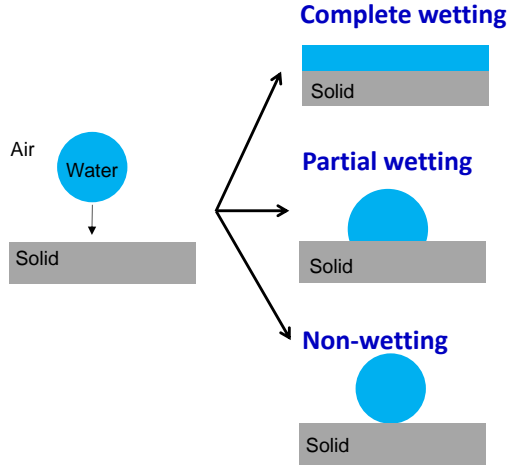


Figure 1.6 Possible wetting configurations of a water droplet on a homogeneous solid substrate.

Wetting in disperse multiphase systems plays a major role in many industrial processes, related to encapsulation, enhanced oil recovery, water purification, food technology, or defoaming. An analysis of wetting in these systems was first reported in the early 1970s by Torza and Mason⁴⁶ and was revisited recently by Pannacci et al.⁴⁷ and Guzowski et al.⁴⁸ These authors found that the wetting of a liquid droplet by a second fluid in a third immiscible fluid medium can result in three possible wetting morphologies (non-wetting, partial engulfment, and complete engulfment of one drop by the other), which were successfully predicted based on the spreading coefficients of three fluids. A fluid i will spread spontaneously at the interface of two immiscible fluids j and k if its spreading coefficient $S_i = \gamma_{jk} - (\gamma_{ik} + \gamma_{ij})$ is positive, where γ_{ij} , γ_{jk} , and γ_{ik} are the respective interfacial tensions.⁴⁶⁻⁴⁸ For the wetting behavior of a colloidal multiphase system, three cases can be distinguished: if the spreading coefficient of the continuous medium phase is positive, the droplets will be non-wetting and try to separate; if, by contrast, one of the droplet phases has a positive spreading coefficient, it will fully engulf

the other droplet (complete wetting); the case of partial wetting is realized when none of the three phases has a positive spreading coefficient.

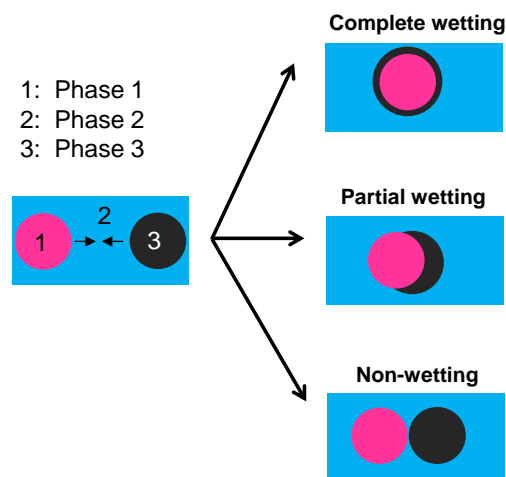


Figure 1.7 Possible wetting configurations for three immiscible fluids.

Each of the three wetting configurations has different applications. The complete engulfment of one drop inside another can be used to encapsulate active substances in the inner droplet for controlled release, and has been exploited in contrast-enhanced ultrasonography, gas flotation, encapsulation, and defoaming.^{3,49-51} Partial engulfment is used in the synthesis of anisotropic particles with promise for applications such as drug delivery, imaging, and sensing.⁵²⁻⁵⁴ The non-wetting configuration can be used to provide a fluid spacer phase that prevents the coalescence of neighboring plugs in plug-flow microfluidics.⁵⁵ All of these applications call for a specific wetting morphology. A given fluid system, however, does not always adopt the desired wetting configuration; hence there is significant and widespread interest in methods to tune or even actively reconfigure the wetting configuration on demand. Surfactants are the traditional tool for

achieving a desired wetting configuration, because they can alter spreading coefficients by adsorbing at fluid-fluid interfaces and reduce their interfacial tensions. A recent study demonstrates the use of surfactants to actively reconfigure wetting states in a colloidal system consisting of three and four-phase complex emulsions.⁵⁶

1.6 Thesis motivations and objectives

Common colloidal systems such as particle suspensions, foams, and emulsions are simply fine dispersions of one phase in another. More complex systems containing multiple dispersed fluids (gas bubbles and liquid droplets or droplets of different immiscible liquids) also occur naturally and even play increasingly important roles in industrial applications such as cosmetics, pharmaceutical formulations, water purification, or food processing. Their various applications depend both on their stability and on their intrinsic wetting morphology. Surfactants traditionally serve as stabilizers and wetting modifiers, but solid particles can sometimes achieve the same goal; moreover, they can have the advantage of providing better resistance to harsh application conditions, posing fewer environmental concerns, and allowing for easier recovery. We are therefore motivated to answer the following two questions:

- (a) Can particles act as stabilizers in colloidal multiphase systems?
- (b) Can particles act as wetting modifiers in colloidal multiphase systems?

1.7 Thesis outline

Chapter 2 presents a new class of soft materials, capillary foams, which are obtained by frothing a particle suspension in the presence of a small amount of oil.

Chapter 3 studies the stabilization mechanism of capillary foams.

Chapter 4 studies the formation stages and the effects of process parameters on the formation of capillary foams.

Chapter 5 explores in more detail the preparation routes of capillary foams. In addition, we create vividly colored wet and dried foams, which are difficult to prepare using traditional methods, and load-bearing porous solids.

Chapter 6 demonstrates that colloidal particles can be used as efficient wetting modifiers to promote “bubble wetting” or to trigger progressive “bubble de-wetting”.

Chapter 7 investigates the interfacial activities of isotropic silica particles at fluid-fluid interfaces and develops a thermodynamic model to predict the effective interfacial tensions and packing density of particles at fluid-fluid interfaces.

Chapter 8 summarizes primary findings of this research and present recommendations for future investigations.

1.8 References

1. Hiemenz, P. C., Principles of colloid and surface chemistry. M. Dekker New York: 1986.
2. Evans, D. F.; Wennerström, H., The colloidal domain: where physics, chemistry, biology, and technology meet. Wiley-VCH New York: 1999.
3. Tiarks, F.; Landfester, K.; Antonietti, M., Preparation of polymeric nanocapsules by miniemulsion polymerization. *Langmuir* 2001, 17 (3), 908-918.
4. Denkov, N. D.; Marinova, K. G.; Tcholakova, S. S., Mechanistic understanding of the modes of action of foam control agents. *Advances in Colloid and Interface Science* 2014, 206, 57-67.
5. Moosai, R.; Dawe, R. A., Gas attachment of oil droplets for gas flotation for oily wastewater cleanup. *Sep Purif Technol* 2003, 33 (3), 303-314.
6. Ramsden, W., Separation of solids in the surface-layers of solutions and 'Suspensions' (Observations on surface-membranes, bubbles, emulsions, and mechanical coagulation). Preliminary Account. *P R Soc London* 1903, 72 (479), 156-164.
7. Pickering, S. U., Emulsions. *J Chem Soc* 1907, 91, 2001-2021.
8. Pieranski, P., Two-dimensional interfacial colloidal crystals. *Phys Rev Lett* 1980, 45 (7), 569-572.
9. Binks, B. P.; Lumsdon, S. O., Influence of particle wettability on the type and stability of surfactant-free emulsions. *Langmuir* 2000, 16 (23), 8622-8631.
10. Binks, B. P.; Horozov, T. S., Colloidal particles at liquid interfaces. Cambridge University Press: 2006.
11. Dinsmore, A. D.; Hsu, M. F.; Nikolaides, M. G.; Marquez, M.; Bausch, A. R.; Weitz, D. A., Colloidosomes: Selectively permeable capsules composed of colloidal particles. *Science* 2002, 298 (5595), 1006-1009.

12. Binks, B. P.; Horozov, T. S., Aqueous foams stabilized solely by silica nanoparticles. *Angew Chem Int Edit* 2005, 44 (24), 3722-3725.
13. Aussillous, P.; Quere, D., Liquid marbles. *Nature* 2001, 411 (6840), 924-927.
14. Binks, B. P.; Murakami, R., Phase inversion of particle-stabilized materials from foams to dry water. *Nat Mater* 2006, 5 (11), 865-869.
15. Simovic, S.; Prestidge, C. A., Nanoparticle layers controlling drug release from emulsions. *Eur J Pharm Biopharm* 2007, 67 (1), 39-47.
16. Eskandar, N. G.; Simovic, S.; Prestidge, C. A., Nanoparticle coated emulsions as novel dermal delivery vehicles. *Curr Drug Deliv* 2009, 6 (4), 367-373.
17. Bragg, J. R., Oil recovery method using an emulsion. Google Patents: 1999.
18. Sullivan, A. P.; Kilpatrick, P. K., The effects of inorganic solid particles on water and crude oil emulsion stability. *Ind Eng Chem Res* 2002, 41 (14), 3389-3404.
19. Crossley, S.; Faria, J.; Shen, M.; Resasco, D. E., Solid nanoparticles that catalyze biofuel upgrade reactions at the water/oil interface. *Science* 2010, 327 (5961), 68-72.
20. Herzig, E.; White, K.; Schofield, A.; Poon, W.; Clegg, P., Bicontinuous emulsions stabilized solely by colloidal particles. *Nat Mater* 2007, 6 (12), 966-971.
21. Cates, M. E.; Clegg, P. S., Bijels: a new class of soft materials. *Soft Matter* 2008, 4 (11), 2132-2138.
22. Zhang, L.; Mikhailovskaya, A.; Yazhgur, P.; Muller, F.; Cousin, F.; Langevin, D.; Wang, N.; Salonen, A., Precipitating sodium dodecyl sulfate to create ultrastable and stimuable foams. *Angewandte Chemie* 2015, 127 (33), 9669-9672.
23. Weaire, D. L.; Hutzler, S., The physics of foams. Oxford University Press: 2001.
24. Dickinson, E., Adsorbed protein layers at fluid interfaces: interactions, structure and surface rheology. *Colloid Surface B* 1999, 15 (2), 161-176.

25. Hunter, T. N.; Pugh, R. J.; Franks, G. V.; Jameson, G. J., The role of particles in stabilising foams and emulsions. *Advances in Colloid and Interface Science* 2008, 137 (2), 57-81.
26. Blanco, E.; Lam, S.; Smoukov, S. K.; Velikov, K. P.; Khan, S. A.; Veleev, O. D., Stability and viscoelasticity of magneto-Pickering foams. *Langmuir* 2013, 29 (32), 10019-10027.
27. Poulichet, V.; Garbin, V., Cooling particle-coated bubbles: destabilization beyond dissolution arrest. *Langmuir* 2015, 31 (44), 12035-12042.
28. Gonzenbach, U. T.; Studart, A. R.; Tervoort, E.; Gauckler, L. J., Ultrastable particle-stabilized foams. *Angew Chem Int Edit* 2006, 45 (21), 3526-3530.
29. Dickinson, E.; Ettelaie, R.; Kostakis, T.; Murray, B. S., Factors controlling the formation and stability of air bubbles stabilized by partially hydrophobic silica nanoparticles. *Langmuir* 2004, 20 (20), 8517-8525.
30. Alargova, R. G.; Warhadpande, D. S.; Paunov, V. N.; Veleev, O. D., Foam superstabilization by polymer microrods. *Langmuir* 2004, 20 (24), 10371-10374.
31. Guevara, J. S.; Mejia, A. F.; Shuai, M.; Chang, Y. W.; Mannan, M. S.; Cheng, Z. D., Stabilization of Pickering foams by high-aspect-ratio nano-sheets. *Soft Matter* 2013, 9 (4), 1327-1336.
32. Binks, B. P., Particles as surfactants - similarities and differences. *Curr Opin Colloid In* 2002, 7 (1-2), 21-41.
33. Bizmark, N.; Ioannidis, M. A.; Henneke, D. E., Irreversible adsorption-driven assembly of nanoparticles at fluid interfaces revealed by a dynamic surface tension probe. *Langmuir* 2014, 30 (3), 710-717.
34. Stocco, A.; Rio, E.; Binks, B. P.; Langevin, D., Aqueous foams stabilized solely by particles. *Soft Matter* 2011, 7 (4), 1260-1267.
35. Dickinson, E., Food emulsions and foams: Stabilization by particles. *Curr Opin Colloid In* 2010, 15 (1-2), 40-49.

36. Lam, S.; Velikov, K. P.; Velev, O. D., Pickering stabilization of foams and emulsions with particles of biological origin. *Curr Opin Colloid In* 2014, 19 (5), 490-500.
37. Studart, A. R.; Gonzenbach, U. T.; Akartuna, I.; Tervoort, E.; Gauckler, L. J., Materials from foams and emulsions stabilized by colloidal particles. *J Mater Chem* 2007, 17 (31), 3283-3289.
38. Fameau, A. L.; Lam, S.; Velev, O. D., Multi-stimuli responsive foams combining particles and self-assembling fatty acids. *Chem Sci* 2013, 4 (10), 3874-3881.
39. Binks, B. P.; Murakami, R.; Armes, S. P.; Fujii, S.; Schmid, A., pH-responsive aqueous foams stabilized by ionizable latex particles. *Langmuir* 2007, 23 (17), 8691-8694.
40. Lam, S.; Blanco, E.; Smoukov, S. K.; Velikov, K. P.; Velev, O. D., Magnetically responsive Pickering foams. *J Am Chem Soc* 2011, 133 (35), 13856-13859.
41. Gonzenbach, U. T.; Studart, A. R.; Tervoort, E.; Gauckler, L. J., Stabilization of foams with inorganic colloidal particles. *Langmuir* 2006, 22 (26), 10983-10988.
42. Koos, E.; Willenbacher, N., Capillary forces in suspension rheology. *Science* 2011, 331 (6019), 897-900.
43. Butt, H. J., Controlling the flow of suspensions. *Science* 2011, 331 (6019), 868-869.
44. Mayer, D.; Surfaces, I., *Colloids: principles and applications*. Wiley New York: 1999.
45. Tian, Y.; Su, B.; Jiang, L., Interfacial material system exhibiting superwettability. *Adv Mater* 2014, 26 (40), 6872-6897.
46. Torza, S.; Mason, S., Three-phase interactions in shear and electrical fields. *J Colloid Interf Sci* 1970, 33 (1), 67-83.
47. Pannacci, N.; Bruus, H.; Bartolo, D.; Etchart, I.; Lockhart, T.; Hennequin, Y.; Willaime, H.; Tabeling, P., Equilibrium and nonequilibrium states in microfluidic double emulsions. *Phys Rev Lett* 2008, 101 (16), 164502- 164505.

48. Guzowski, J.; Korczyk, P. M.; Jakiela, S.; Garstecki, P., The structure and stability of multiple micro-droplets. *Soft Matter* 2012, 8 (27), 7269-7278.
49. Xu, J. H.; Chen, R.; Wang, Y. D.; Luo, G. S., Controllable gas/liquid/liquid double emulsions in a dual-coaxial microfluidic device. *Lab Chip* 2012, 12 (11), 2029-2036.
50. Chu, L. Y.; Utada, A. S.; Shah, R. K.; Kim, J. W.; Weitz, D. A., Controllable monodisperse multiple emulsions. *Angew Chem Int Edit* 2007, 46 (47), 8970-8974.
51. Garrett, P., Defoaming: theory and industrial applications. CRC Press: 1992.
52. Walther, A.; Muller, A. H. E., Janus Particles: synthesis, self-assembly, physical properties, and applications. *Chem Rev* 2013, 113 (7), 5194-5261.
53. Lone, S.; Cheong, I. W., Fabrication of polymeric Janus particles by droplet microfluidics. *Rsc Adv* 2014, 4 (26), 13322-13333.
54. Huang, X. P.; Qian, Q. P.; Wang, Y. P., Anisotropic particles from a one-pot double emulsion induced by partial wetting and their triggered release. *Small* 2014, 10 (7), 1412-1420.
55. Chen, D. L. L.; Li, L.; Reyes, S.; Adamson, D. N.; Ismagilov, R. F., Using three-phase flow of immiscible liquids to prevent coalescence of droplets in microfluidic channels: Criteria to identify the third liquid and validation with protein crystallization. *Langmuir* 2007, 23 (4), 2255-2260.
56. Zarzar, L. D.; Sresht, V.; Sletten, E. M.; Kalow, J. A.; Blankschtein, D.; Swager, T. M., Dynamically reconfigurable complex emulsions via tunable interfacial tensions. *Nature* 2015, 518 (7540), 520-524.

CHAPTER 2

CAPILLARY FOAMS: A SMALL AMOUNT OF OIL MAKES A BIG DIFFERENCE

2.1 Introduction

Liquid foams arise both in nature and in many commercial products and processes, including pharmaceutical formulation, food processing, wastewater treatment, and cosmetics.¹⁻³ Dried foam materials are widely used to fabricate thermally insulating materials⁴ and low-weight structures, as well as in tissue engineering. Long-term stability in the liquid state is desirable for many foam-based systems, but often difficult to achieve. All foams are thermodynamically unstable due to liquid surface tension and will separate into two distinct phases given enough time. Therefore stabilizers such as surfactants are commonly added to stabilize foams kinetically. Foam bubbles can alternatively be stabilized by adsorbing colloidal particles;⁵⁻⁹ and the resulting “Pickering foams” can achieve superior long-term stability. Often, however, solid particles of a given material do not have the required wettability to stabilize gas bubbles. In that case, particle-stabilized foams can only be achieved by substituting a different type of particle or by adjusting the particle wettability via surface modification.^{10,11}

In this chapter, we report a new type of foam material (“capillary foams”) that dramatically expands the range of viable particles for foam stabilization, and in which gas bubbles are stabilized by the combined action of particles and a small amount of an immiscible secondary liquid. Our study focuses on water-based foams with different oils

as the secondary liquid. We find that the presence of a small amount of oil can lead to stable foams even when the particles cannot stabilize foam bubbles by themselves.

2.2 Materials and Methods

2.2.1 Materials

Polyvinyl chloride particles with different size and wettability (Vinnolit SA 1062/7 and Vinnolit P70F) were obtained from Vinnolit, Germany. Polyethylene (PE) particles were purchased from Polysciences, Inc., USA. The silica samples (Aerosil 200) were obtained from Evonik, USA and then treated with trimethoxymethylsilane as provided by Sigma-Aldrich. Cellulose powder was purchased from Sigma-Aldrich and then modified with poly(maleic anhydride-1-octadecene) obtained from Polysciences, Inc., USA. The glass samples were obtained from Potters Industries LLC as Spherglass 5000 solid glass microspheres. The glass was cleaned with acetone. The aluminum oxide particles were purchased from Sigma-Aldrich. Monodisperse silica spheres (SS03N, 0.96 μ m) were obtained from Bangs Laboratories, Inc. Scanning electron micrographs of particles used in this study and particles size distribution are shown in Figures 2.1 and 2.2, respectively.

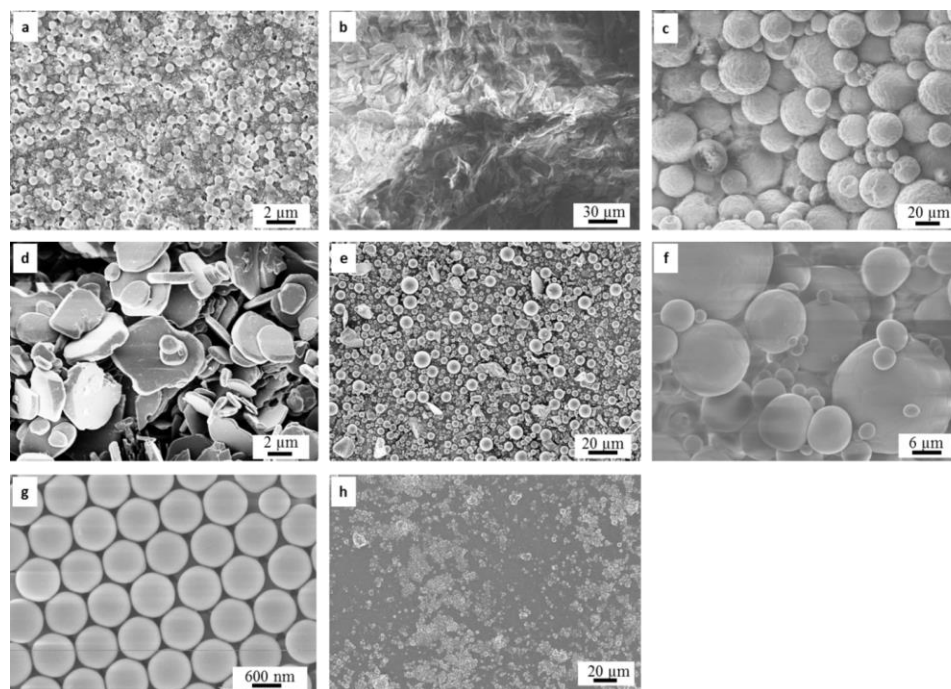


Figure 2.1 SEM images of the particles used in this study. (a) Modified silica (Aerosil 200), mean diameter: 619.15 nm. (b) Modified cellulose powder, mean diameter: 33.90 μm . (c) PVC Vinnolit SA/1062/7, mean diameter: 29.59 μm . (d) Aluminum oxide particles, mean diameter: 5.27 μm . (e) Glass (Spherglass 5000), mean diameter: 4.44 μm . (f) Polyethylene particles, mean diameter: 9.65 μm . (g) Monodisperse silica spheres (SS03N), diameter: 0.96 μm . (h) PVC Vinnolit P70F, mean diameter: 0.93 μm .

The secondary fluids used in this chapter were trimethylolpropane trimethacrylate (TMPTMA, Sigma-Aldrich), paraffin (Sigma-Aldrich), and diisononyl phthalate (DINP, Sigma-Aldrich). Polyvinyl chloride particles (Vinnolit SA1062/7) were washed with deionized water several times before use. All the chemicals were used as received, unless otherwise noted. Ultra-pure water with a resistivity of 18.2 $\text{M}\Omega\cdot\text{cm}$ (Barnstead) was used.

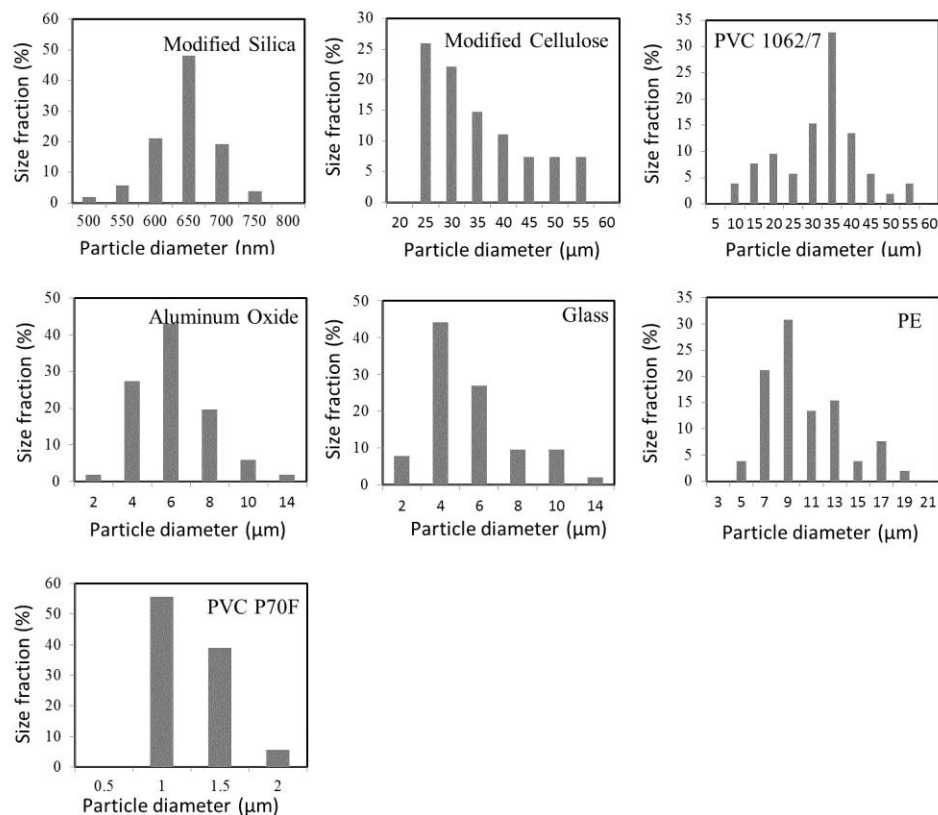


Figure 2.2 Particle size distributions.

2.2.2 Surface tension and interfacial tension measurements

To measure the equilibrium surface and interfacial tensions, equal volumes of water and oil were vigorously stirred overnight to achieve mutual saturation, and then separated by centrifuge prior to the experiment. The surface tension of oil against air was measured with a Lauda TVT-2 drop volume tensiometer. Interfacial tensions of water against air and oil were measured via shape analysis of pendant drops with a Ramé-hart model 250 goniometer. The surface and interfacial tensions are reported in Table 2.1. Reported surface and interfacial tensions are averages over five independent measurements.

Table 2.1 Surface and interfacial tensions of fluids used in this study. Equilibrium interfacial tension data of TMPTMA were obtained from reference 12. The equilibrium surface and interfacial tensions were used to calculate the interfacial energy change and effective spreading coefficient, where a, o, w represent the air, oil, water phase respectively. γ' is the equilibrium surface/interfacial tension and γ is the surface/interfacial tension of pure liquids.

	Equilibrium surface and interfacial tensions			Surface and interfacial tensions of pure liquids		
	γ'_{ao} (mN/m)	γ'_{aw} (mN/m)	γ'_{ow} (mN/m)	γ_{ao} (mN/m)	γ_{aw} (mN/m)	γ_{ow} (mN/m)
TMPTMA	32.86	51.74	18.99	32.55	72.80	18.49
DINP	32.13	57.43	19.56	30.68	72.80	22.24
Paraffin oil	32.95	72.00	49.22	31.26	72.80	49.39

2.2.3 Foam preparation and characterization

A suspension of particles in water as the primary liquid was obtained by initially dispersing the particles via sonication; then a small amount (0.5-3.0 wt%) of immiscible secondary fluid was added. The resulting suspension was frothed using a rotor-stator homogenizer (IKA UltraTurrax T10, stator diameter of 8 mm and rotor diameter of 6.1 mm) at 30000 rpm for 1 minute (3×20 s with 20 s rest periods). The wet foam was characterized with respect to foam stability. The foam stability was assessed by monitoring foam height over time at ambient temperature. Confocal laser scanning microscopy (CLSM) was performed using a Zeiss LSM 510 VIS Confocal Microscope. Nile red (0.01 wt %) was used as a staining agent for the oil phase using excitation at 543 nm and emission above 560 nm. The wet foam containing TMPTMA was settled by exposure to UV light (SpectroLine Longlife Filter, wavelength 365 nm) for 2 hours and

then dried in the oven at 70 °C for 16 hours. SEM images of gold coated surfaces were taken using a Zeiss Ultra60 field emission scanning electron microscope (FE-SEM; Carl Zeiss Microscopy, LLC North America, Peabody, MA) operated at an accelerating voltage of 5 kV.

2.3 Results and Discussion

2.3.1 Capillary foams: a small amount of oil makes a big difference

We find that the presence of a small amount of oil can lead to stable foams even when the particles cannot stabilize foam bubbles by themselves, as illustrated in Figure 2.3: in the absence of oil, mechanical frothing of an aqueous suspension of polyvinyl chloride particles produced only a very small foam head, and this foam disintegrated within 24 hours; but if as little as 0.5 wt% (with respect to the water bulk) of photopolymerizable oil trimethylolpropane trimethacrylate (TMPTMA), paraffin oil, or diisononyl phthalate (DINP) was added to the particle suspension prior to frothing, a large amount of foam was formed, which showed no significant degradation over several weeks (Figure 2.3b). Similar behaviour was observed for other types of particles (modified cellulose, modified silica, and glass, see Figure 2.4). This synergy of oil and particulate foam stabilizers is remarkable because oils are usually considered detrimental for foam stability^{13,14} and are commonly used as defoaming agents.^{15,16}

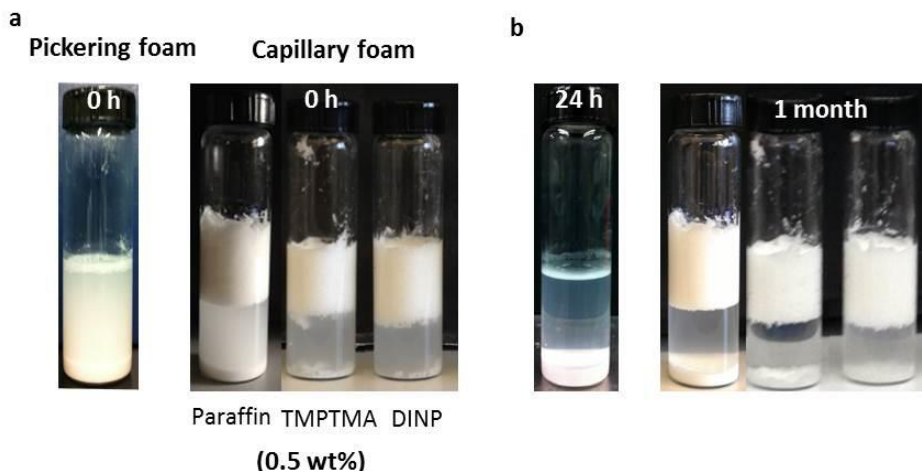


Figure 2.3 Stable foams requiring both particles and a secondary liquid. (a) Attempts of producing foams via frothing in the presence of PVC (Vinnolit SA 1062/7) particles only (14.16 wt%), and of both particles and a secondary liquid combined (14.16 wt% total, including 0.5 wt% of the secondary liquid). (b) Photographs of the same samples after 24 hours or 1 month.

We have prepared capillary foams with water as the bulk fluid (primary liquid) and air as the bubble phase, varying the “oil” (secondary liquid) and the particle type in a study covering a variety of particle sizes, shapes, and wettabilities (see Figures 2.4). Oils explored include TMPTMA, paraffin, and DINP; the particles include polyvinyl chloride (PVC) of different size and wettability (Vinnolit SA 1062/7 and Vinnolit P70F), polyethylene (PE), modified silica (aerosol 200), monodisperse silica spheres (SS03N), glass, aluminium oxide, and modified cellulose.

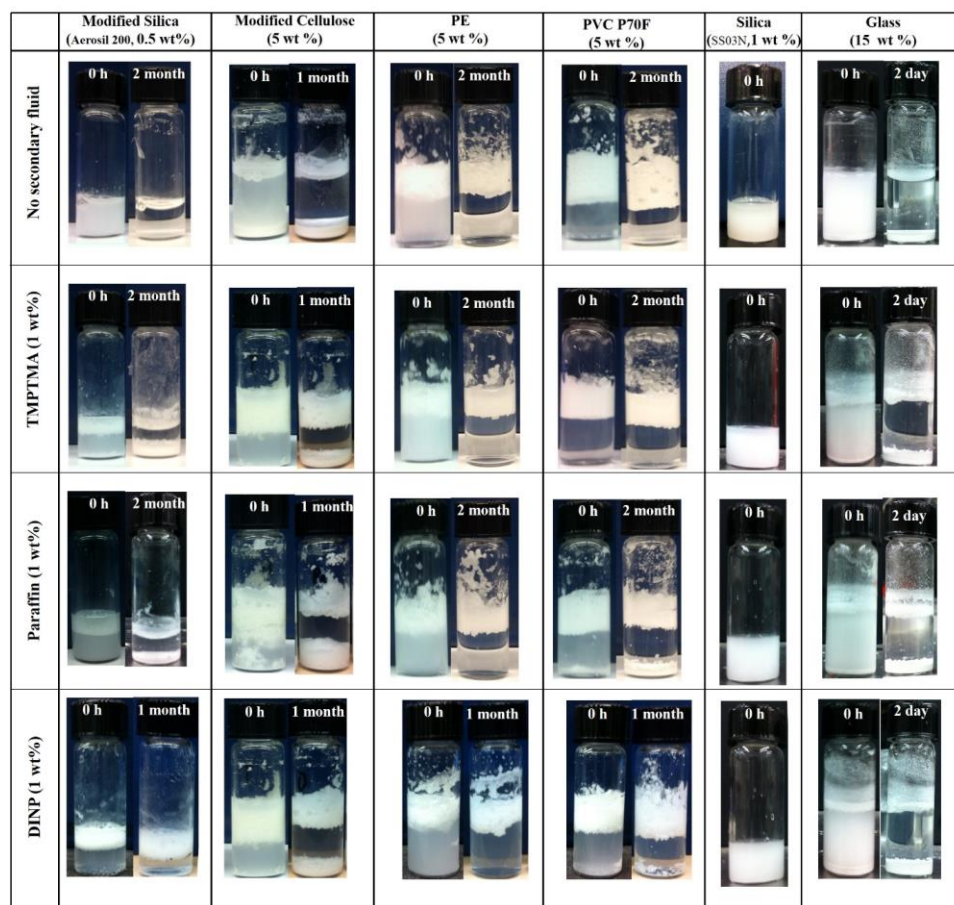


Figure 2.4 Experimental observations of foam stability where a variety of particles and fluid combinations were tested. The particles tested cover a range of particle size, shapes and wettability.

Figure 2.5a-j shows SEM images of a dried capillary foam with TMPTMA as the oil (Sigma-Aldrich, treated with Al_2O_3 to remove inhibitor, and enriched with 5 wt.% of the photo-initiator benzoin-isobutylether) and either PE particles, PVC 1062/7 particles or glass particles, whereas Figure 2.5k-m shows the location of the (dye-labelled) oil in the corresponding wet foams, as seen by confocal microscopy.

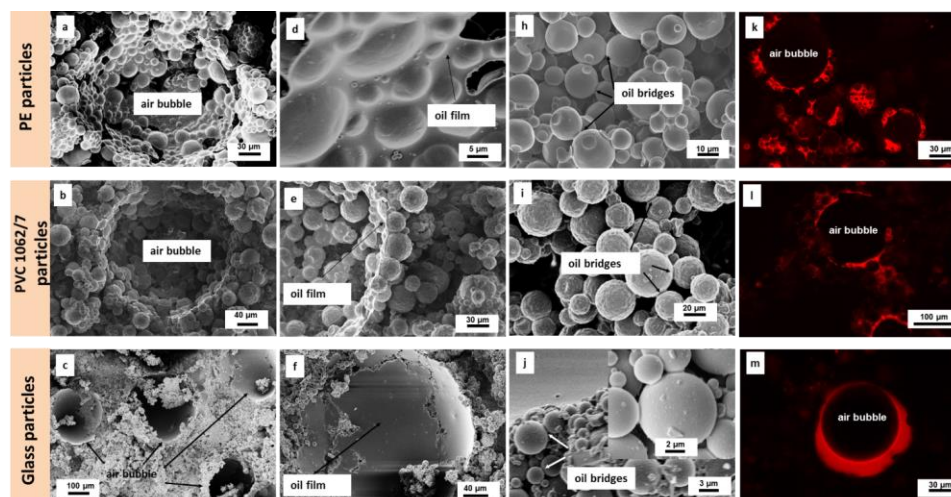


Figure 2.5 Combined adsorption of particles and secondary fluid at bubble surfaces of a capillary foam. (a-c) SEM images of a dried capillary foam formed by addition of gas bubbles and 1 wt% TMPTMA as the secondary fluid to suspensions of PE or PVC Vinnolit 1062/7 or glass particles in water with a solids loading of 10 vol.%. The secondary fluid was first solidified by photo-polymerization, and then the water was removed by drying. (d-f) Close-up of particles and polymerized secondary fluid surrounding a gas bubble. (h-j) Network of particles and polymerized secondary fluid bridges in the aqueous suspension bulk. (k-m) Confocal microscope image of the wet capillary foam with the secondary fluid TMPTMA labelled by Nile red.

Figure 2.5d-f and k-m suggests an accumulation of oil around the bubble surfaces. On the other hand, small oil bridges are also seen to connect the particles in the bulk suspension between the bubbles (Figure 2.5h-j) into a particle network. Such networks of particles connected via oil bridges are held together by capillary forces, much like the water-bridged grains of sand in a sand castle, and were already reported in 2011 for bubble-free particle suspensions that gel when mixed with a small amount of an immiscible liquid.^{17,18} In capillary foams, the particle network appears to provide a matrix that connects and immobilizes the (particle- and oil-decorated) bubbles. We surmise that this particle network also contributes to foam stability against bubble coalescence by hindering liquid drainage. Nonetheless, the formation of particle networks in the liquid bulk does not by itself guarantee effective bubble stabilization. Figure 2.6a

shows a failed attempt of producing stable capillary foam using hydrophilic silica particles and TMPTMA, a particle/oil combination that does lead to networks of oil-bridged particles (Figure 2.6b,c). Frothing of this suspension in the presence of oil produced no significant foam head.

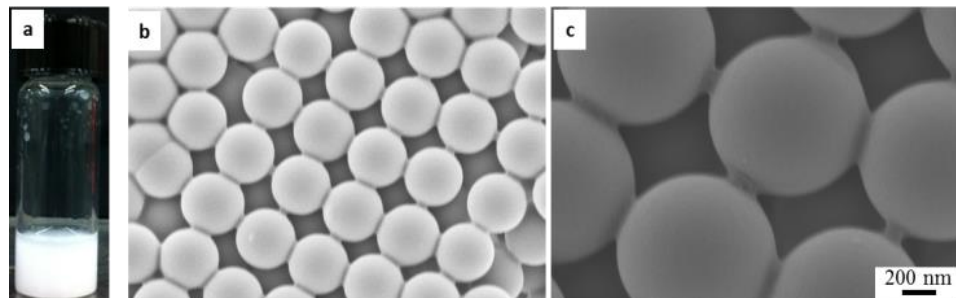


Figure 2.6 Network formation without foam stabilization. (a) Failed attempt of producing capillary foam from a silica particle suspension (2 wt.%) in the presence of secondary fluid TMPTMA (3 wt.%, with respect to the amount of bulk phase water). (b-c) SEM images of a dried silica particles suspension. The secondary fluid was solidified by photo-polymerization prior to water removal.

2.3.2 Evidence that secondary liquid alone cannot stabilize foams

We report that the addition of a secondary liquid can lead to stable foams even when the particles do not have the required wetting behavior to stabilize air bubbles by themselves and find that stabilization of bubbles requires both particles and a secondary liquid. In order to further support the synergistic action of particles and a secondary fluid on the stabilization of capillary foams, here we investigate whether the foam bubbles can be stabilized in the presence of only a secondary fluid. Figure 2.7 shows that no foam head is produced when frothing a particle-free systems with only a secondary fluid, such as Paraffin, TMPTMA or DINP (14.16 wt%).



Figure 2.7 Attempts of producing foam via frothing in the presence of secondary liquids only (14.16 wt. %).

2.4 Conclusions

In summary, we have reported a new class of liquid foams materials in which gas bubbles are stabilized by the synergistic action of particles and a small amount of an immiscible secondary liquid. The practical implications of this finding are significant: particle-stabilized aqueous foams play a role in many industrial processes, but the particle wettability requirements for bubble stabilization have so far severely limited the choice of particle stabilizers. The addition of a small amount of oil provides a convenient and timesaving alternative to surface modification and greatly broadens the range of suitable particles. Tuning and functionalization options afforded by the combined presence of particles and a secondary liquid in capillary foams make these materials extremely versatile, with expected applications ranging from drug delivery to oil recovery.

2.5 References

1. Mezzenga, R.; Schurtenberger, P.; Burbidge, A.; Michel, M., Understanding foods as soft materials. *Nat Mater* 2005, 4 (10), 729-740.
2. Rajagopalan, R.; Hiemenz, P. C., Principles of colloid and surface chemistry. Marcel Dekker New-York: 1986.
3. Evans, D. F.; Wennerstrom, H., Colloidal domain. Wiley-Vch: 1999.
4. Mills, N., Polymer foams handbook: engineering and biomechanics applications and design guide. Butterworth-Heinemann: 2007.
5. Binks, B. P., Particles as surfactants - similarities and differences. *Curr Opin Colloid In* 2002, 7 (1-2), 21-41.
6. Alargova, R. G.; Warhadpande, D. S.; Paunov, V. N.; Velev, O. D., Foam superstabilization by polymer microrods. *Langmuir* 2004, 20 (24), 10371-10374.
7. Binks, B. P.; Horozov, T. S., Colloidal particles at liquid interfaces. Cambridge University Press: 2006.
8. Wege, H. A.; Kim, S.; Paunov, V. N.; Zhong, Q. X.; Velev, O. D., Long-term stabilization of foams and emulsions with in-situ formed microparticles from hydrophobic cellulose. *Langmuir* 2008, 24 (17), 9245-9253.
9. Binks, B. P.; Murakami, R., Phase inversion of particle-stabilized materials from foams to dry water. *Nat Mater* 2006, 5 (11), 865-869.
10. Binks, B. P.; Horozov, T. S., Aqueous foams stabilized solely by silica nanoparticles. *Angew Chem Int Edit* 2005, 44 (24), 3722-3725.
11. Gonzenbach, U. T.; Studart, A. R.; Tervoort, E.; Gauckler, L. J., Ultrastable particle-stabilized foams. *Angew Chem Int Edit* 2006, 45 (21), 3526-3530.
12. Ding, A. L.; Goedel, W.A., Experimental investigation of particle-assisted wetting. *J Am Chem Soc* 2006, 128(15), 4930-4931.

13. Lee, J.; Nikolov, A.; Wasan, D., Stability of aqueous foams in the presence of oil: on the importance of dispersed vs solubilized oil. *Ind Eng Chem Res* 2013, 52 (1), 66-72.
14. Denkov, N. D.; Marinova, K. G.; Tcholakova, S. S., Mechanistic understanding of the modes of action of foam control agents. *Adv Colloid Interfac* 2014, 206, 57-67.
15. Garrett, P., Defoaming: theory and industrial applications. CRC Press: 1992.
16. Denkov, N. D., Mechanisms of foam destruction by oil-based antifoams. *Langmuir* 2004, 20 (22), 9463-9505.
17. Koos, E.; Willenbacher, N., Capillary forces in suspension rheology. *Science* 2011, 331 (6019), 897-900.
18. Butt, H. J., Controlling the flow of suspensions. *Science* 2011, 331 (6019), 868-869.

CHAPTER 3

STABILIZATION MECHANISM OF CAPILLARY FOAMS

3.1 Introduction

We propose, based on the experimental observations in the previous chapter, that the synergistic adsorption of particles and oil around the gas bubbles bears strong resemblance to the phenomenon of “particle-assisted wetting” of a macroscopic air-water interface by a drop of oil that would be non-wetting in the absence of particles, which can be quantified by effective spreading coefficient of oil phase. To get stable capillary foams, a system should have positive spreading coefficient, forming oil-coated bubbles. In addition, just like oil droplets in a Pickering emulsion, the oil-coated bubbles in a capillary foam need to be stabilized by particles with a strong tendency to adsorb at the oil-water interface (the outer interface for capillary foams) where they can serve as a mechanical barrier to coalescence. The particle affinity to this interface can be characterized by the contact angle θ_{wop} ; it is maximal for angles close to 90° .

We will discuss the calculation of effective spreading coefficient and measurement of particle affinity to the outer interface for capillary foams. Upon completion of these calculations and measurements, we are able to theoretically estimate whether the formation of capillary foams should be expected at a given particle and oil combination, and will compare such theoretical predictions to the experimental results from chapter 2.

3.2 Materials and Methods

3.2.1 Materials

The gelling agent for the water phase used in the gel trapping method was gellan gum (Kelcogel, CPKelco). The hot gelling solution was purified by passing it twice through a C18–silica chromatographic column (Phenomenex) preactivated with an acetonitrile (Sigma-Aldrich)-water (80:20) mixture. Sulfuric acid and hydrogen peroxide were purchased from VWR international and EMD Millipore, respectively.

3.2.2 Contact angle measurements

The recently developed gel-trapping technique (GTT) has proven to be a powerful method for determining particle contact angles at a fluid-fluid interface and was used in this work.¹⁻³ The GTT involves spreading colloidal particles at a water-oil or water-air interface and subsequent gelling of the aqueous phase with a non-surface-active gelling agent.⁴ The top phase is removed and replaced with curable polydimethylsiloxane (PDMS), which is then cured and peeled off the gel. The PDMS replica of the interface with entrapped particles was imaged by Scanning Electron Microscope (SEM). The height of protrusion, h , and the equatorial radius, R , of particles at the interface were obtained from the SEM images (Figure 3.1). The particle contact angle is given by³

$$\theta = \arccos\left(\frac{h}{R} - 1\right) \quad (1)$$

The value of the particle contact angle was determined by averaging over a large number of particles.

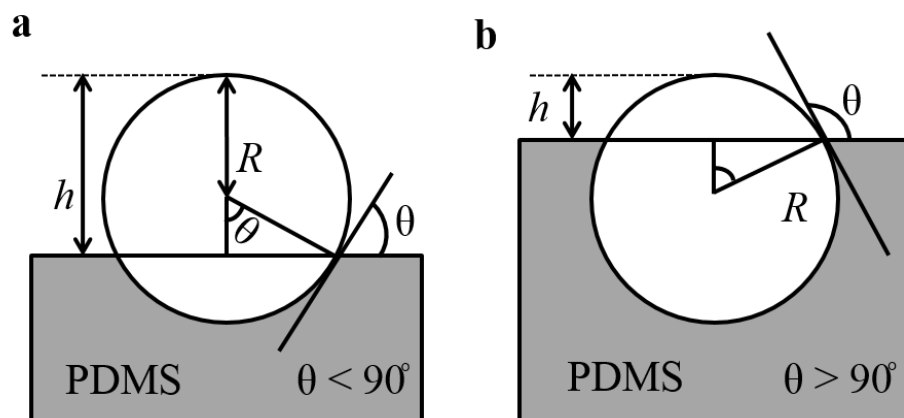


Figure 3.1 Schematic representation of a PDMS replica with trapped particle. (a) Contact angle smaller than 90° . (b) Contact angle larger than 90° .

The GTT protocol reported in the literature typically starts with the introduction of particles to interface using a spreading solvent such as isopropanol (IPA). Here, the particles were delivered to the interface using mechanical force instead of a spreading solvent, because spreading solvents have been demonstrated to affect the particle wetting properties, IPA for instance making particles appear more hydrophobic.⁴ Our sample preparation protocol for GTT proceeded as follows: in the case of air-water interface, 0.001 wt % particles were dispersed in water by sonication (VWR Model B2500A- MT ultrasonic cleaner) for 30 minutes and then delivered to the air-water interface by homogenization (IKA UltraTurrax T10, stator diameter of 8 mm and rotor diameter of 6.1 mm) in a Petri dish. Air bubbles were removed with a mild vacuum (100 mbar), and the sample temperature was raised to 50–55 °C. An aqueous 3 wt% solution of gel solution was added to the hot aqueous phase. The system was then cooled quickly to 25°C to set the gel and immobilize the particles at the interface. PDMS was spread on the top of the aqueous gel and cured to generate a PDMS replica with trapped particles. For the case of oil-water interface, the same procedure was used to prepare the aqueous

dispersion, deliver the particles to the interface, and remove air bubbles. Then the oil was carefully added at the air-water interface. The sample was moved to the oven at 50-55 °C. An aqueous 3 wt% solution of gel solution was added to the hot aqueous phase. The system was cooled quickly to 25 °C to set the gel. Then, the oil phase was carefully removed and immediately replaced with PDMS.

After curing the PDMS layer at room temperature for 48 h, it was peeled off the aqueous gel (along with the entrapped particles at the interface) and washed with pure hot water to remove any gel residues from the PDMS surface. The PDMS replica with trapped particles were prepared for imaging with SEM by coating with a gold nanolayer in a Hummer 5 Gold/Palladium Sputter and the contact angle was calculated from geometric parameters obtained by SEM.

The hydrophilic silica particles (SS03N) used in this study could not be trapped in the PDMS replica of the oil-water interface because of their low affinity for the interface. In this case the contact angle was estimated using macroscopic contact angle measurements with a Ramé-Hart goniometer on a glass slide pretreated with “piranha solution” (3:1 mixture of concentrated sulfuric acid and hydrogen peroxide) to mimic the surface wettability of bare silica particle. For the contact angle of oil/water interface, the glass substrate was submerged in a quartz cell filled with water and contact angle measurements were carried out on an inverted sessile oil drop. The contact angle for the air/water interface was estimated from observation of sessile water drops in air.

3.2.3 Preparation details for the mixed layer of secondary fluid and particles at a macroscopic air-water interface

0.01 wt% particles were dispersed in water by sonication for 30 minutes and then delivered to the air/water interface by homogenization with an IKA UltraTurrax T10 homogenizer in a Petri dish. Air bubbles were removed by exposure to a mild vacuum (100 mbar). Next, TMPTMA (with 5 wt% photoinitiator benzoinisobutylether) was added to the air-water interface slowly and carefully. A mixed wetting layer of oil and particles formed and was solidified by photo-polymerization (after 48 hours, using irradiation with UV light of 365 nm wavelength for 5 hours) and transferred to solid substrates such as gold electron microscope grids for subsequent imaging analysis.

3.2.4 The interfacial free energy of capillary foams and the effective oil spreading coefficient

Ordinary liquid foams are two phase systems in which a large volume of gas is dispersed as bubbles in a continuous liquid phase. We consider the case of air as the gas phase and water as the continuous liquid. Aqueous foams are thermodynamically unstable due to the large interfacial free energy cost associated with the bubble surfaces. If the continuous water phase contains suspended colloidal particles of appropriate wettability, these particles can adsorb strongly to the air-water interface and hinder the coalescence of foam bubbles kinetically; such particle-stabilized foams are often referred to as Pickering foams in analogy to the particle-stabilized Pickering emulsions.

In the capillary foams investigated in our study, the air-water interface is replaced (at least to a large extent, if not entirely) by a film of oil (the secondary liquid), where particles now adsorb to the oil film interface with the air bubble or with the continuous water phase. The adsorption state (oil-water interface or the air-oil interface) yielding the lower interfacial energy was considered the preferred (predicted) state of the bubble

surface in the capillary foams. Here we estimate the total interfacial energy change (inverse of effective spreading coefficient) for capillary foams from different particles and secondary fluid combinations. To this end the following simplifying assumptions and notations are adopted:

- (1) The internal energy, pressure, and temperature are assumed constant, and the small entropy changes due to particle adsorption are neglected.
- (2) Particles are considered spherical and effects of particle surface charge and size polydispersity are neglected.
- (3) Gravitational force and particle-particle interactions are neglected against surface and interfacial tension forces.
- (4) Particles are initially dispersed in the water phase.
- (5) Effects of bubble curvature are neglected.
- (6) The interfacial tensions of the oil/water, air/oil, air/water, air/particle, water/particle and oil/particle interfaces are denoted as γ_{ow} , γ_{oa} , γ_{aw} , γ_{ap} , γ_{wp} and γ_{op} . In systems containing both water and oil, mutual saturation of the two liquid phases is assumed.
- (7) θ_{wop} and θ_{aop} denote the particle contact angle at the water/oil and air/oil interfaces measured through the oil phase as is customary in the literature on particle-assisted wetting. θ_{awp} is the particle contact angle at the air/water interface measured through the water phase as customary in the literature on Pickering emulsions.

The interfacial energy per unit bubble area in a Pickering foam is the adsorption energy of particles attaching to the bubble surfaces,

$$\frac{G_{\text{Pickering}}^{\text{intf}}}{A} = \gamma_{aw} + \frac{n_p}{A} \Delta G_{\text{Pickering}}, \quad (2)$$

where n_p is the number of particles attached onto the air-water interface, and $\Delta G_{\text{pickering}}$ is the adsorption energy per particle, given by

$$\Delta G_{\text{Pickering}} = -\pi R^2 \gamma_{aw} (1 - \cos \theta_{awp})^2. \quad (3)$$

Combining Eqs. 2 and 3 and normalizing by the bubble surface area yields for the interfacial energy per unit bubble area of the Pickering foam

$$\frac{G_{\text{Pickering}}^{\text{intf}}}{A} = \gamma_{aw} \left[1 - \phi (1 - \cos \theta_{awp})^2 \right], \quad (4)$$

where $\phi = n_p \pi R^2 / A$ is the packing density (area fraction) of the particles adsorbed in the interface. Similar considerations can be applied to capillary foams. The interfacial energy change per unit bubble area in capillary foam is the sum of the free energy required for spreading an oil film at that interface with the assistance of adsorbed particles.

$$\frac{G_{\text{capillary}}^{\text{intf}}}{A} = \gamma_{aw} - S_{\text{eff}} = \gamma_{aw} - S_o + \frac{n_p}{A} \Delta G, \quad (5)$$

where S_{eff} is the effective spreading coefficient accounting for particles adsorption at one of the oil interfaces, $S_o = \gamma_{aw} - (\gamma_{oa} + \gamma_{ow})$ is the standard spreading coefficient of the oil, and ΔG is again a particle's energy change upon transfer from the water bulk to an interface.

Spreading of the oil around the air bubbles requires that particles adsorb at the oil-water interface (case i), or the oil-air interface (case ii), or at both interfaces; and the particle wettability dictates which, if any, of these scenarios are realized. For the case i of particles adsorbing at the oil-water interface, the particle adsorption energy ΔG_i , is given by

$$\Delta G_i = -\pi R^2 \gamma_{ow} (1 + \cos \theta_{wop})^2. \quad (6)$$

Therefore, the interfacial energy of the capillary foam with particles adsorbed at the oil-water interface is given by

$$\frac{G_{capillary, i}^{intf}}{A} = \gamma_{aw} - S_{eff, i} = \gamma_{aw} - S_o - \phi \gamma_{ow} (1 + \cos \theta_{wop})^2, \quad (7)$$

where ϕ again stands for the particle packing fraction, this time in the oil-water interface. For the case ii of particles adsorbed at the air-oil interface, the energy change upon bringing particles from the water bulk to the air-oil interface, ΔG_{ii} , is given by

$$-\frac{\Delta G_{ii}}{\pi R^2} = \gamma_{oa} \sin^2 \theta_{aop} + 2 \left[\cos \theta_{aop} (\gamma_{ap} - \gamma_{op}) + (\gamma_{wp} - \gamma_{ap}) + (\gamma_{wp} - \gamma_{op}) \right]. \quad (8)$$

The interfacial tensions involving the particle surface are not directly accessible experimentally, but can be eliminated using Young's equations

$$\gamma_{ap} - \gamma_{op} = \gamma_{oa} \cos \theta_{aop}, \quad (9)$$

$$\gamma_{wp} - \gamma_{ap} = -\gamma_{aw} \cos \theta_{awp}. \quad (10)$$

$$\gamma_{wp} - \gamma_{op} = \gamma_{ow} \cos \theta_{wop}. \quad (11)$$

Equation 8 then takes the form

$$-\frac{\Delta G_{ii}}{\pi R^2} = \gamma_{oa} (1 + \cos^2 \theta_{aop}) + 2(\gamma_{ow} \cos \theta_{wop} - \gamma_{aw} \cos \theta_{awp}). \quad (12)$$

Hence, the interfacial energy per unit bubble area for a capillary foam with particles adsorbed at the air-oil interface is

$$\frac{G_{\text{capillary,ii}}^{\text{intf}}}{A} = \gamma_{aw} - S_{\text{eff,ii}} = \gamma_{aw} - S_o - \phi \left[\gamma_{oa} (1 + \cos^2 \theta_{aop}) + 2(\gamma_{ow} \cos \theta_{wop} - \gamma_{aw} \cos \theta_{awp}) \right]. \quad (13)$$

The particle contact angles θ_{wop} and θ_{awp} were measured by GTT, and the contact angle

θ_{aop} was inferred from the measured contact angles ($\theta_{wop}, \theta_{awp}$) and the measured

interfacial tensions ($\gamma_{ow}, \gamma_{oa}, \gamma_{aw}$) via Young's relation:

$$\gamma_{oa} \cos \theta_{aop} = \gamma_{aw} \cos \theta_{awp} + \gamma_{ow} \cos \theta_{wop} \quad (14)$$

Equations (7) and (13) were used to calculate the interfacial free energy change per unit bubble surface area and effective spreading coefficient for scenarios i (particles

adsorb at the oil-water interface) and ii (particles adsorb at the air-oil interface), assuming for both cases an interfacial particle packing density (area fraction) ϕ of 70% based on a crude estimate from microscopic observations. A positive effective spreading coefficient ($S_{eff} > 0$) means that the spreading of secondary fluid around gas bubbles with the help of particles is thermodynamically favorable.

For some of the larger particles used in this study, SEM images suggest that particles may simultaneously penetrate both interfaces of the oil film around the droplets. A thermodynamic model for this scenario, which would have to take into account the film thickness and thus the fraction of oil not spread at the droplet surfaces, is beyond the scope of the present study.

3.3 Results and Discussion

We propose that the synergistic adsorption of particles and oil around the gas bubbles bears strong resemblance to the phenomenon of “particle-assisted wetting” of a macroscopic air-water interface by a drop of oil that would be non-wetting in the absence of particles.⁵⁻⁷ This requires that particles adsorb at the oil-water interface (Figure 3.2b i) or the oil-air interface (Figure 3.2b ii), or both, rather than at the air-water interface as in a classical Pickering foam. Which of these interfaces experiences particle adsorption depends on the particle wettability.

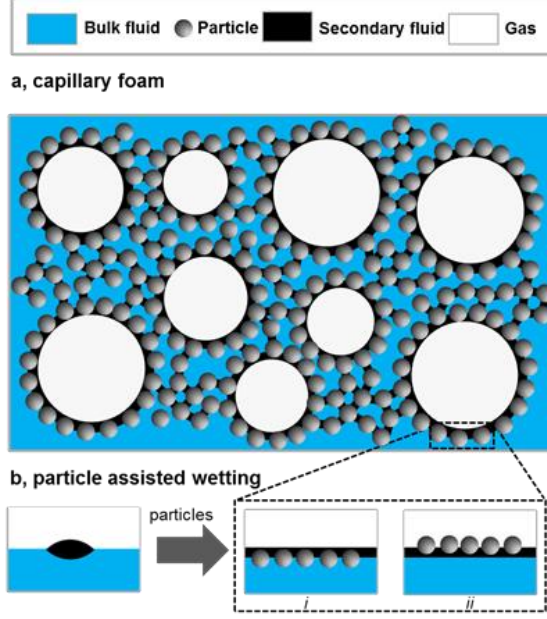


Figure 3.2 Schematic illustration of capillary foams. (a) In capillary foams, suspension particles and the secondary liquid jointly adsorb at the interface of gas bubbles. The decorated bubbles are further entrapped in a network of excess particles in the primary liquid bridged by a secondary liquid. (b) Particles adsorbing preferentially at an interface of the secondary liquid can mediate the spreading of a secondary liquid film around the gas bubbles, in direct analogy to the “particle-assisted wetting” of a macroscopic air-water interface by a drop of oil. Depending on their wetting properties, the particles can adsorb at oil-water interface (i) or the oil-air interface (ii) (or both).

The effect can be explained by the net reduction in interfacial free energy arising from the adsorption of particles at the newly formed oil-water or oil-air interface: spreading of the oil in the presence of particles becomes thermodynamically favourable for positive values of an “effective spreading coefficient” given by

$$S_{eff} = S_o - \frac{n_p}{A} \Delta G \quad (15)$$

Here $S_o = \gamma_{aw} - (\gamma_{ow} + \gamma_{ao})$ is the spreading coefficient of the oil as commonly defined and accounts for the energy change upon replacing the air-water interface by an oil-water and air-oil interface with respective tensions γ_{ow} and γ_{ao} ; A is the total surface area of the

bubbles, n_p is the number of particles adsorbed at the oil-water interface (Figure 3.2b, i) or the air-oil interface (Figure 3.2b, ii), and ΔG is the average free energy change associated with a particle adsorption event, given by









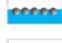





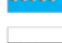








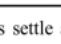
$$\Delta G_i = -\pi R^2 \gamma_{ow} (1 + \cos \theta_{wop})^2 \quad (16)$$

for adsorption at the oil-water interface and by

$$\Delta G_{ii} = -\pi R^2 \left[\gamma_{oa} (1 + \cos^2 \theta_{aop}) + 2(\gamma_{ow} \cos \theta_{wop} - \gamma_{aw} \cos \theta_{awp}) \right] \quad (17)$$

for adsorption at the air-oil interface, where R denotes the average particle radius, θ_{wop} , θ_{aop} are the equilibrium contact angles of the particle with the oil-water and air-oil interface as measured through the oil phase, and θ_{awp} is the contact angle at the air-water interface, measured through the water phase. This description neglects effects of bubble curvature and accounts for particle interaction only indirectly through the bubble coverage.

Table 3.1 Comparison between experimental observations and theoretical estimates for foams from a variety of particle and fluids combinations. θ_{awp} and θ_{owp} are particle contact angles at air-water interface and oil-water interface respectively. S_{eff} is the effective spreading coefficient. The cellulose and aluminum oxide particles are not included here because it is challenging to measure contact angles for these irregularly shaped particles.

Particles	Secondary fluid [oil]	θ_{awp} (°)	θ_{owp} (°)	Predicted state	S_{eff} (mN/m)	Experimental observation
Silica (SS03N)	None	22.32				Unstable
	TMPTMA	22.83	132.80		1.26	Unstable
	DINP	27.00	155.00		5.86	Unstable
	Paraffin	22.32	144.90		-9.02	Unstable
Glass	None	42.65				Unstable
	TMPTMA	32.63	124.21		2.45	Semi-stable*
	DINP	32.76	124.53		8.32	Semi-stable*
	Paraffin	42.65	128.78		-5.34	Semi-stable*
Modified Silica (Aerosil 200)	None	38.30				Unstable
	TMPTMA	31.88	98.84		9.43	Stable
	DINP	41.88	118.50		9.50	Stable
	Paraffin	38.30	109.52		5.15	Stable
PVC SA 1062/7	None	27.35				Unstable
	TMPTMA	21.84	94.84		11.05	Stable
	DINP	20.51	83.45		22.76	Stable
	Paraffin	27.35	105.32		8.53	Stable
PE	None	101.20				Stable
	TMPTMA	98.16	77.87		38.95	Stable
	DINP	120.05	102.64		86.12	Stable
	Paraffin	101.20	73.05		52.52	Stable
PVC P70F	None	98.76				Stable
	TMPTMA	91.94	106.91		18.69	Stable
	DINP	88.81	112.10		17.03	Stable
	Paraffin	98.76	75.42		45.60	Stable

* Only a small amount foam is formed, and most particles settle at the container bottom.

We obtained estimates for the effective oil spreading coefficient in our capillary foams from equations 15-17 with measured values for the surface and interfacial tensions γ_{ij} and for the particle contact angles θ_{ijp} , assuming an interfacial particle packing density (area fraction) $\phi = \pi R^2 n_p / A$ of 70% based on a crude estimate from microscopic observations. Results for the oil/particle combinations of our study are shown in Table 3.1 and Figure 3.3a, which also indicates the experimentally achieved foam stability. All studied systems that produced stable capillary foams upon frothing have a positive effective spreading coefficient and are thus expected to experience oil-spreading around the air bubbles. Conversely, however, the successful spreading of the oil, either by itself ($S_o > 0$) or with the help of particles ($S_{eff} > 0$), does not guarantee good foam stability (Figure 3.3a). Just like oil droplets in a Pickering emulsion, the oil-coated bubbles in a capillary foam need to be stabilized by particles with a strong tendency to adsorb at the oil-water interface (the outer interface for capillary foams) where they can serve as a mechanical barrier to coalescence. The particle affinity to this interface is characterized by the contact angle θ_{wop} ; it is maximal for angles close to 90° .⁸

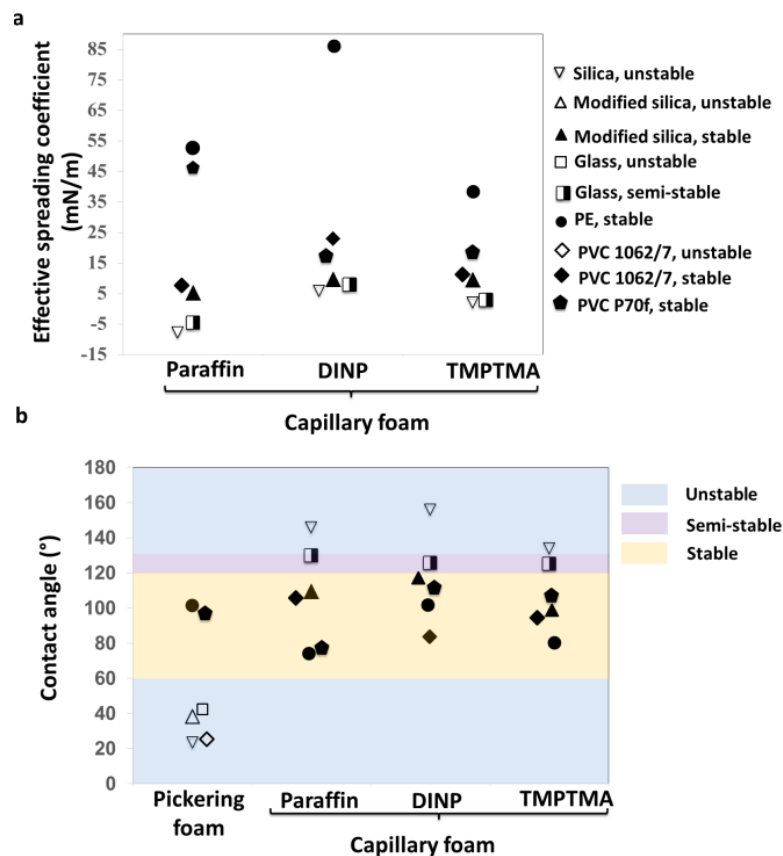


Figure 3.3 The effective oil spreading coefficient S_{eff} (a) and the equilibrium particle contact angle (b) at the air-water interface for Pickering foams and at the oil-water interface for capillary foams from a variety of particle/oil combinations. Full marks are used for systems that produce stable foam heads upon frothing, open markers denote patently unstable systems, and the half-open marker (“semi-stable”) is for systems developing only a very small, albeit durable, foam head and a large sediment of particles not participating in bubble stabilization. The standard spreading coefficient S_o of paraffin oil, DNP and TMPTMA are -10.17 mN/m, 5.74 mN/m and -0.11 mN/m respectively.

The data shown in Figure 3.3b illustrate the importance of the contact angle for foam stability. Systematically, particles with a weak affinity to the outer interface (contact angle below 60° or above 130°) led to unstable foams that disintegrated within one or two days, whereas particles with a strong affinity to the outer interface (contact angle in the range from 60° to 120°) yielded foams that remain intact for weeks or months. (Particles with intermediate contact angles from 120° to 130° stabilized only a

small amount of foam, and most particles were found to sediment instead of participating in foam stabilization.)

The hydrophilic PVC particles used in the foaming experiments of chapter 2 represent a case in point: their contact angle with an air-water interface mimicking the bubble surface in a classical Pickering foam is below 30° (Figure 3.4a), which points at a low affinity for the interface and explains their poor performance as a Pickering foam stabilizer. By contrast, the same particles form contact angles near 90° with oil-water interfaces (Figure 3.4b-d) mimicking the outer interface of oil-coated bubbles in the stable capillary foams of Figure 2.3 of chapter 2.

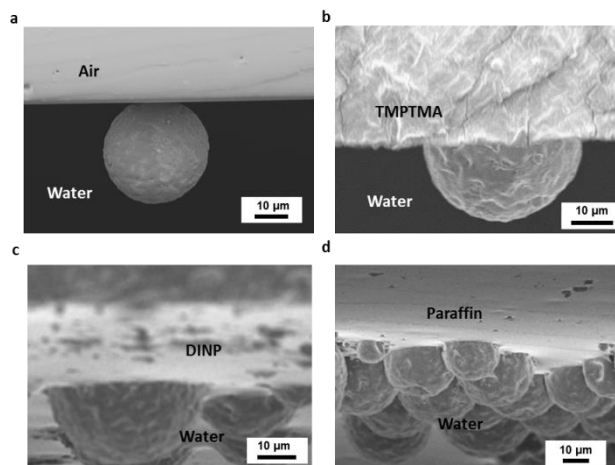


Figure 3.4 SEM image of PVC particles trapped in the PDMS replica of a macroscopic air-water interface (a) and of several oil-water interfaces (b-d) using the gel trapping technique. The visible part of particle originally resided in the water phase.

For PVC (Vinnolit SA 1062/7) particles in water with added TMPTMA and air bubbles, the model predicts a free energy change per unit area of $-S_{eff,i} = -11.05 \text{ mJ/m}^2$ for spreading of an oil film around them if the particles adsorb to the oil-water interface at an assumed area coverage of 70%; by contrast, if the particles instead adsorbed to the

oil-air interface, the predicted energy change would be $-S_{eff,ii} = +4.55 \text{ mJ/m}^2$. From this, one would expect the particles to adsorb preferentially at the oil-water interface. Experimentally, a layer of TMPTMA, spread at a macroscopic air-water interface with the help of the same PVC particles, was solidified by photo-polymerization. Figure 3.5a shows an SEM image of the solidified oil layer with the particles adsorbed in the oil-water interface with a three-phase contact angle near 90° , favoring strong particle adsorption. Hence the SEM images of Figure 3.5 are consistent with the spreading and stabilization of an oil film at the bubble surface by PVC particles (Vinnolit SA 1062/7) preferentially adsorbing at the oil-water interface.

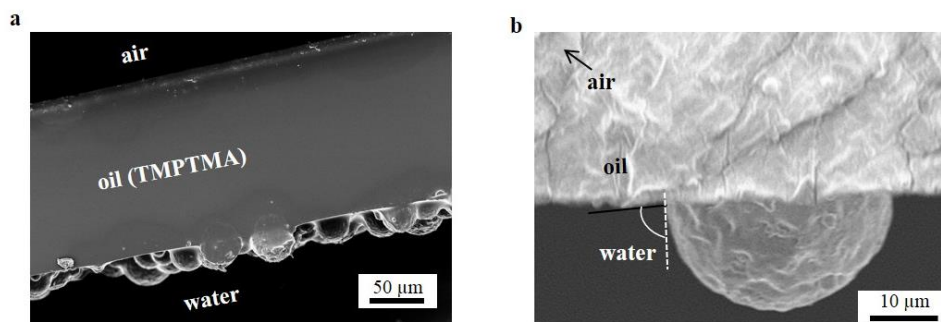


Figure 3.5 Experimental observation of the particle location at the interface. (a) SEM image of the mixed layers of TMPTMA and particles formed on an air-water interface. (b) SEM image of PVC particles trapped on the PDMS replica of oil-water interface using the gel trapping technique. The visible part of particle has been immersed in the water phase.

3.4 Conclusions

In summary, we have reported a new class of liquid foams materials in which gas bubbles are stabilized by the synergistic action of particles and a small amount of an immiscible secondary liquid. The particles can promote spreading of the minority liquid around the gas bubbles, and the newly formed liquid-liquid interface can be easier for liquid-dispersible particles to stabilize than the gas-liquid interface of a classical Pickering foams. To get stable capillary foams, the particles and oil should jointly adsorb on the bubble surface, forming oil-coated bubbles. In addition, the oil-coated bubbles in a capillary foam need to be stabilized by particles with a strong tendency to adsorb at the oil-water interface (the outer interface for capillary foams) where they can serve as a mechanical barrier to coalescence.

3.5 References

1. Paunov, V. N., Novel method for determining the three-phase contact angle of colloid particles adsorbed at air-water and oil-water interfaces. *Langmuir* 2003, 19 (19), 7970-7976.
2. Cayre, O. J.; Paunov, V. N., Contact angles of colloid silica and gold particles at air-water and oil-water interfaces determined with the gel trapping technique. *Langmuir* 2004, 20 (22), 9594-9599.
3. Arnaudov, L. N.; Cayre, O. J.; Stuart, M. A. C.; Stoyanov, S. D.; Paunov, V. N., Measuring the three-phase contact angle of nanoparticles at fluid interfaces. *Phys Chem Chem Phys* 2010, 12 (2), 328-331.
4. Maestro, A.; Bonales, L. J.; Ritacco, H.; Rubio, R. G.; Ortega, F., Effect of the spreading solvent on the three-phase contact angle of microparticles attached at fluid interfaces. *Phys Chem Chem Phys* 2010, 12 (42), 14115-14120.
5. Goedel, W. A., A simple theory of particle-assisted wetting. *Europhys Lett* 2003, 62 (4), 607-613.
6. Xu, H.; Goedel, W. A., From particle-assisted wetting to thin free-standing porous membranes. *Angew Chem Int Edit* 2003, 42 (38), 4694-4696.
7. Ding, A. L.; Goedel, W. A., Experimental investigation of particle-assisted wetting. *J Am Chem Soc* 2006, 128 (15), 4930-4931.
8. Binks, B. P.; Lumsdon, S. O., Influence of particle wettability on the type and stability of surfactant-free emulsions. *Langmuir* 2000, 16 (23), 8622-8631.

CHAPTER 4

CAPILLARY FOAMS: FORMATION STAGES AND EFFECTS OF PROCESS PARAMETERS

4.1 Introduction

Aqueous foams are found in everyday life; they also play important roles in many industrial applications, such as enhanced oil recovery, froth flotation, cosmetic, and food processing.¹⁻²¹ In previous chapters, a new class of liquid foams (“capillary foams”) was discovered.²² In capillary foams, the gas bubbles are stabilized against coalescence neither by surface active molecules (as in classical foams), nor by particles adsorbed at the gas-liquid interface. Capillary foams are obtained by frothing a suspension of colloidal particles in the presence of a small amount of an immiscible oil phase. The addition of a small amount of oil provides a convenient and timesaving alternative to surface modification and greatly broadens the range of suitable particles. The formation of stable capillary foams using particles and oil as stabilizing agents opens many applications including foods, oil recovery, high strength porous materials. In the prepared capillary foams, particle networks are formed in which particles are connected by oil bridges with strong capillary force. In addition, particles and a thin oil film jointly adsorb on bubble surfaces, contributing the stabilization of gas bubbles. However, we do not know the formation stages of capillary foams. In addition, what are influences of process parameters on the formation of capillary foams?

In this chapter, we explored in more detail the formation stages of capillary foams. In addition, we investigated the influence of particle concentration and wettability

on the formation of capillary foams. Finally, capillary foams were prepared at different oil fractions by using a chemically-diverse set of oils with different interfacial properties. A detailed understanding of the foam formation and the effects of material and process parameters will lay the foundation for the targeted development of capillary foams toward future applications.

4.2 Materials and Methods

4.2.1 Materials

Polyvinyl chloride particles (PVC, Vinnolit SA1062/7, average particle size 14.8 μm , particle density 1.41 g/cm^3) were obtained from Vinnolit, Germany. Wacker-Chemie AG (Germany) provided amorphous fumed silica particles with various degrees of hydrophobicity: 100% SiOH, 70% SiOH, 50% SiOH, and 32% SiOH. The methylsilyl modification was performed by the manufacturer through reaction with dichlorodimethylsilane.^{23,24} Since the partially hydrophobic silica particles (70%, 50%, and 32% SiOH) were not wetted well by DI water, aqueous dispersions were prepared by first dispersing the particles in acetone and then transferring the particles to the DI water using repeated centrifugation and replacement of supernatant. Direct measurement of particle contact angle, for example, by gel trapping method,²⁵ freeze-fracture shadow-casting cryo-scanning electron microscopy (FreSCa cryo-SEM),²⁶ or digital holography,²⁷ is a challenging issue for fumed silica particles with a few hundred nanometers and nonspherical shapes. The wettability of silica particles was characterized by measuring the contact angle of a water drop in air on a pressed tablet of silica particles. Particle hydrodynamic radius in water of silica particles was measured by dynamic light

scattering using a Malvern Zetasizer Nano ZS90. The hydrodynamic radius and wettability of silica particles are shown in Table 4.1. Trimethylolpropane trimethacrylate (TMPTMA), silicone oil, and paraffin oil were purchased from Sigma-Aldrich. Surface and interfacial tensions of oils used in this study are shown in Table 4.2. Ultrapure water with a resistivity of 18.2 M Ω •cm (Barnstead) was used.

Table 4.1 Hydrodynamic radius and wettability of silica particles coated with various extends of methylsilyl groups. Contact angle data of 100% SiOH particles were obtained from reference 28.

Particle	Coating	Particle hydrodynamic radius (nm) in water	Contact angle at air-water interface (°)
100%	Bare	251.73 \pm 18.86	20.42 \pm 5.21
70%	30% methylsilyl	212.57 \pm 2.06	42.11 \pm 3.70
50%	50% methylsilyl	208.83 \pm 3.84	85.67 \pm 5.89
32%	68% methylsilyl	239.17 \pm 21.70	114.06 \pm 9.41

Table 4.2 Surface and interfacial tensions of oils used in this study. Interfacial tension data of TMPTMA were obtained from reference 29. Here, γ is the equilibrium surface/interfacial tension, where a, o, w denotes the air, oil, and water phase. S is the spreading coefficient.

	γ_{aw}	γ_{ow}	γ_{ao}	S_o
Paraffin oil	72.00	49.22	32.95	-10.17
TMPTMA	51.74	18.99	32.86	-0.11
Silicone oil	72.00	43.15	19.00	9.85

4.2.2 Preparation and characterization of capillary foams

Suspensions of particles in water at desired particle fractions were prepared. A small amount of oil (the mass percentage of oil is with respect to bulk water, unless otherwise noted) was added to the resulting particle suspension and frothed by using a rotor–stator homogenizer (IKA UltraTurrax T10, stator diameter of 8 mm and rotor diameter of 6.1 mm) at 30 000 rpm or by using a commercial handheld mixer (Rival 5-Speed Hand Mixer) at the maximum speed. The wet foam was characterized by monitoring initial foam volume and stability, which was assessed by monitoring foam height over time at ambient temperature.

4.3 Results and Discussion

4.3.1 Formation stages of capillary foams

Previous chapters have demonstrated that capillary foams can be prepared by frothing a particle suspension in the presence of a small amount of oil.²² In capillary foams, two primary structures are known to distinguish capillary foams from surfactant-stabilized and Pickering foams. First, interconnected particle networks formed by capillary or pendular oil bridges between particles span the space between bubbles, reducing their mobility.³⁰⁻³² In addition, particles and a thin oil film jointly adsorb on bubble surfaces to contribute the stabilization of gas bubbles (Figure 4.1). However, we do not know the order in which these stages form in capillary foams. For example, do particle networks form first and followed by particles and oil adsorption on the bubble surfaces, or is the reverse true? Alternatively, do particle networks and oil-coated bubbles form simultaneously?

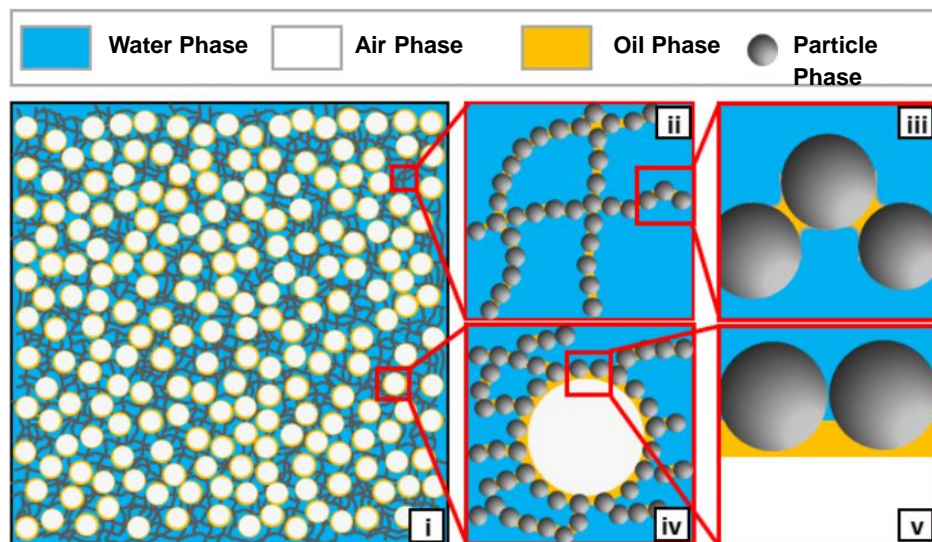


Figure 4.1 Structure of capillary foams. The system contains a continuous water phase, a gas phase, an oil phase, as well as particles. The agitation of the mixture results in a space-spanning network of particles in water (ii) connected by bridges of oil phase (iii), with air bubbles embedded in the network (iv) via a joint adsorption of particles and a thin oil film.

To address these questions, we studied the formation stages of capillary foams prepared with PVC 1062/7 particles in the presence of a small amount of oil. PVC particles were suspended in water at a particle concentration of 10 wt%. 1 wt% TMPTMA was then added as oil phase. Mechanical frothing of this particle suspension generated a large amount of foams after 4 minutes (Figure 4.2a). Interestingly, Figure 4.2a shows that liquid-bridged particle clusters and spanning particle networks were first formed after 40 seconds, i.e., the formation of a capillary suspension.^{31,32} Figure 4.2a demonstrates that during capillary foam formation, particle networks are formed first prior to the trapping of air bubbles. As a further test of the formation stages of capillary foams, we prepared foams with combinations of PVC particles and a diverse set of oils (Figures 4.2b and c). These images further demonstrate that particle networks are formed first and then air bubbles are entrapped in capillary foams (Figure 4.2d).

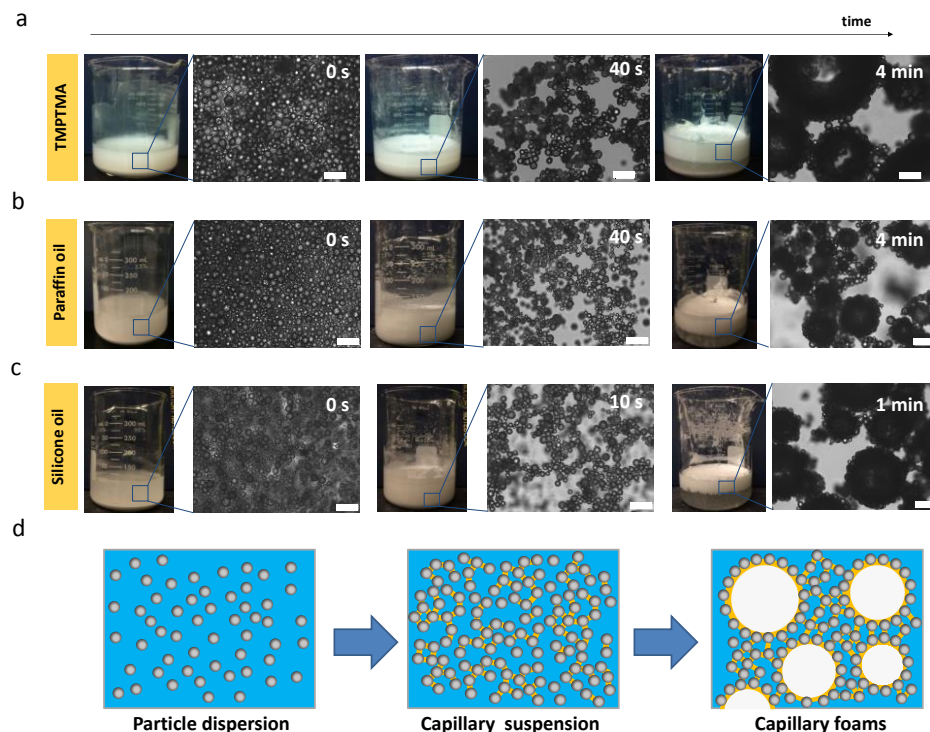


Figure 4.2 Formation stages of capillary foams. Photographs and corresponding microscope images of PVC particle suspension in the presence of 1 wt% (a) TMPTMA, (b) Paraffin oil, and (c) Silicone oil during several stages of frothing. Scar bars are 110 μm . (d) Schematic illustration of suspension morphologies during formation of capillary foams.

Mechanical frothing of a particle suspension (Figure 4.3a) in the presence of a small amount of oil generates air bubbles and oil droplets throughout the suspension (Figure 4.3b). The particles in the suspension could at this point adsorb directly at air-water interface, forming particle-coated bubbles (Figure 4.3c). However, the contact angle of PVC particles in the air-water interface is below 30° ,²² which points to a low affinity for the interface and makes the adsorption of particles in the interface unlikely. These structures are not observed. What is actually observed is that particles encounter oil droplets and form particle networks linked by capillary or pendular bridges of oil, due to the specific oil-particle-water wetting conditions (Figure 4.3d). An alternative

possibility is that oil droplets generated during agitation could encounter bubbles and spread on the air-water interface in the absence of particles if the spreading coefficient is positive (Figure 4.3e). The formation of oil-coated bubbles will be energetically favorable for oils with a positive spreading coefficient, which for the oils investigated is only true for silicone oil. Just like the adsorption of particles on an emulsion droplet, the formation of oil bridges between particles can also lower the interfacial energy. However, Figure 4.2 clearly shows the preferential formation of spanning particle networks for the combinations of PVC particles and oils with various interfacial properties. These experimental observation of particle networks instead of oil-coated bubbles initially suggests that competition between these two process is either kinetically controlled or that particle networks formation has a larger reduction in interfacial energy compared with the formation of oil-coated bubbles. Clearly, the air bubbles are entrapped to the whole suspension only after the formation of spanning particle networks (Figure 4.3f). We also point out that two additional possible configurations are that oil droplets could become coated with adsorbed particles (Pickering emulsions) or oil droplets coalesce with one another, neither of which were observed for the oils and particles chosen here in the presence of air bubbles.

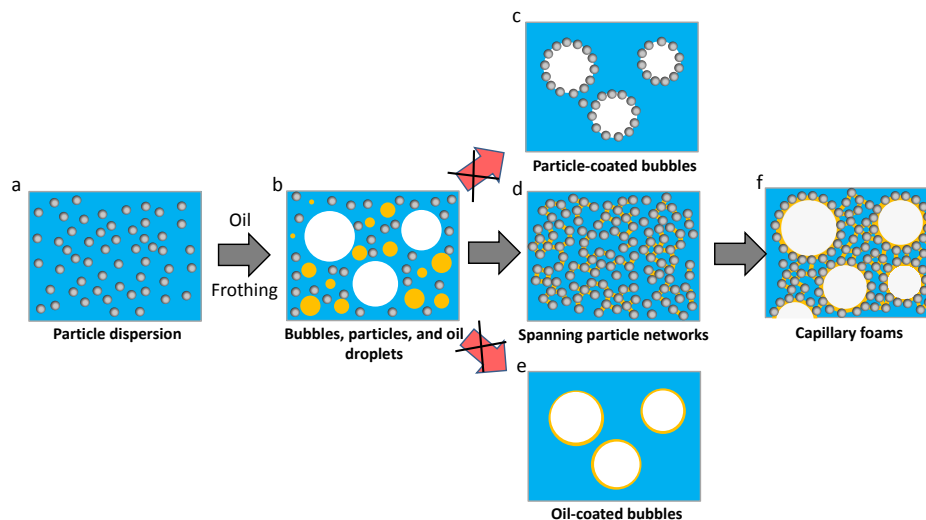


Figure 4.3 Possible formation stages of capillary foams. (a) Particle dispersion. (b) Mixture of generated air bubbles, oil droplets, and particles in water. (c) Particle-coated bubbles. (d) Spanning particle networks in a capillary suspension. (e) Oil-coated bubbles. (f) Capillary foams.

4.3.2 Effect of particle concentration

Particle concentration has been found to have a strong effect on the formation and stability of Pickering foams or emulsions against coalescence.^{33,34} We investigated the effect of particle concentration on the formation and stability of capillary foams and found a dramatic dependence of foamability on the concentration of added particles. The particle concentration of PVC particles was varied in the range from 5 to 40 wt%, as shown in Figure 4.4. In all prepared capillary foams, the oil phase was TMPTMA and its amount was kept constant at 1 wt%. As the fraction of particles increased from 5 to 20 wt%, the foam volume increased rapidly. However, upon a further increase of the particle concentration to 30 or 40 wt%, the suspension became gel-like and, thus, it was difficult to entrap and disperse gas bubbles. As the number of available particles in the bulk phase increases, more gas bubbles will be incorporated into a tenuous network of particles connected by oil bridges. The formation of gels at higher particle concentrations may be

caused by the formation of particle clusters and spanning particle networks held together by strong capillary forces. The gelled suspensions were too viscous to allow entrapment of bubbles. Photograph of capillary foams stabilized with different concentrations of PVC particles after 5 months are shown in Figure 4.4b. In general, these capillary foams are very stable. The long-term stability of capillary foams is contributed by the mechanical barriers of a film of oil and particles at the bubble surfaces and a network of space-spanning particles that connects bubbles.²²

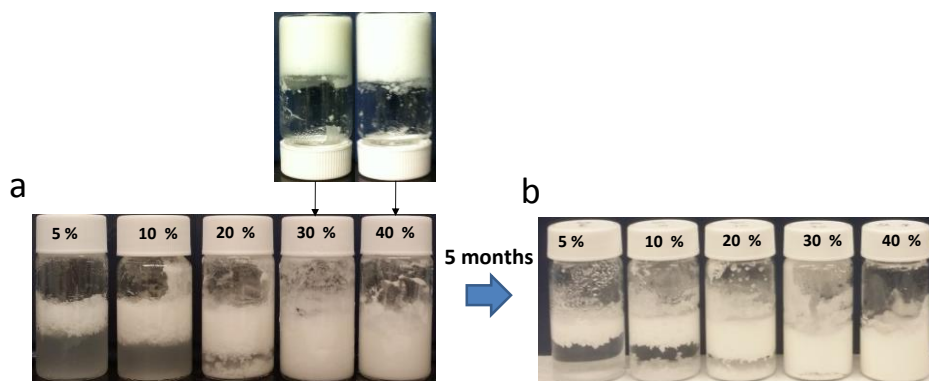


Figure 4.4 Photograph of capillary foams stabilized with different concentrations of PVC particles. The photograph was taken at (a) 0 minute and (b) 5 months after preparation.

4.3.3 Effect of particle wettability

Capillary foams made by particles and a small amount of oil are stable over several months. The wettability of particles is crucial for the preparation of stable capillary foams. To study the influence of particle wettability on the formation of capillary foams, a series of dimethyldichlorosilane-modified silica particles with systematically varied hydrophobicity, ranging from completely hydrophilic (100% SiOH) to hydrophobic (32% SiOH), were used. We also compared the foamability of foams

stabilized only by particles (Pickering foams) and foams stabilized by particles and a small amount of oil (capillary foams). In all capillary foams, the oil phase was TMPTMA and its amount was kept constant at 1 wt% and the particle concentration was 3 wt% (Figure 4.5). In all Pickering foams, the particle concentration was also kept constant at 3 wt%. For foams stabilized only by particles (Pickering foams), the relatively hydrophilic particles, 100% and 70% SiOH, cannot stabilize foam bubbles. With further increase of particle hydrophobicity to 50% and 32% SiOH, air bubbles are stabilized and the foam volume increases progressively with the increase of particle hydrophobicity. The maximum initial foam volume was achieved for particles with a surface hydrophobicity of 32% SiOH (Figure 4.5). With the increase of particle hydrophobicity from completely hydrophilic (100% SiOH) to relatively hydrophobic (32% SiOH), the affinity of particles to the air-water interface increases and, thus, more and more air bubbles are covered by particles.¹⁴

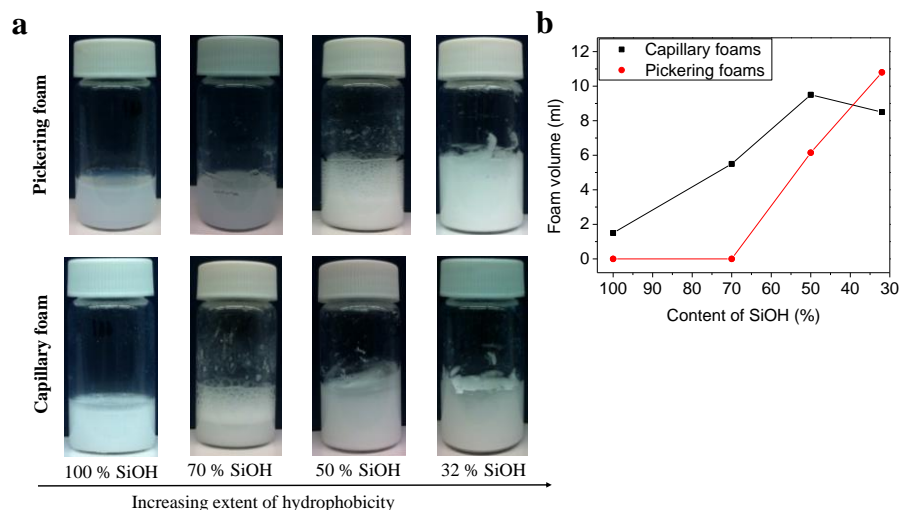


Figure 4.5 Effects of particle hydrophobicity on the formation of Pickering and capillary foams. (a) Photographs of foams prepared by using particles with various hydrophobicity. (b) Initial foam volume as a function of particle wettability.

The addition of a small amount of oil (1 wt %) helps the hydrophilic particles (100 and 70% SiOH) stabilize foams. For capillary foams, the initial volume of foams increases progressively with the increase of particle hydrophobicity from 100% to 50% SiOH (Figure 4.5). The volume of foams drops with a further increase of particle hydrophobicity to 32% SiOH (Figure 4.5). In capillary foams, oil spreads on bubble surfaces, and the original air-water interface is replaced with air-oil and oil-water interfaces.²² Since oil is more polar than air, hydrophilic silica particles have stronger affinity to the oil-water interface in capillary foams than that to the air-water interface in Pickering foams. For Pickering foams, the maximum initial foam volume was achieved by 32% SiOH silica particles which have a strong affinity to the air-water interface. It was not surprising that a reduction of initial foam volume was observed in the corresponding capillary foams.

4.3.4 Effects of oil types and fractions

Stable capillary foams can be prepared by using particles and a small amount of oil. This raises interesting questions: can capillary foams be prepared with oils of various interfacial properties? How much oil is needed in order to get stable capillary foams? What are effects of oil types on the formation of capillary foams? To answer these questions, we prepared capillary foams with oils of different interfacial properties by varying the concentration of oils. The interfacial properties of oil phase can be quantified by the spreading coefficient of oil phase on the air-water interface. Three types of oils, paraffin oil, TMPTMA, and silicone oil, were used in this study. The spreading coefficients of paraffin oil, TMPTMA, and silicone oil are -10.17 mN/m, -0.11 mN/m, and 9.85 mN/m, respectively. For PVC particle suspensions, we varied the amount of oil phase (silicone oil, TMPTMA or paraffin oil) from 0.025 wt% to 5 wt% (Figure 4.6). Figure 4.6 shows that capillary foams can be prepared with a diverse set of oils with different interfacial properties. As the fraction of oil increased, foam volume first increased and then reached a plateau. In the absence of oil, particles are settled at the bottom of the container.²² However, with the addition of oil, some particles and oil jointly adsorb on the bubble surface and form capillary foams while others still stay on the bottom of the container. All the particles and oils are accumulated on the top of the suspension and form capillary foams with a further addition of oils. The increase of foam volumes is caused by the incorporation of (oil- and particle-coated) gas bubbles into a tenuous network of particles stabilized by oil bridges. The drained water phase below the foam becomes clearer from left to right, suggesting that more and more particles are used to stabilize foams. Although capillary foams can be prepared with a diverse set of oils

with different interfacial properties, less oil is needed to make all particles accumulate at the foam area for oils with positive spreading coefficient (or close to positive). Photographs of foams after 5 months are shown in Figures 4.6b, d, f, indicating that capillary foams prepared by oils with positive spreading coefficient (or close to positive spreading coefficient) can maintain their stability for months. For foams stabilized by paraffin oil ($S_o = -10.17$ mN/m), some foams disappear and particle networks settle on the bottom of container. Figure 4.6 suggests that capillary foams can be prepared with a diverse set of oils. The spreading coefficient of oil has strong effects on both the amount of oil needed to obtain stable foams and the stability of the prepared foams.

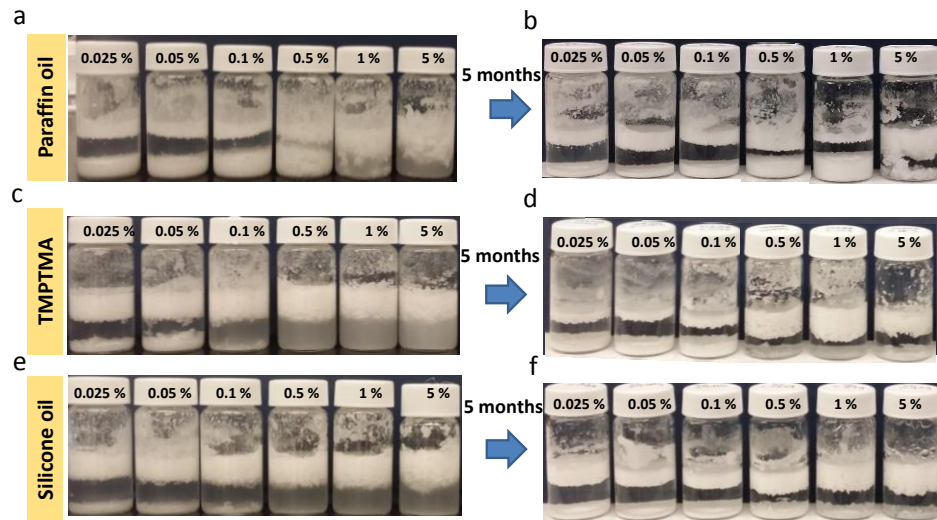


Figure 4.6 Effects of oil types and fractions on the formation and stability of capillary foams. Capillary foams prepared with 10 wt% PVC particles in the presence of 1 wt% (a) Paraffin oil, (c) TMPTMA, and (e) Silicone oil. (b, d, f) Appearances of foams after 5 months. The equilibrium spreading coefficients S_o of paraffin oil, TMPTMA, and silicone oil are -10.17 mN/m, -0.11 mN/m, and 9.85 mN/m, respectively.

4.4 Conclusions

In this chapter, we studied the formation stages of capillary foams and reported that particle networks are formed first and then air bubbles are entrapped. In addition, we have systematically investigated the influence of the particle concentration and wettability on the preparation of capillary foams. As the fraction of particle increased, foam volume first increased and then reached a plateau, where system becomes too viscous to entrap air bubbles. Finally, to illustrate the effects of oils, capillary foams were prepared with a diverse set of oils with different interfacial properties. Capillary foams can be prepared with a diverse set of oils. The spreading coefficient of oil has strong effects on both the amount of oil needed to obtain stable foams and the stability of foams. A detailed understanding of the foam formation and the effects of material and process parameters will lay the foundation for the targeted development of capillary foams toward future applications, which may range from the fabrication of load-bearing, lightweight porous materials, to enhanced oil recovery, advanced froth flotation, wastewater treatment, and oil spill remediation.

4.5 References

1. Hiemenz, P. C., Principles of colloid and surface chemistry. M. Dekker New York: 1986.
2. Evans, D. F.; Wennerström, H., The colloidal domain: where physics, chemistry, biology, and technology meet. Wiley-Vch: 1999.
3. Weaire, D. L.; Hutzler, S., The physics of foams. Oxford University Press: 2001.
4. Zhang, L.; Mikhailovskaya, A.; Yazhgur, P.; Muller, F.; Cousin, F.; Langevin, D.; Wang, N.; Salonen, A., Precipitating sodium dodecyl sulfate to create ultrastable and stimuable foams. *Angewandte Chemie* 2015, 127 (33), 9669-9672.
5. Hunter, T. N.; Pugh, R. J.; Franks, G. V.; Jameson, G. J., The role of particles in stabilising foams and emulsions. *Advances in Colloid and Interface Science* 2008, 137 (2), 57-81.
6. Blanco, E.; Lam, S.; Smoukov, S. K.; Velikov, K. P.; Khan, S. A.; Veleev, O. D., Stability and viscoelasticity of magneto-Pickering foams. *Langmuir* 2013, 29 (32), 10019-10027.
7. Poulichet, V.; Garbin, V., Cooling particle-coated bubbles: destabilization beyond dissolution arrest. *Langmuir* 2015, 31 (44), 12035-12042.
8. Gonzenbach, U. T.; Studart, A. R.; Tervoort, E.; Gauckler, L. J., Ultrastable particle-stabilized foams. *Angew Chem Int Edit* 2006, 45 (21), 3526-3530.
9. Binks, B. P.; Murakami, R., Phase inversion of particle-stabilized materials from foams to dry water. *Nat Mater* 2006, 5 (11), 865-869.
10. Dickinson, E.; Ettelaie, R.; Kostakis, T.; Murray, B. S., Factors controlling the formation and stability of air bubbles stabilized by partially hydrophobic silica nanoparticles. *Langmuir* 2004, 20 (20), 8517-8525.
11. Alargova, R. G.; Warhadpande, D. S.; Paunov, V. N.; Veleev, O. D., Foam superstabilization by polymer microrods. *Langmuir* 2004, 20 (24), 10371-10374.

12. Binks, B. P., Particles as surfactants - similarities and differences. *Curr Opin Colloid In* 2002, 7 (1-2), 21-41.
13. Bizmark, N.; Ioannidis, M. A.; Henneke, D. E., Irreversible adsorption-driven assembly of nanoparticles at fluid interfaces revealed by a dynamic surface tension probe. *Langmuir* 2014, 30 (3), 710-717.
14. Stocco, A.; Rio, E.; Binks, B. P.; Langevin, D., Aqueous foams stabilized solely by particles. *Soft Matter* 2011, 7 (4), 1260-1267.
15. Dickinson, E., Food emulsions and foams: Stabilization by particles. *Curr Opin Colloid In* 2010, 15 (1-2), 40-49.
16. Lam, S.; Velikov, K. P.; Velev, O. D., Pickering stabilization of foams and emulsions with particles of biological origin. *Curr Opin Colloid In* 2014, 19 (5), 490-500.
17. Studart, A. R.; Gonzenbach, U. T.; Akartuna, I.; Tervoort, E.; Gauckler, L. J., Materials from foams and emulsions stabilized by colloidal particles. *J Mater Chem* 2007, 17 (31), 3283-3289.
18. Fameau, A. L.; Lam, S.; Velev, O. D., Multi-stimuli responsive foams combining particles and self-assembling fatty acids. *Chem Sci* 2013, 4 (10), 3874-3881.
19. Binks, B. P.; Murakami, R.; Armes, S. P.; Fujii, S.; Schmid, A., pH-responsive aqueous foams stabilized by ionizable latex particles. *Langmuir* 2007, 23 (17), 8691-8694.
20. Lam, S.; Blanco, E.; Smoukov, S. K.; Velikov, K. P.; Velev, O. D., Magnetically responsive Pickering foams. *J Am Chem Soc* 2011, 133 (35), 13856-13859.
21. Gonzenbach, U. T.; Studart, A. R.; Tervoort, E.; Gauckler, L. J., Stabilization of foams with inorganic colloidal particles. *Langmuir* 2006, 22 (26), 10983-10988.
22. Zhang, Y.; Wu, J.; Wang, H. Z.; Meredith, J. C.; Behrens, S. H., Stabilization of liquid foams through the synergistic action of particles and an immiscible liquid. *Angew Chem Int Edit* 2014, 53 (49), 13385-13389.

23. Worthen, A. J.; Bagaria, H. G.; Chen, Y. S.; Bryant, S. L.; Huh, C.; Johnston, K. P., Nanoparticle-stabilized carbon dioxide-in-water foams with fine texture. *J Colloid Interf Sci* 2013, 391, 142-151.
24. Binks, B. P.; Lumsdon, S. O., Influence of particle wettability on the type and stability of surfactant-free emulsions. *Langmuir* 2000, 16 (23), 8622-8631.
25. Paunov, V. N., Novel method for determining the three-phase contact angle of colloid particles adsorbed at air-water and oil-water interfaces. *Langmuir* 2003, 19 (19), 7970-7976.
26. Isa, L.; Lucas, F.; Wepf, R.; Reimhult, E., Measuring single-nanoparticle wetting properties by freeze-fracture shadow-casting cryo-scanning electron microscopy. *Nat Commun* 2011, 2.
27. Kaz, D. M.; McGorty, R.; Mani, M.; Brenner, M. P.; Manoharan, V. N., Physical ageing of the contact line on colloidal particles at liquid interfaces. *Nat Mater* 2012, 11 (2), 138-142.
28. Kostakis, T.; Ettelaie, R.; Murray, B. S., Effect of high salt concentrations on the stabilization of bubbles by silica particles. *Langmuir* 2006, 22 (3), 1273-1280.
29. Ding, A. L.; Goedel, W. A., Experimental investigation of particle-assisted wetting. *J Am Chem Soc* 2006, 128 (15), 4930-4931.
30. Rabinovich, Y. I.; Esayanur, M. S.; Moudgil, B. M., Capillary forces between two spheres with a fixed volume liquid bridge: Theory and experiment. *Langmuir* 2005, 21 (24), 10992-10997.
31. Koos, E.; Willenbacher, N., Capillary forces in suspension rheology. *Science* 2011, 331 (6019), 897-900.
32. Koos, E.; Johannsmeier, J.; Schwebler, L.; Willenbacher, N., Tuning suspension rheology using capillary forces. *Soft Matter* 2012, 8 (24), 6620-6628.
33. De Folter, J. W.; van Ruijven, M. W.; Velikov, K. P., Oil-in-water Pickering emulsions stabilized by colloidal particles from the water-insoluble protein zein. *Soft Matter* 2012, 8 (25), 6807-6815.

34. Wong, J. C. H.; Tervoort, E.; Busato, S.; Gonzenbach, U. T.; Studart, A. R.; Ermanni, P.; Gauckler, L. J., Designing macroporous polymers from particle-stabilized foams. *J Mater Chem* 2010, 20 (27), 5628-5640.

CHAPTER 5

CAPILLARY FOAMS: STABILIZATION AND FUNCTIONALIZATION OF POROUS LIQUIDS AND SOLIDS

5.1 Introduction

Liquid suspensions of solid colloidal particles (Figure 5.1a) are ubiquitous in nature and are widely used in industry, including pharmaceutical formulations, foods, coatings, adhesives, and cosmetics.¹⁻³ Colloidal particles can adsorb strongly to liquid-gas or liquid-liquid interfaces of foams and emulsions and form a protective particle layer around gas bubbles or liquid droplets.⁴⁻⁸ The adsorption of particles with appropriate wettability tends to lower interfacial energy so significantly that the particle attachment is practically irreversible.⁴⁻¹⁰ Consequently, any coalescence of particle-covered bubbles or emulsion droplets results in an increase in interfacial particle concentration. Once a sufficiently high interfacial coverage is reached, further coalescence is effectively inhibited and the covered emulsion droplets or foam bubbles become highly stable.^{10,11} Particle-stabilized emulsions or foams, often called “Pickering emulsions” or “Pickering foams,” have been prepared by agitating particle suspensions with an added immiscible liquid or a gas. Depending on the wetting properties of particles, either oil-in-water or water-in-oil emulsions can be stabilized if the added fluid is a liquid (Figure 5.1b),¹² and either particle-decorated (“armored”) foam bubbles in liquid suspension or liquid drops (“liquid marbles”) in a continuous gas phase can be stabilized if the added fluid is a gas (Figures 5.1d,e).^{12,13} Even more complex multi-phase colloidal systems, such as combined dispersions of particles, oil, and air in an aqueous medium, have received less

attention in the scientific literature, but they are nonetheless relevant industrially, *e.g.* for oil recovery, food products like ice cream, cosmetics, or pharmaceuticals.¹⁴⁻¹⁶

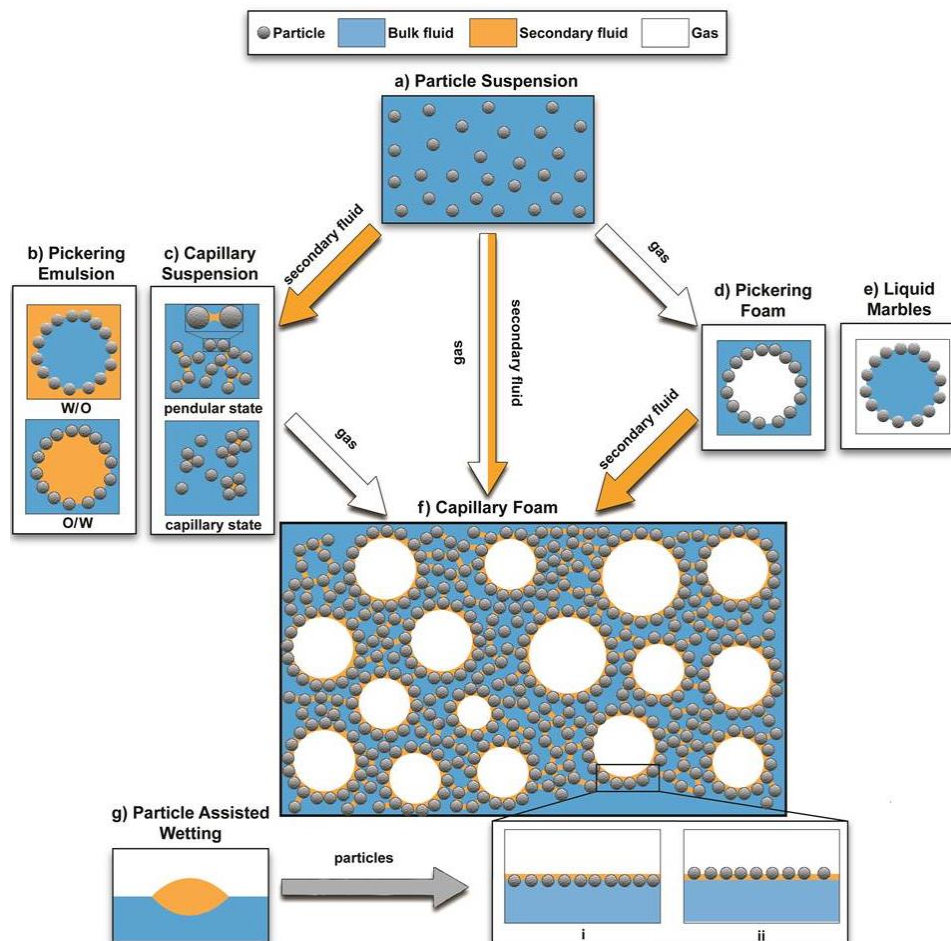


Figure 5.1 Multi-phase colloidal systems prepared from particle dispersions. (a) Particle suspensions are the starting point. (b) Suspension mixing with a large amount of secondary liquid can result in “Pickering emulsion” drops of oil-in-water or water-in-oil stabilized with hydrophilic or hydrophobic particles, respectively. (c) Mixing with a small amount of secondary liquid can result in the formation of a capillary suspension in which particles are connected by bridges of secondary liquid (either forming “pendular” menisci between particle pairs or the center of “capillary” agglomerates, depending on which liquid wets the particles preferentially). (d), (e) Suspension mixing with a gas phase can lead to “armored bubbles” (particle- stabilized bubbles that connect, at high concentration, forming a “Pickering foam”), to “liquid marbles” (particle stabilized droplets in air), depending on the particle wettability. (f) In capillary foams, suspension particles and the secondary liquid jointly adsorb at the interface of the gas bubbles with the primary liquid. The decorated bubbles are further entrapped in a network of excess particles in the primary liquid bridged by a secondary liquid. (g) Particles

adsorbing preferentially at the interface of the secondary liquid can mediate the spread of the secondary liquid film around the gas bubbles, which is directly analogous to the “particle-assisted wetting” of a macroscopic air-water interface by a drop of oil. Depending on their wetting properties, the particles can adsorb at the oil-water interface (i) or the oil-air interface (ii).

In 2011, it was reported that the addition of a small amount (0.05-10 wt%) of an immiscible secondary liquid to a particle suspension can transform the suspension from a viscous fluid into an elastic gel (“capillary suspension”), in which particles at a relatively low volume fraction form a system-spanning network (Figure 5.1c), held together by the capillary forces associated with small liquid bridges between the particles.¹⁷⁻¹⁹ In previous chapters, we have shown that a new type of foam material (“capillary foams”) can be formed from a particle dispersion by introducing both gas bubbles and a small amount of an immiscible secondary liquid (Figure 5.1f).²⁰ In these foams particles again are connected via bridges of the minority liquid, and the resulting network partly serves to entrap and immobilize gas bubbles. More importantly, the particles and the secondary liquid can jointly adsorb at bubble surfaces and stabilize the foam bubbles in a synergistic manner: While particles alone are known to stabilize foams if their wetting properties are appropriate, the addition of a secondary liquid can lead to stable foams even when the particles do not have the required wetting behavior to stabilize foam bubbles. In the case of aqueous foams with an oil as the secondary liquid, for instance, particles may readily adsorb at the air-oil or oil-water interface (but not at the air water interface), and thereby promote spreading of the oil around the gas bubbles,²⁰ in close analogy to the “particle-assisted wetting” of a planar water surface by an oil drop (Figure 5.1g).^{21,22} In order to get stable capillary foams, the oil should successfully spread around gas bubbles, forming

oil-coated bubbles. In addition, the particle should have a strong affinity to adsorb at the oil-water interface (the outer interface of capillary foams).²⁰

In this chapter, we show that capillary foams can be prepared alternatively by either introducing air and oil simultaneously to a particle suspension, by frothing a capillary suspension, or by mixing oil into a Pickering foam. To illustrate some of the application potential, we demonstrate the preparation of intensely colored foams that are notoriously difficult to achieve with traditional methods, and the preparation of load-bearing porous solids.

5.2 Materials and Methods

5.2.1 Materials

Polyvinyl chloride particles (Vinnolit SA1062/7, average particle size 14.9 μm , particle density 1.41g/cm³) were obtained from Vinnolit, Germany. The polyethylene (PE) particles were purchased from Polysciences, Inc., USA. Trimethylolpropane trimethacrylate (TMPTMA) and sodium dodecyl sulfate (SDS) were purchased from Sigma-Aldrich, and benzoin isobutyl ether was purchased from TCI America. Nile red, allura red, oil Blue N, and FD&C blue No.1 dye were purchased from Sigma-Aldrich. Ultra-pure water with a resistivity of 18.2 M Ω ·cm (Barnstead) was used as the bulk phase of the foams in this study.

5.2.2 Preparation and characterization of load-bearing, lightweight porous materials

The main processing steps can be summarized as the dispersion of particles, the introduction of secondary fluid and gas bubbles, and the solidification and drying of foams (as shown in Figure 5.2).

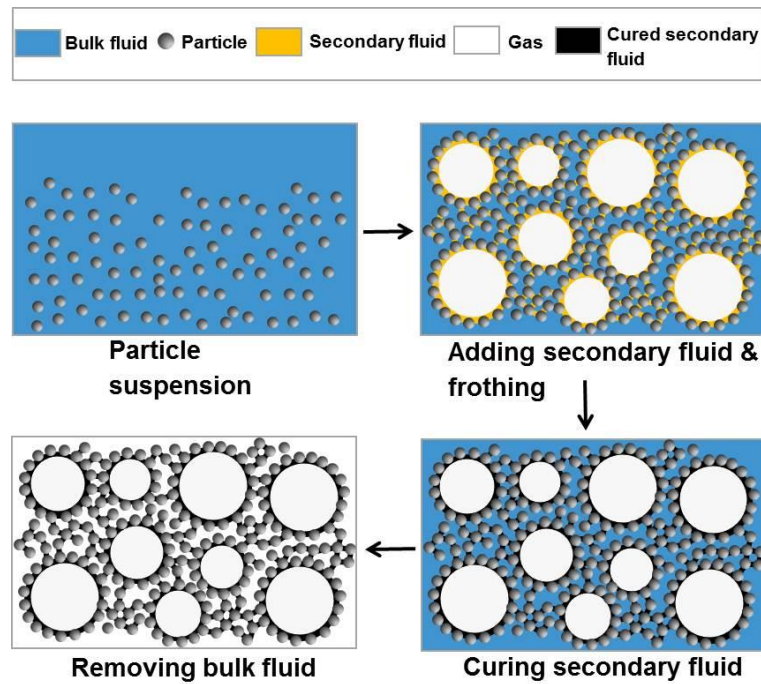


Figure 5.2 Processing steps for the preparation of load-bearing, lightweight porous solids.

- (1) A suspension of particles in water as the primary liquid was obtained by dispersing the initially dried particles with the help of sonication.
- (2) A small amount (0.14-6 wt%) of immiscible secondary fluid (the mass percentage of secondary fluid is with respect to water bulk in this study, unless otherwise noted) was added to the resulting particle suspension and frothed using a rotor-

stator homogenizer (IKA UltraTurrax T10, stator diameter of 8 mm and rotor diameter of 6.1 mm) at 30,000 rpm or a hand mixer (Rival 5-Speed Hand Mixer) at the maximum speed. The TMPTMA was treated with Al_2O_3 to remove inhibitor, and enriched with 6 wt % of the photoinitiator benzoin isobutyl ether.

- (3) The wet foam containing TMPTMA was cured by exposure to UV light (SpectroLine Longlife Filter, wavelength 365 nm) and then dried in an atmospheric oven (Fisher Scientific Co.) at 70 °C.

The porosity ε of dried foam was calculated by using $\varepsilon = (1 - \rho_b / \rho_p)$, where ρ_b is the bulk density of the foams and ρ_p is the particle density. The bulk density ρ_b of foam was calculated by measuring sample mass and volume.

5.2.3 Preparation and characterization of colored foams

Colored foams stabilized by SDS surfactant were formed by hand-shaking the water dispersion of surfactant and dye 20 times. Colored particle-stabilized foams (Pickering foam) were prepared by frothing a suspension of particles and dissolved dye using a rotor-stator homogenizer (IKA UltraTurrax T10, stator diameter of 8 mm and rotor diameter of 6.1 mm, 30,000 rpm). For the preparation of colored capillary foams, a suspension of particles in water was obtained by dispersing the particles via sonication and then the dye solution, consisting of dye dissolved in the oil phase, was added. The resulting suspension was frothed using a rotor-stator homogenizer (IKA UltraTurrax T10, with a stator diameter of 8 mm, and a rotor diameter of 6.1 mm) at 30,000 rpm. The wet foam was characterized using a Zeiss LSM 510 VIS confocal microscope (excitation at 543 nm and emission above 560 nm).

5.2.4 Spectral acquisition of foam area using hyperspectral technology

The foams were collected from each sample using a small clean metal spatula and placed on a microscope slide, covering about a $0.5 \times 0.5 \text{ mm}^2$ area (with no cover slip). Using a PARISS® hyperspectral imaging system (LightForm, Inc., Asheville, NC, USA), the color (in specular reflectance mode) of each foam was acquired under a Nikon 80i microscope outfitted with a monochrome Retiga 2000DC, CCD camera (QImaging, BC, Canada). Wavelength calibration was performed with a MIDL Hg^+/Ar^+ emission lamp (LightForm, Inc, NC, USA) and accuracy was recorded and verified to be better than 2 nm using a $50 \text{ }\mu\text{m}$ slit. To avoid heterogeneity of data due to complex surface geometry, lack of plane focus, and sometimes movement of the foam, only one snapshot of spectral acquisition was done (taking less than 30 ms), covering a $5 \times 0.005 \text{ mm}^2$ line across the foam surface, with a 10x objective. All spectra (ranging from 400 nm to 900 nm) from one individual sample (line) showing > 99 % closeness of fit were identified by one or two single representative spectra. Percent reflectance was calculated by dividing the sample spectra by a silver mirror reference standard with optimal reflectance in the range of visible wavelengths (Thorlabs, Newton NJ, USA).

5.2.5 Optical density acquisition of bulk liquid of foam

Bulk liquid aliquots (200 μL) from each sample were placed in wells of a UV transparent 96-well plate (Corning Costar). Each well was scanned for optical density (% transmittance) using a Spectramax I3 (Molecular Devices, Sunnyvale, CA), with a 1 nm incremental step from 230-930 nm.

5.3 Results and Discussion

5.3.1 Water-based capillary foams can be prepared by introducing air and oil simultaneously or by either frothing a capillary suspension or mixing oil into a Pickering foam

Starting with 10 wt% PE particle suspension (Figure 5.3a), mechanical frothing produced PE particles stabilized foam (Figure 5.3b). Figure 5.3c shows an image of a particle suspension prepared with 2 wt% trimethylpropane trimethacrylate (TMPTMA) and followed by stirring (60 rpm, 30 minutes). Figure 5.3g is a SEM image of the corresponding dried suspension from Figure 5.3c. Figure 5.3g shows that particles are connected by bridges of TMTPMA, confirming that capillary suspensions are formed in the bulk liquid of the suspension in Figure 5.3c. To study the possible routes of preparing capillary foams, we prepared foams by: (1) introducing air bubbles and TMPTMA simultaneously to the PE particles suspension in which 2 wt% TMPTMA was initially added to the container of suspension and then introduced to the whole suspension simultaneously with air bubble by mechanical frothing (Figure 5.3e); (2) mechanically frothing a capillary suspension (Figure 5.3f); (3) introducing TMPTMA to a PE particles stabilized foam in which 2 wt% TMPTMA was added and frothed again (Figure 5.3d). Figures 5.3h, i, j show SEM images of the stabilized bubble of the corresponding dried foams in Figures 5.3d, e, f, respectively. For the dried capillary suspension and foams, the secondary fluid was first solidified by photopolymerization, and then the water was removed by drying. The polymerization of TMPTMA results in a gel at a conversion degree of only 3 to 4%, effectively preserving the structure existing in the suspension. Since the small conversion at gelation is not expected to change the surface and

interfacial properties of the TMPTMA significantly, the oil-phase networks of the capillary suspension and foam are not expected to change substantially during further polymerization of TMPTMA.²³ The images in Figures 5.3h, i, j indicate that solidified TMPTMA spreads around gas bubbles and connects the particles in the bulk water phase, and is taken to reflect the structure in the liquid state prior to TMPTMA polymerization. Figures 5.3h, i, j suggest that both particles and a thin oil film adsorb on the bubble surface and therefore capillary foams were formed in Figures 5.3d, e, f. We can conclude that capillary foams can be prepared through multiple routes.

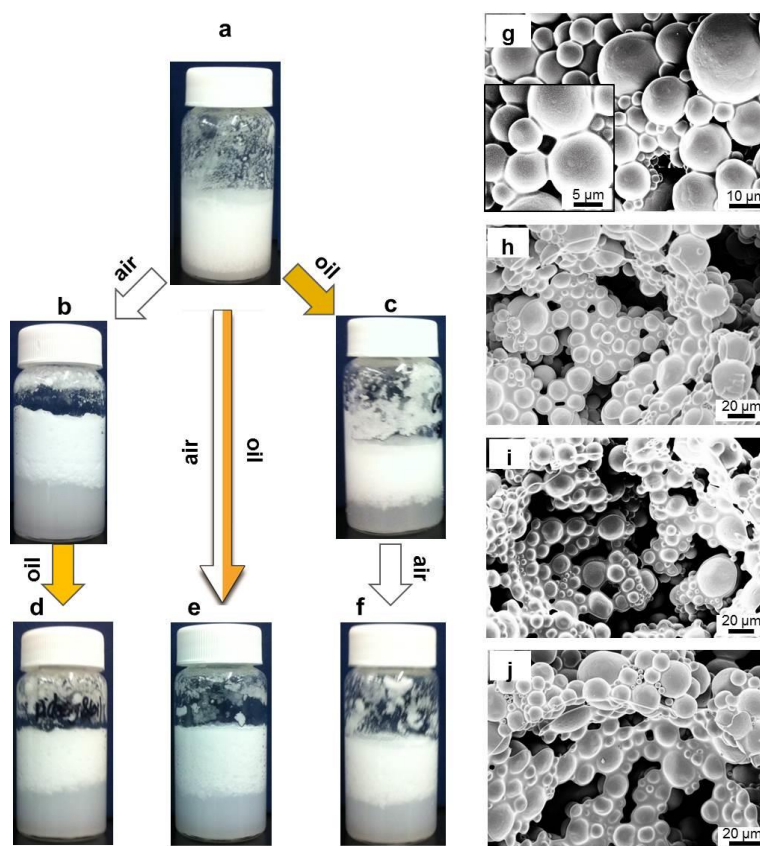


Figure 5.3 Capillary foams were prepared through multiple routes. (a) 10 wt% PE particles suspensions. (b) Mechanical frothing of suspension produced a Pickering foam. (c) Suspension mixing with 2 wt% oil (TMPTMA) resulted in the formation of a capillary suspension. Capillary foams were prepared by (d) mixing 2 wt% oil

(TMPTMA) to a Pickering foam (e) introducing 2 wt% oil (TMPTMA) and air bubbles simultaneously to a particles suspension (f) introducing air bubble to a capillary suspension. TMPTMA was treated with Al_2O_3 to remove inhibitor, and enriched with 5 wt % of the photoinitiator benzoin isobutyl ether. (g) SEM image of dried capillary suspension in (c). The particles were bridged by the minority oil phase. (h-j) SEM images of corresponding dried foam in (d), (e), and (f), respectively. Both particles and a thin oil film adsorbed on the bubble surface. For dried capillary suspension and foam, the secondary liquid was first solidified by photopolymerization, and then the water was removed by drying.

Figure 5.1 illustrates the connection between capillary foams and other colloidal multiphase systems, such as capillary suspensions or Pickering foams, and that the latter can be intermediates in the preparation of capillary foams. It would nonetheless be wrong to think of capillary foams simply as a Pickering foam with some added oil or as a capillary dispersion with some added gas bubbles: some particles suitable for capillary foams simply do stabilize an intermediate Pickering foam, and the ones that do, require a major rearrangement, as oil adsorbs at the previously particle-stabilized air-water interface. Similarly, the bubbles added to a capillary dispersion do not simply become entrapped in the existing particle network but also get “coated” via joint adsorption of oil and particles, and as shown previously the formation of a capillary networks is not sufficient to stabilize capillary foams.²⁰

5.3.2 Load-bearing, lightweight moldable porous solid foams

Mold casting, which is widely used in fabrication processes, is inexpensive and easy to control. To show that capillary foams are in principle amenable to this technique, we prepared wet capillary foams as described before and transferred them into different simple molds by hand, cured them under UV light, and then dried them in an oven at 70 °C overnight (Figures 5.4a,b). Figure 5.4 demonstrates that capillary foams can be

molded into various shapes, and the moldability supports the application of these foams as materials for various applications.

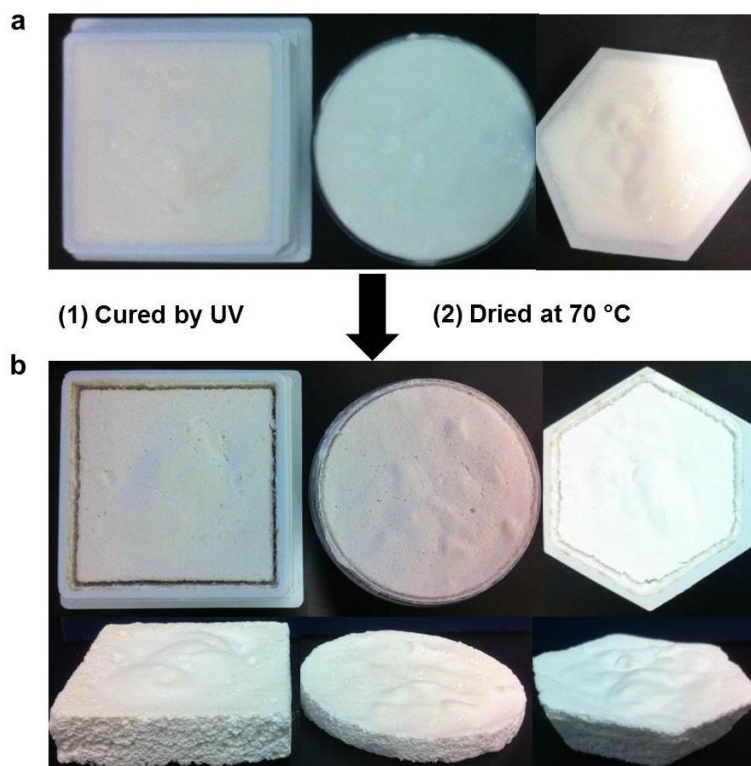


Figure 5.4 Mold casting of capillary foams. (a) The prepared capillary foams with 25.2 vol% PVC 1062/7 particle concentration and 2.92 wt% TMPTMA were molded into containers of various shapes by hand. (b) Capillary foams were cured under UV light and then dried in the oven.

In capillary foams, particles and an oil film jointly adsorb on the bubble surface and the resulting mixed particle/oil coated bubbles are entrapped in a network of excess particles connected by bridges of oil.²⁰ Dried capillary foam consists of pores originating from the original gas bubbles and the interparticle spaces in the initially liquid part of the foam. Because the walls of such dry foams consist of a porous (particle) network, these foams can achieve high overall porosity and low mass density. Moreover, the secondary

liquid originally connecting the particles reinforces the particle network, enhancing its mechanical strength. For example, it is possible to solidify the secondary liquid prior to the removal of the primary liquid, thereby avoiding the need to apply high temperature thermal sintering that is often used to enhance the mechanical properties of porous solids prepared from particles.^{24,25} Dried capillary foams such as shown in Figure 5.5a show promise as lightweight, load-bearing, functional materials. In this case the secondary liquid TMPTMA was solidified by UV-initiated polymerization prior to removal of the bulk water.^{21,22} We expect that the optimization of foam mechanical properties can be attained through the adjustment of preparation and drying conditions as well as through alternative methods of solidifying the secondary fluid. Similarly, it is conceivable that properties can be tuned for use in thermal and acoustic insulation, packaging, transportation, shock absorption, and tissue scaffolding. Although the adaptation of capillary foams for a particular use is beyond the scope of this study, we anticipate that this new type of foam material will be a robust subject for future application-oriented research.

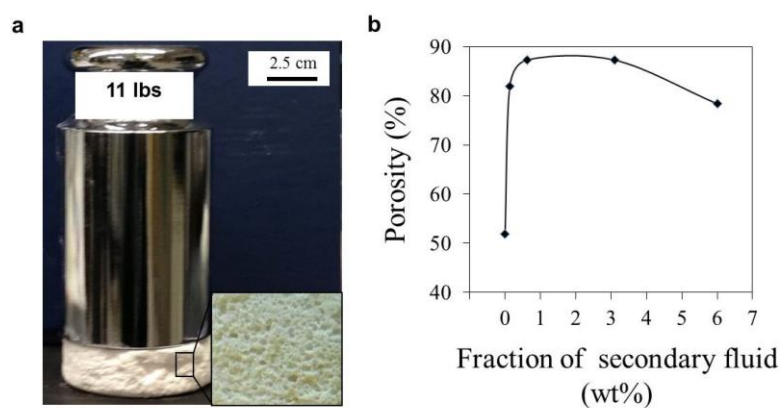


Figure 5.5 Functional load-bearing, lightweight porous materials from capillary foams. (a) Photograph of 11 lbs weight on a cured and dried foam with a density of

0.24 g/cm³ and porosity of 82.97 %. The foams were prepared from PVC (Vinnolit SA 1062/7) particles with a solid content of 21 vol % and 1.5 wt% TMPTMA by a hand mixer (Rival 5-Speed Hand Mixer) running at the maximum speed. (b) Variation in porosity with the amount of secondary fluid phase for prepared porous solids from capillary foam.

We investigated the effect of the amount of secondary fluid on the porosity of dried capillary foams and found a dramatic dependence of porosity on the concentration of added secondary liquid. Figure 5.5b shows the porosity of materials with initial PVC 1062/7 particle loading of 10 vol% and various amounts of TMPTMA. As the fraction of secondary fluid increased, porosity first increased rapidly and then reached a plateau of 87.3 % (The corresponding mass density of foams initially decreased from 0.68 g/cm³ and then reached a plateau of 0.18 g/cm³). However, porosity began to decrease to 78.37 % (mass density: 0.30 g/cm³) at 3.09 wt% oil concentration. The increase of porosity at low oil concentration is caused by the incorporation of gas bubbles stabilized by the synergistic action of particles and oils. The decrease of porosity at high oil concentration may be attributed to the reduction of the volume of particle networks caused by the formation of more attractive capillary bridges in the suspension. In all cases, the porosity is higher than both that of the corresponding Pickering foam without secondary fluid and that of capillary suspensions without introduction of gas bubbles.^{26,27}

5.3.3 Intensely colored capillary foam

Aqueous foams are inherently unstable. Their instability arises from the large gas-water interfacial energy which the foam systems tend to reduce by decreasing the total interfacial area via bubble coalescence and Ostwald ripening. Surfactant, such as SDS, is typically added to reduce interfacial energy by its adsorption at the air-water interface.

Figure 5.6a shows the results of foaming a colored aqueous liquid with 0.05 wt% SDS, indicating an intense color in the bottom solution but weak coloration of the foam phase. The color intensity of the bulk liquid phase was determined by transmitted light spectrometry. Measuring the color intensity of foam phase by using transmitted light spectrometry is difficult due to the diffusion and scattering of incident light in foams.²⁸ The color intensities of foams were measured by using hyperspectral imaging in reflectance mode. Quantitative analysis of the color intensity of dyes in the bulk liquid and foam phased is shown in Figures 5.6b, c, which demonstrates the strong absorbance in bulk liquid and weak reflectance for the foams at wavelengths of 500 nm and 630 nm. It appears that the majority of dye is concentrated in the bulk solution rather than in the thin films between the bubbles, as is observed qualitatively in the images. This appearance is typical of surfactant-stabilized foams made from colored liquids.²⁸

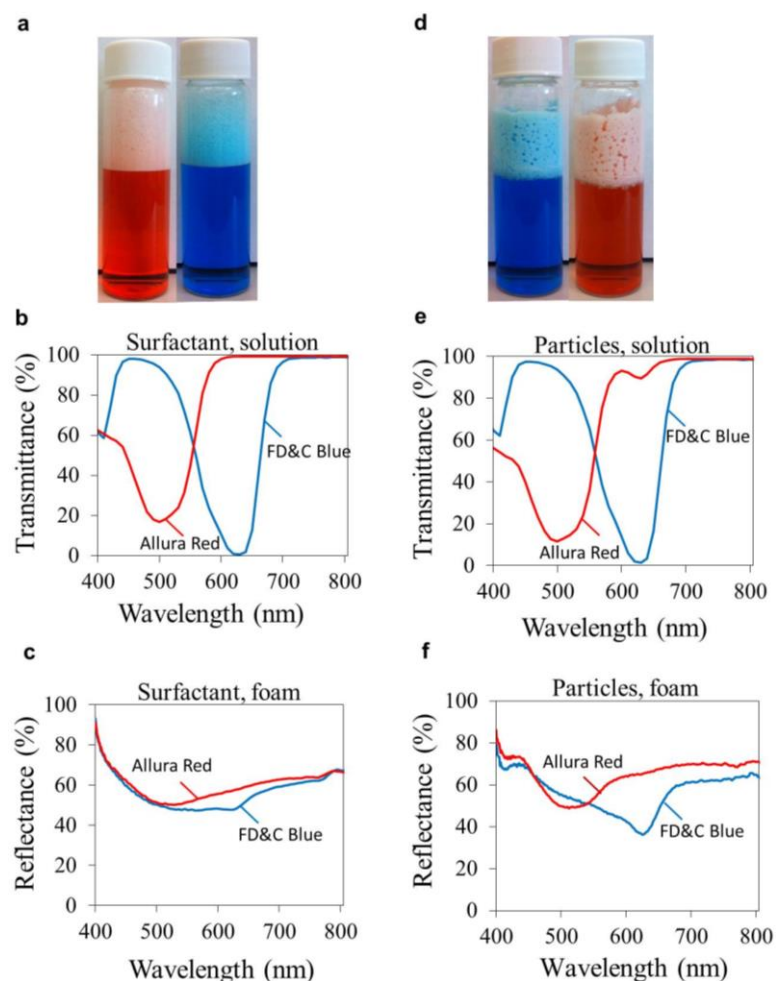


Figure 5.6 Photographs and spectra of colored foams formed by traditional foaming methods. (a) Photographs of foams stabilized by 0.05 wt% SDS surfactant and colored by 0.003 wt % allura red (left) or FD&C blue NO.1 (right) dye. (b) Transmittance spectra of bulk liquid suspension of the foam in (a). (c) Reflectance spectra of foam area of the foam in (a). (d) Photographs of foams stabilized by 7.41 wt% PE particles and colored by 0.0028 wt % allura red (right) or FD&C blue NO. 1 (left). (e) Transmittance spectra of bulk suspension of the corresponding foams stabilized by PE particles in (d). (f) Reflectance spectra of foam area of the corresponding foams stabilized by PE particles in (d).

Foam bubbles can alternatively be stabilized by colloidal particles, and the resulting foams are often called “Pickering foams”. Colored Pickering foams stabilized by PE particles are shown in Figure 5.6d. Like the colored foams stabilized by surfactant, Figure 5.6d shows intense coloration in the bulk liquid phase and weak coloration of the

foam areas. Figures 5.6e, f quantify this with strong absorbance for the bulk liquid phase but weak reflectance for foams at wavelengths of 500 nm and 630 nm. The majority of colorants are concentrated in the bulk solution. The color intensity of the very thin films between the bubbles is insufficient to impart intense color to the foam. Sejong Kim and coworkers²⁸ reported a method of imparting intense color to foams stabilized with cellulose particles in which the dye was embedded in the particles during the synthesis process. However, it is not straightforward to dye many of the particles used to stabilize foams in industry, for example silica and alumina particles.

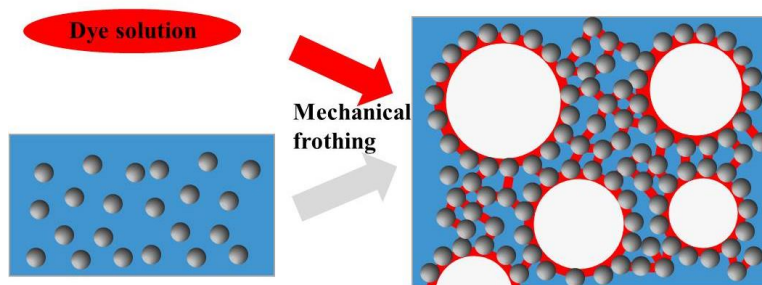


Figure 5.7 Schematic of the formation of colored capillary foam. The dye is dissolved in the secondary fluid. During the foaming process, dyes adsorb onto the bubble surfaces, and they are bridged by particles in the region between bubbles.

The utilization of both particles and an oil phase in the capillary foams described above suggests an alternative method for incorporating a dye into the thin liquid films surrounding foam bubbles. To demonstrate this principle, described schematically in Figure 5.7, particles were dispersed in the water and the dye was dissolved in the oil phase, the oil-based dye solution was added to the aqueous dispersion and the mixture was frothed. Based on our previous study, we expect that the particles facilitate spreading of oil-dye solution around the air bubbles.²⁰ In the region between the gas bubbles, the

particles are expected to be bridged by the dye solution. Figures 5.8a, c show images of intensely colored capillary foams prepared in this manner, indicating weak coloration in the bulk phase but intense coloration of the foam area. Figures 5.8b, d quantitatively demonstrate the weak absorbance for the liquid phase and strong reflectance for the foam phase. Figures 5.8a, c show confocal microscopy images of wet capillary foams dyed with Nile red, in which both the particles and the oil are adsorbed on the surfaces of air bubbles. In addition, the particles between the bubbles are connected by oil bridges, shown in Figures 5.8a, c (inserts). Therefore, the colorant is concentrated both on the bubble surfaces and in the liquid films between the bubbles.

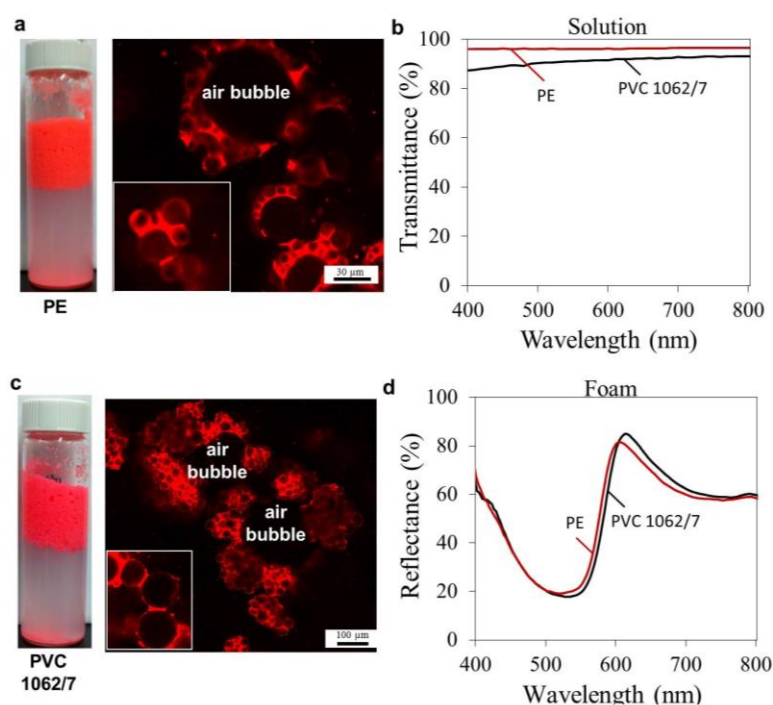


Figure 5.8 Intensely colored capillary foam. (a,c) Photographs and confocal microscope images of colored foams stabilized by 2 wt% dye solution (0.37 mg of Nile red was dissolved in 0.5 g TMPTMA) and 7.41 wt% PE or PVC 1062/7 particles. Inserts in (a) and (c) are confocal microscopic images of the particle network among the bubbles. The additional zoom factors for the inserts are 1.61 and 3.05, respectively. (b) Transmittance spectra of bulk suspension of the corresponding capillary foam. (d) Reflectance spectra of foam area of the corresponding capillary foams.

Capillary foam retained its intense coloration even after drying, as shown in Figures 5.9a and b. Figure 5.9c shows that the dried color foam retained its strong reflectance. By contrast, the corresponding wet foams stabilized by surfactant or by particles did not yield intensely colored dried foams. The surfactant stabilized colored foams coalesced and fully disintegrated during the drying process. For particle-stabilized colored foams, dyes concentrated on the external surfaces rather than within the interior of the dried foam, as shown in Figure 5.9d.

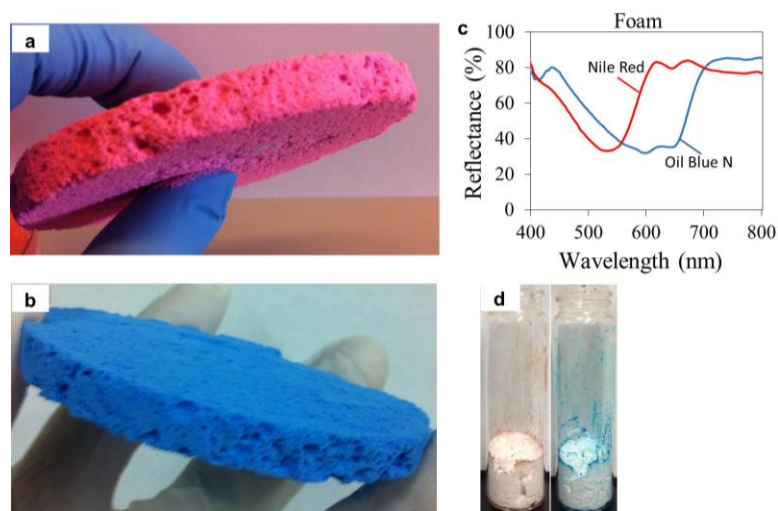


Figure 5.9 Images of dried color foams. (a) Dried capillary foams stabilized by the synergistic action of 18.5 vol% PVC 1062/7 particles and 4 wt% TMPTMA (1.5 mg of Nile red was dissolved in 2g TMPTMA). (b) Dried capillary foams formed from the synergistic action of 10 vol% PVC 1062/7 particles and 5 wt% TMPTMA (10.2 mg of oil blue N was dissolved in 2 g TMPTMA). (c) Reflectance spectra of the corresponding dried foams in (a) and (b). (d) Dried Pickering foam stabilized by 7.41 wt% PE particles and colored by 0.003 wt % allura red (left) or FD&C blue NO.1 (right).

5.4 Conclusion

In this chapter, we reported that capillary foams can be prepared by either introducing air and oil simultaneously to a particle suspension, by frothing a capillary suspension, or by mixing oil into a Pickering foam. In addition, capillary foams provide a general, novel processing route for preparing load-bearing porous solids and intensely colored liquid or solid dried foams. Porous solids formed from capillary foams have porosity on different length scales originating from the original gas bubbles and the particle network in the original liquid phase. Moreover, the secondary liquid originally connecting the particles in the wet foam could be polymerized to further reinforce the particle network before removal of the primary liquid. We also successfully prepared intensely colored liquid and dried foams by introducing an oil-based dye solution and gas bubbles to an aqueous particle suspension. Capillary foams retained their intense coloration even after drying, whereas foams stabilized by surfactant or particles did not allow for intense coloring in either the wet or dry state. Clearly the presence of the minority liquid phase in capillary foams gives rise to many new opportunities for foam processing, further examples of which shall be explored in a forthcoming paper.

5.5 References

1. Hiemenz, P. C.; Rajagopalan, R. Principles of colloidal and surface chemistry; Dekker New York: 1997.
2. Evans, D. F.; Wennerstrom, H. The colloidal domain: where physics, chemistry, biology, and technology meet. Wiley-VCH New York: 1999.
3. Binks, B. P.; Horozov, T. S. (eds) Colloidal particles at liquid interfaces. Cambridge Univ. Press: 2006.
4. Binks, B. P. Particles as surfactants—similarities and differences. *Curr. Opin. Colloid Interface Sci.* 2002, 7 (1-2), 21–41.
5. Lin, Y.; Skaff, H.; Emrick, T.; Dinsmore, A. D.; Russell, T. P. Nanoparticle assembly and transport at liquid-liquid interfaces. *Science* 2003, 299(5604), 226–229.
6. Subramaniam, A. B.; Abkarian, M.; Mahadevan, L.; Stone, H. A. Non-spherical bubbles. *Nature* 2005, 438(7070), 930.
7. Dinsmore, A. D.; Hsu, M. F.; Nikolaidis, M. G.; Marquez, M.; Bausch, A. R.; Weitz, D. A. Colloidosomes: Selectively permeable capsules composed of colloidal particles. *Science* 2002, 298(5595), 1006-1009.
8. Kaz, D. M.; McGorty, R.; Mani, M.; Brenner, M. P.; Manoharan, V. N. Physical ageing of the contact line on colloidal particles at liquid interfaces. *Nat. Mater.* 2012, 11(2), 138-142.
9. Alargova, R. G.; Warhadpande, D. S.; Paunov, V. N.; Velev, O. D. Foam super stabilization by polymer microrods. *Langmuir* 2004, 20(24), 10371–10374.
10. Aveyard, R.; Binks, B. P.; Clint, J. H. Emulsions stabilised solely by colloidal particles. *Adv. Colloid Interface Sci.* 2003, 100, 503– 546.
11. Gonzenbach, U. T.; Studart, A. R.; Tervoort, E.; Gauckler, L. J. Ultrastable particle-stabilized foams. *Angew. Chem. Int. Edit.* 2006, 45(21), 3526-3530.

12. Binks, B. P.; Murakami, R. Phase inversion of particle-stabilized materials from foams to dry water. *Nat. Mater.* 2006, 5(11), 865-869.
13. Aussillous, P.; Quéré, D. Liquid marbles. *Nature* 2001, 411(6840), 924–927.
14. Wege, H. A.; Kim, S.; Paunov, V. N.; Zhong, Q. X.; Velev, O. D. Long-term stabilization of foams and emulsions with in-situ formed microparticles from hydrophobic cellulose. *Langmuir* 2008, 24(17), 9245-9253.
15. Salonen, A.; Lhermerout, R.; Rio, E.; Langevin, D.; Saint-Jalmes, A. Dual gas and oil dispersions in water: production and stability of foamulsion. *Soft Matter* 2012, 8(3), 699-706.
16. Patel, A. R.; Drost, E.; Blijdenstein, T. B.; Velikov, K. P. Stable and temperature-responsive surfactant-free foamulsions with high oil-volume fraction. *ChemPhysChem* 2012, 13(17), 3777-3781.
17. Koos, E.; Willenbacher, N. Capillary forces in suspension rheology. *Science* 2011, 331(6019), 897-900.
18. Butt, H. J. Controlling the flow of suspensions. *Science* 2011, 331(6019), 868-869.
19. Koos, E. Capillary suspensions: Particle networks formed through the capillary force. *Curr. Opin. Colloid Interface Sci.* 2014, 1(6), 575-584.
20. Zhang, Y.; Wu, J.; Wang, H. Z.; Meredith, J. C.; Behrens, S. H., Stabilization of Liquid Foams through the Synergistic Action of Particles and an Immiscible Liquid. *Angew Chem Int Edit* 2014, 53 (49), 13385-13389.
21. Xu, H.; Goedel, W. A. Particle-assisted wetting. *Langmuir* 2003, 19(12), 4950-4952.
22. Ding, A. L.; Goedel, W. A. Experimental investigation of particle-assisted wetting. *J. Am. Chem. Soc.* 2006, 128(15), 4930-4931.
23. Ding, A. L. PhD. Dissertation, Chemnitz University of Technology, 2007.
24. Gonzenbach, U. T.; Studart, A. R.; Tervoort, E.; Gauckler, L. J. Macroporous ceramics from particle-stabilized wet foams. *J. Am. Ceram. Soc.* 2007, 90(1), 16-22.

25. Studart, A. R.; Gonzenbach, U. T.; Akartuna, I.; Tervoort, E.; Gauckler, L. J. Materials from foams and emulsions stabilized by colloidal particles. *J. Mater. Chem.* 2007, 17(31), 3283-3289.
26. Dittmann, J.; Koos, E.; Willenbacher, N. Ceramic capillary suspensions: novel processing route for macroporous ceramic materials. *J. Am. Ceram. Soc.* 2013, 96(2), 391-397.
27. Dittmann, J.; Koos, E.; Willenbacher, N. Micro structural investigations and mechanical properties of macro porous ceramic materials from capillary suspensions. *J. Am. Ceram. Soc.* 2014, 97(12), 3787-3792.
28. Kim, S.; Barraza, H.; Velez, O. D. Intense and selective coloration of foams stabilized with functionalized particles. *J. Mater. Chem.* 2009, 19(38), 7043-7049.

CHAPTER 6

BUBBLE MEETS DROPLET: PARTICLE-ASSISTED RECONFIGURATION OF WETTING MORPHOLOGIES IN COLLOIDAL MULTIPHASE SYSTEMS

6.1 Introduction

Wetting phenomena are ubiquitous both in nature and play key functions in various industrial processes and products.^{1,2} Three distinct wetting morphologies (complete wetting, partial wetting, and non-wetting) can be found in colloidal multiphase systems.³⁻⁵ Each of these three morphologies can have practical benefits, and controlling the morphology is desirable for applications ranging from oil recovery to separations.⁶⁻¹³ It is known that the wetting morphology depends on the balance of interfacial tensions and can thus be modified with surfactant additives.^{14,15} However, surfactants suffer from drawbacks such as chemical degradation under harsh application conditions, potential environmental pollution, and recovery difficulty.¹⁶⁻²²

Unlike surfactants, which adsorb at and desorb from an interface very rapidly under the effect of thermal fluctuations, particles with suitable wettability can be strongly adsorbed to the interface of immiscible fluids because of high adsorption energy.²²⁻²⁴ Since the pioneering work of Ramsden and Pickering in the early 20th century,^{25,26} numerous studies have reported the fabrication of ultra-stable colloidal multiphase systems, such as foams,²⁷⁻³⁰ emulsions,^{31,32} liquid marbles,^{33,34} colloidosomes,^{35,36} and bijels,³⁷ using colloidal particles. Particle-stabilized colloidal multiphase systems have

applications in cosmetics, food products, wastewater treatment, and oil recovery processes. Goedel found that particles can assist the spreading of trimethylpropane trimethacrylate (TMPTMA) at a planar air-water interface.³⁸⁻⁴¹ Although it was recognized more than a century ago that particles can act as stabilizers in colloidal multiphase systems, it is still unknown whether particles can also act as wetting modifiers. For example, can particles be used to induce or prevent the spreading of an oil droplet around gas bubbles in a colloidal multiphase system? One may also wonder whether the wetting configuration in systems with particle-laden interfaces can be predicted based on an effective interfacial tension or spreading coefficient of the particle-coated interface. Another question is whether particles afford the ability to actively reconfigure the wetting morphology, i.e., to change an existing configuration in situ through the controlled addition of appropriately selected particles.

We addressed these questions in this chapter and demonstrated that the wetting configuration of a colloidal multiphase system can be tuned by selection of appropriate colloidal particles, as predicted by an effective spreading coefficient. The wetting and engulfment of an air bubble by an oil droplet in a water medium was used as a model system which is relevant in a wide variety of industrial processes such as contrast-enhanced ultrasonography, gas flotation, and defoaming. We also demonstrated the particle-mediated dynamic reconfiguration of the wetting state and show that particles can be used both to promote “bubble wetting” and induce the complete bubble engulfment by an oil drop and to trigger “bubble de-wetting”, *i.e.* substantially reduce the oil-bubble contact area. A mechanistic understanding of this reconfiguration process was obtained by measuring the effective dynamic surface and interfacial tensions obtained by

axisymmetric drop shape analysis. The tunability is attributed to changes in interfacial energy caused by the adsorption of particles at fluid-fluid interfaces. This study yields a new strategy to predict and control the wetting configuration in colloidal multiphase systems, with potential benefits in a wide range of research fields, industrial processes, and commercial products.

6.2 Materials and Methods

6.2.1 Materials

Hexadecane, tripropylene glycol diacrylate (TPGDA), and Nile red were purchased from Sigma-Aldrich. Hexadecane was purified by using basic alumina and silica gel to remove any surface active contamination. TPGDA was purified by using basic alumina. Ultrapure water with a resistivity of 18.2 M Ω ·cm was used as the aqueous phase. Silica particles were received in powder form and were gifts from Wacker-Chemie: MM038-5 (68% methylsilyl capped, 32% SiOH). Since the partially hydrophobic silica particles (32% SiOH) were not wetted well by DI water, aqueous dispersions were prepared by first dispersing the particles in acetone and then transferring the particles to the DI water using repeated centrifugation. The zeta potential of silica particles is -46.3 mV which is obtained by phase analysis light scattering, Malvern Zetasizer Nano ZS90. Ethyl cellulose (EC) particles were synthesized by following the reported method.⁴²⁻⁴⁴ Briefly, 1 wt% of EC (Sigma-Aldrich, product code: 247499-100G) in acetone was prepared using a magnetic stirrer with 1100 rpm at 45 °C until EC particles were dissolved. An equal volume of ultrapure DI water (18.2 M Ω ·cm) was then quickly poured into the prepared EC solution under stirring (1100 rpm), and the solution turned

turbid as a result of EC nanoparticle nucleation and growth. The solution was then enriched in water where all the acetone and part of the water was removed by evaporation. For the preparation of Nile red labeled-EC particles, Nile red and EC with the mass ratio of 1:100 were dissolved in acetone when preparing 1 wt% EC in acetone solution. All the following procedures are similar with the steps of synthesizing of dye-free EC particles. During the precipitation process, EC particles were labeled with Nile red by incorporating the dye into the particles.⁴⁵ Hypromellose phthalate (grade HP 55) was provided by Shin Etsu Chemical Co., Ltd. (Tokyo, Japan). The starting materials was purified by centrifugation (sedimentation and re-dispersion for 6 cycles) in water. Minor modifications were made to a reported method⁴⁶ of HP 55 nanoparticle synthesis in an aqueous medium. Briefly, a solution of 1 wt% purified HP 55 in acetone was prepared. An equal volume of ultrapure DI water was then quickly poured into the prepared HP 55 solution, which became turbid upon nanoparticle nucleation and growth. The solution was enriched in water where all the acetone and part of the water removed by evaporation under continuous stirring. For the preparation of Nile red labeled-HP 55 particles, Nile red and HP 55 with the mass ratio of 1:100 were dissolved in acetone when preparing 1 wt% HP 55 in acetone solution. All the following procedures are similar with the steps of synthesizing of dye-free HP 55 particles. The obtained EC and HP 55 particle suspensions were passed three times through a C18–silica chromatographic column (Phenomenex) that had been preactivated with an acetonitrile–water (80:20) mixture and flushed several times with hot DI water. Before the particle dispersions were used in an experiment, the purified HP55 solution was diluted to specific particle concentration using DI water and its pH was tuned to 4.35 by adding 0.01 M hydrochloric acid to

reduce the electrostatic barrier to particles adsorption. The EC dispersion was diluted to specific particle concentration with DI water and the pH was tuned to 6.0 by using 0.01 M hydrochloric acid. Both EC and HP 55 particles dispersions in water are negative charged in water.^{42,46} These pH values were chosen for purely practical reasons based on balancing the kinetics of adsorption (which becomes very slow at high pH) versus the opacity of the suspension (aggregations are formed and the resulting suspension becomes difficult to image the bubble and drop at low pH). The hydrodynamic radius of EC and HP 55 particles was measured by dynamic light scattering using a Malvern Zetasizer Nano ZS90. The morphologies of EC and HP 55 particles were observed by a scanning electron microscope (SEM). One drop of 0.2 wt% particles dispersion was placed on glass side and left to air dry. After the evaporation of the water, the particles were prepared for imaging with an SEM by coating them with a gold nanolayer in a Hummer 5 Gold/Palladium Sputter.

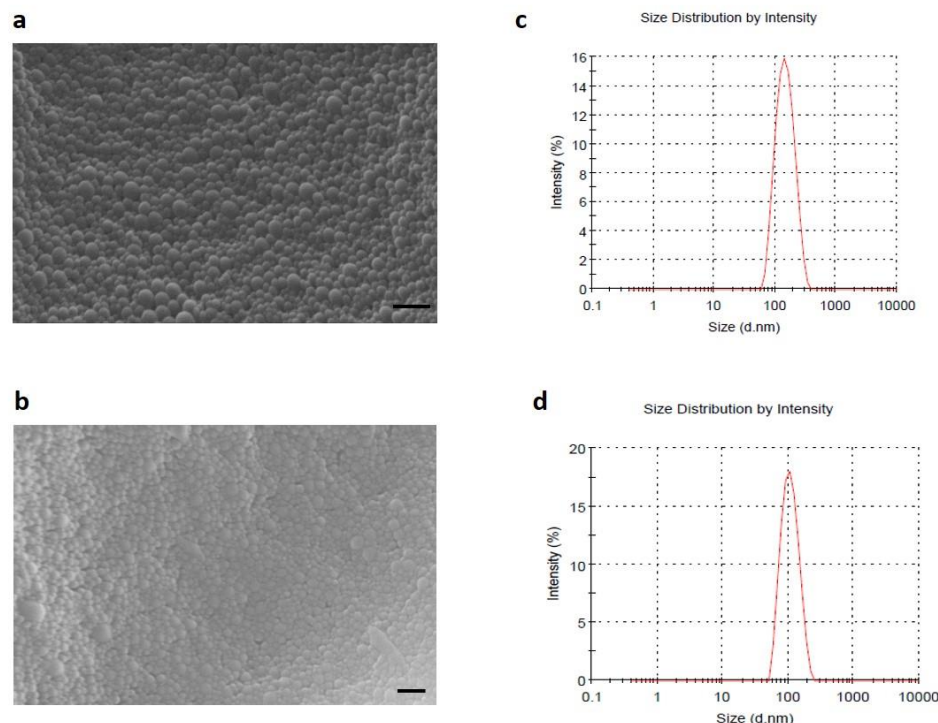


Figure 6.1 SEM images and size distributions of particles used in this study. SEM image of (a) HP 55 and (b) EC particles. Scale bars are 200 nm. Intensity-weighted particles size distribution of (c) HP 55 and (d) EC particles obtained from dynamic light scattering by inversion of the scattering intensity autocorrelation function. The Z-average sizes of the EC and HP55 particles are 102.3 nm and 137.4 nm, respectively. The corresponding coefficients of variation are 13% and 10%, respectively.

6.2.2 A single air bubble and oil droplet were generated and brought into contact

The experimental setup consisted of one square capillary (VitroCom, Inc., with an inner diameter of 1 mm and an outer diameter of 1.4 mm unless otherwise mentioned) to hold the sample and two round capillary tubes (VitroCom, Inc., with an inner diameter of 0.7 mm, an outer diameter of 0.87 mm) through which the air bubble and oil droplet were injected. The square capillary was pretreated with “piranha solution” (a 3:1 mixture of concentrated sulfuric acid and 30 % hydrogen peroxide) for 1.5 h. One end of each round capillary tube was shaped into a tapered orifice using a flaming/brown micropipette puller; this end could be used to introduce the air bubble or oil droplet. The other end of

the round capillary was connected to a microsyringe (containing air or oil) by using polytetrafluoroethylene (PTFE) tubing. A single air bubble was generated in a petri dish with DI water or particle suspension using a microsyringe and then transferred into the square capillary prefilled with DI water or particle suspension (Figure 6.2a). Next, a single oil droplet was dispensed directly into the square capillary through the second injection tube with a slowly and manually operated microsyringe (Figure 6.2b). The generated bubble and oil droplet were kept in the device to allow particles to adsorb on the bubble and oil droplet surfaces (Figure 6.2c); then they were brought into contact through the buoyancy force on the air bubble (Figure 6.2d). The morphologies were studied in the microfluidic device after the air bubble and oil drop made contact (Figure 6.2e). The radius of oil droplet and air bubble were kept to be around 300 - 400 μm .

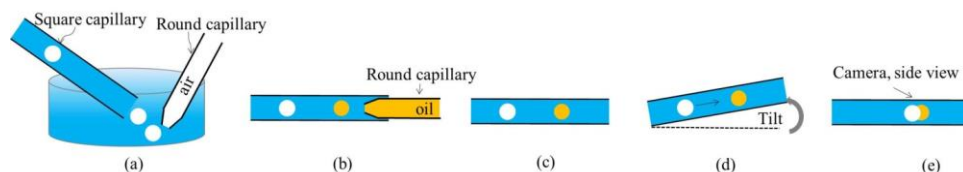


Figure 6.2 (a) A single air bubble was generated and then transferred into the square capillary. (b) A single oil droplet was dispensed directly into the square capillary through the second tapered round tube. (c) The generated bubble and oil droplet were kept in the device to allow particles to adsorb on the bubble and oil droplet surfaces. (d) The bubble and oil droplet were brought into contact by slightly tilting the capillary and exploiting the bubble's buoyancy. (e) The wetting configuration was examined optically in the glass capillary.

6.2.3 Measurement of interfacial tensions

The dynamic surface and interfacial tension was measured via axisymmetric drop shape analysis of pendant drops with a Ramé-hart goniometer. This method has proven

extremely useful to determine the evolution of the interfacial tension due to the adsorption of particles to the interface.⁴⁷⁻⁵² Briefly, an inverted pendant drop of oil or an air bubble immersed in the aqueous phase was created by a syringe with a steel needle, and a high speed CCD camera was programmed to capture the variation of drop/bubble shape with time. The interfacial/surface tension is obtained by analyzing the contour shape resulting from the balance of gravitational forces and tension forces. All experiments were performed at room temperature of 21 °C.

6.3 Results and Discussion

6.3.1 Selection of colloidal multiphase systems

Our study focuses on the wetting of an air bubble by an oil droplet in a water medium. We chose hexadecane and tripropylene glycol diacrylate (TPGDA) as oil phases, because these are commonly found in industrial processes and have different wetting in the absence of particles.⁵³ Particles of ethyl cellulose (EC) and cellulose-derived hypromellose phthalate (HP 55) were used as wetting modifiers because they are readily available, chemically modifiable, and biorenewable.^{46,54-56} The hydrodynamic diameters of the EC and HP55 particles as obtained by dynamic light scattering are 102.3 nm and 137.4 nm, respectively. The corresponding coefficients of variation are 13% and 10%. A glass capillary tube with square cross-section was used to observe the wetting configurations of air-water-oil-particle combinations. One air bubble and one oil droplet were dispensed from microsyringes, transferred to a square capillary containing the aqueous particle dispersion, and kept stationary for 30 minutes to allow for particles to adsorb on their surfaces. Then the bubble and oil droplet were brought into contact by

slightly tilting the capillary and exploiting the bubble's buoyancy. The wetting configuration assumed upon bubble-droplet contact was examined optically in the glass capillary.

For a three-phase system, the final wetting morphology can be determined by knowing at least two spreading coefficients.³⁻⁵ In the scenario of interest to our study, the wetting of an air bubble by an oil drop in an aqueous medium, there are only two kinds of possible wetting configurations: partial and complete wetting. The non-wetting state is energetically unfavorable: because of the high air-water surface tension, γ_{aw} , water cannot spread at an air-oil interface ($S_w = \gamma_{ao} - (\gamma_{aw} + \gamma_{ow}) < 0$ always). Similarly, it is energetically unfavorable for the gas bubble to engulf the oil droplet ($S_a < 0$). Therefore, the final wetting morphology can be determined from knowledge of only the oil spreading coefficient. If the oil phase has a positive spreading coefficient ($S_o > 0$), the oil will engulf the bubble completely, otherwise partial wetting will occur (Figure 6.3).

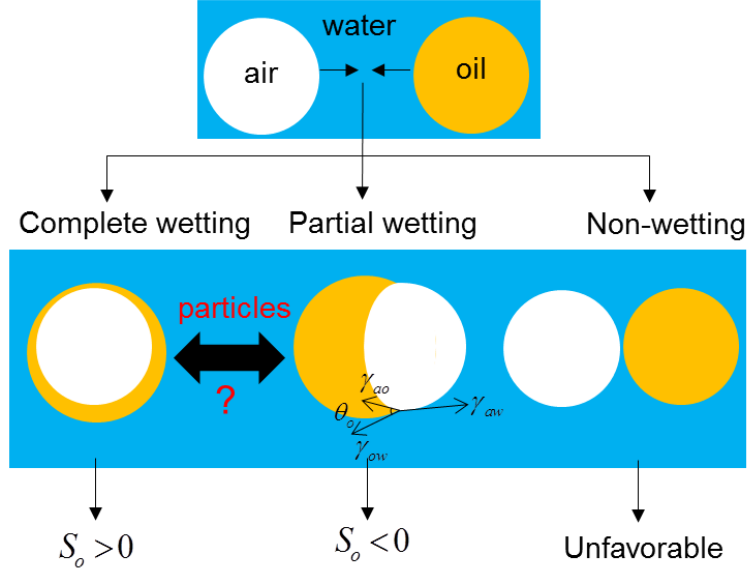


Figure 6.3 Possible wetting morphologies of an air bubble and an oil droplet in water and schematic illustration of equilibrium contact angle at the three-phase contact line. Here $S_o = \gamma_{aw} - (\gamma_{ao} + \gamma_{ow})$, where a, o, w denote the air, oil, and water phase respectively.

6.3.2 Particles can promote bubble wetting

Figure 6.4 shows that the dispersions particle presents in the aqueous medium determine the wetting configuration of the air-hexadecane-water system. In the absence of particles partial engulfment of the bubble by hexadecane was observed (Figure 6.4a), and the presence of up to 0.2 wt% of EC particles did not change this qualitative behavior (Figure 6.4b). By contrast, when the air bubble and hexadecane droplet were brought into contact in water containing 0.2 wt% of HP 55 particles, we observed complete bubble engulfment (Figure 6.4c). We found that these wetting configurations do not change in the following 12 hours. These results show that the wetting morphology of air-hexadecane-water system was changed from partial to complete wetting by using as little as 0.2 wt% HP 55 particles.

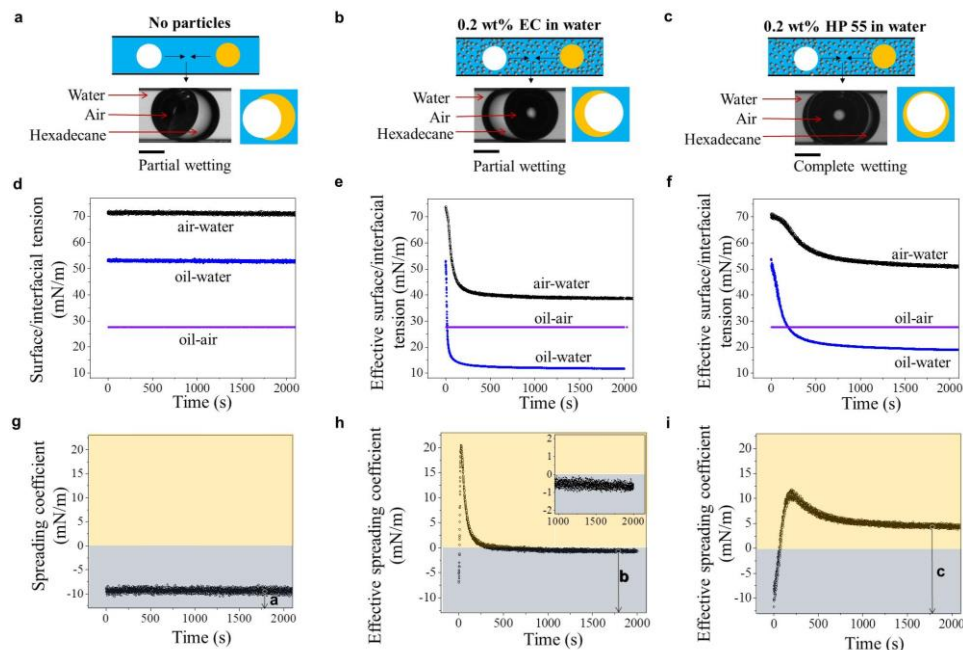


Figure 6.4 Particles promote the bubble wetting. First row: experimental observations of an air bubble and a hexadecane droplet brought into contact in a water medium containing (a) no particles, (b) 0.2 wt% EC particles, and (c) 0.2 wt% HP 55 particles. Scale bars are 500 μm . Second row: the dynamic effective surface and interfacial tension of an air-hexadecane-water system in which the water phase contains (d) no particles, (e) 0.2 wt% EC particles, and (f) 0.2 wt% HP 55 particles. Third row: the dynamic effective spreading coefficient of an air-hexadecane-water system in which the water phase contains (g) no particles, (h) 0.2 wt% EC particles, and (i) 0.2 wt% HP 55 particles. The yellow band indicates the complete wetting regime as predicted based on the of positive effective spreading coefficient ($S'_o > 0$), the grey band indicates the partial wetting regime expected for a negative effective spreading coefficient ($S'_o < 0$).

6.3.3 The change in wetting morphology is attributed to an interfacial energy change caused by the adsorption of particles at fluid-fluid interfaces

We propose that the dependence of the wetting configuration on the presence and type of particles may be attributed to the tuning of interfacial tensions caused by the adsorption of particles in the interfaces.^{43,48,50-52} Dynamic surface tension measurements have proven to be a straightforward and powerful method of quantifying the effective surface or interfacial tension of fluid interfaces containing adsorbed particles, and were

used in this study. The measured effective surface and interfacial tension data yield an effective spreading coefficient of fluid i via

$$S'_i = \gamma'_{jk} - (\gamma'_{ij} + \gamma'_{ik}) \quad (1)$$

We measured the interfacial tension via analysis of a pendant drop shape, which is determined by a balance of gravitational and tension forces. Figures 6.4d, e, f show time-dependent pendant drop tensiometer measurements at the air-water and hexadecane-water interfaces in which the water phase contained no particles, 0.2 wt% EC particles, or 0.2 wt% HP 55 particles, respectively. When the water phase contained no particles, the tensions of the air-water interface and of the hexadecane-water interface were time-independent (Figure 6.4d). On the other hand, when the water phase contained 0.2 wt% HP 55 or 0.2 wt% EC particles, the effective air-water tension γ'_{aw} and effective hexadecane-water tension γ'_{ow} first decreased with time and then reached steady state (Figures 6.4e, f). The decrease in γ'_{aw} and γ'_{ow} is caused by the progressive adsorption of particles at the respective interface over the course of the measurement series. As the interface reaches a plateau coverage by particles, the effective surface and interfacial tension also reached steady value. The particles may also adsorb on the oil-air interface when an air bubble and an oil droplet are brought into contact. The adsorption of particles at the oil-air interface can influence the surface tension of the oil-air interface. Contact angle experiments suggesting that the particles have little influence on the effective oil-air surface tension. Therefore, during the experiment, the air-hexadecane effective surface tension was assumed to be constant. Using Equation (1), we obtained the effective dynamic spreading coefficient of hexadecane (shown in Figures 6.4g, h, i). In

our experiment, the air bubble and hexadecane droplet were retained in the water phase for around 30 minutes to allow particles to adsorb to the interfaces. Therefore, the values of the effective spreading coefficient at 30 minutes were used. Figure 6.4g shows that the oil spreading coefficient in the absence of particles is negative in agreement with the observed partial bubble engulfment. The presence of 0.2 wt% EC particles raises the effective spreading coefficient significantly by reducing the oil-water interfacial tension (Figure 6.4e), but the effect on the effective spreading coefficient S_o' is partly offset by a significant simultaneous reduction of the air-water tension, which results in a negative value of -0.7 mN/m after 30 minutes (Figure 6.4h). Addition of HP 55 particles, by contrast, reduces the oil-water tension much more than the air-water tension (Figure 6.4f), and therefore leads to positive values of the effective spreading coefficient after 3 minutes (Figure 6.4i). As mentioned before, a positive effective spreading coefficient is consistent with the complete bubble engulfment by the oil droplet, whereas a negative value indicates only partial engulfment. The predicted morphologies based on the effective spreading coefficient matched the directly observed wetting configurations in a water phase containing no particles, 0.2 wt% EC particles, and 0.2 wt% HP 55 particles, respectively. For the wetting of air-hexadecane-water in the presence of 0.2 wt% EC particles, the accuracy of the wetting prediction based on the measured effective spreading coefficient may appear doubtful, because the experimental value is very close (within the uncertainty of the tension measurements) to the threshold value of zero. Visual observation and tensiometry consistently suggest that partial wetting occurs. Additionally, we observed that a hexadecane droplet placed on the macroscopic surface of an aqueous 0.2 wt% EC particle dispersion formed a stable oil lens with a finite

contact angle rather than wetting film (Figure 6.5). It therefore seems safe to conclude that in the particle dispersion the steady-state wetting configuration of an air bubble and a hexadecane droplet is indeed one of partial bubble engulfment.

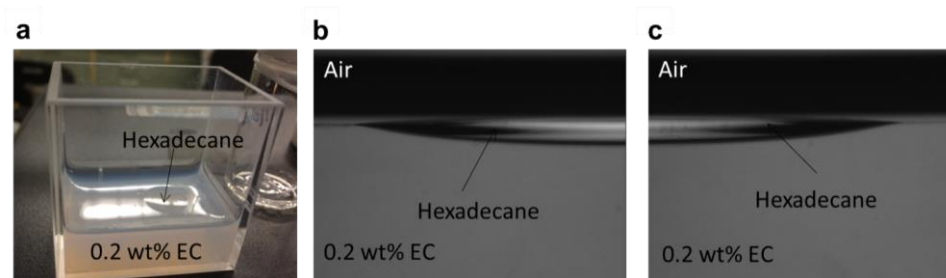


Figure 6.5. Formation of hexadecane oil lens at the macroscopic air-water interface. (a) A top view of hexadecane at the air-water interface where water phase contains 0.2 wt% EC particles. (b,c) Side views of oil lens in (a) using a CCD camera.

6.3.4 Particles can promote bubble de-wetting

As the observations of Figure 6.4 demonstrate, particles can promote bubble wetting and induce the complete bubble engulfment by hexadecane. One may wonder whether particles can also be used to trigger the bubble de-wetting and reduce the wetting area between an oil droplet and a gas bubble. To answer this question, we turned to a system in which hexadecane was replaced by the more polar TPGDA. Since TPGDA has a non-negligible water solubility of 4 g/L, we mutually saturated the TPGDA and water phase before performing the experiments and interfacial measurements so that equilibrium was reached. In the absence of particles, this system forms partial engulfment of an air bubble by the oil as seen in Figure 6.6a. Although the systems maintain partial wetting in the presence of 0.2 wt% EC or HP 55 particles in the water phase (Figure 6.6b, c), the presence of 0.2 wt% EC particles in the water phase induces further de-wetting and substantially reduces the oil-bubble contact (Figure 6.6b). It can be quantified by the

equilibrium contact angle at the three-phase contact line (Figure 6.3).⁵ For the contact angle θ_o , measured through oil phase

$$\cos \theta_o = \frac{\gamma'_{aw} - (\gamma'_{ow} + \gamma'_{ao})}{2\gamma'_{ow}\gamma'_{ao}} \quad (2)$$

where γ'_{aw} , γ'_{ao} , and γ'_{ow} are the respective interfacial tensions and a, w, o denotes air, water, oil phase, respectively. By analyzing the dynamic surface and interfacial tensions (shown in Figures 6.6d,e), we found that the effective spreading coefficient of TPGDA changes from -2.4 mN/m without particles to -7.8 mN/m. The corresponding three-phase contact angle measured through the oil phase increased from 43.2° to 87.4°. These results suggest that particles can be used to promote “bubble de-wetting” and substantially reduce the oil-bubble contact area.

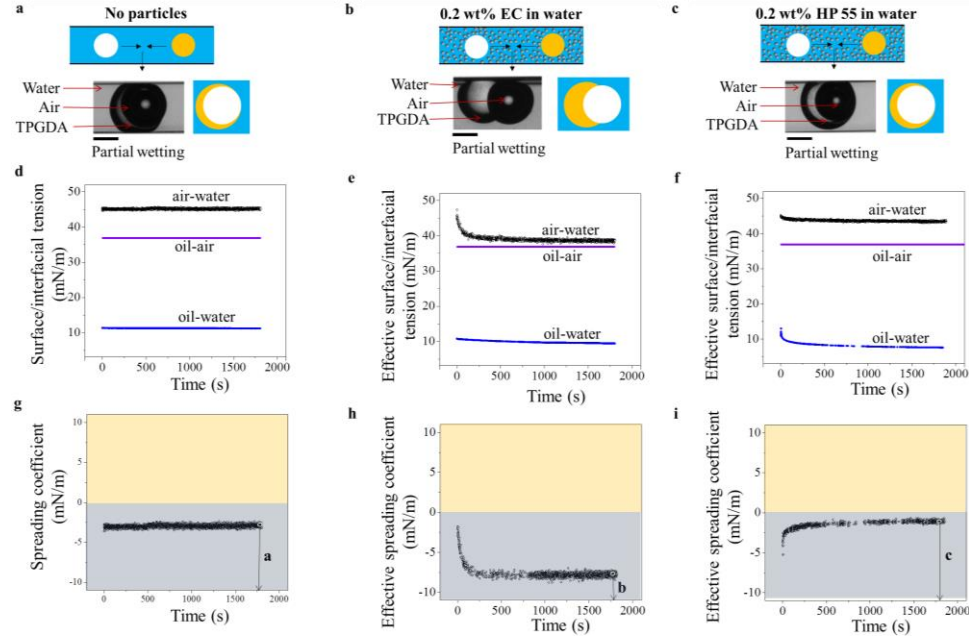


Figure 6.6 Particles promote the bubble de-wetting. Experimental observations of an air bubble and a TPGDA droplet brought into contact in a water phase containing (a) no particles, (b) 0.2 wt% EC particles, and (c) 0.2 wt% HP 55 particles. Scale bars are 500 μm . The dynamic effective surface and interfacial tension of an air-TPGDA-water system in which the water phase contains (d) no

particles, (e) 0.2 wt% EC particles, and (f) 0.2 wt% HP 55 particles. The dynamic effective spreading coefficient of an air-TPGDA-water system in which the water phase contains (g) no particles, (h) 0.2 wt% EC particles, and (i) 0.2 wt% HP 55 particles. The yellow and grey background indicates the different wetting regimes as in Figure 6.4.

6.3.5 Wetting behavior as function of particle concentration

In Figures 6.4 and 6.6, only one specific particle concentration (0.2 wt%) was used to demonstrate that particles can be used to change the wetting configurations. We have further investigated the effect of particle concentration (Figure 6.7). Figure 6.7a shows the stable wetting morphologies and the corresponding effective spreading coefficients of the air-hexadecane-water system for different concentrations of the HP 55 particles (from experiments analogous to those shown in Figure 6.4 c, f, i). Both the visual observation of the bubble-droplet pairs and measured effective spreading coefficient suggest that the wetting morphology changes from partial to complete wetting at the particle concentration around 0.02 wt%. Figure 6.7b shows the corresponding wetting morphologies and effective spreading coefficients of the air-TPGDA-water system in the presence of various concentrations of EC particles (experiments analogous to those shown in Figure 6.6 b, e, h). The observed wetting configuration demonstrates that the presence of only 0.01 wt% already gives rise to significant bubble de-wetting, whereas the measured the effective spreading coefficient suggests that the effect plateaus at a somewhat higher concentration (around 0.03 wt%). This difference might be explained by the difficulty of comparing droplet images taken at slightly different viewing angles and the possibility that full equilibrium had not been reached within the experimental observation period at these very low particle concentrations.

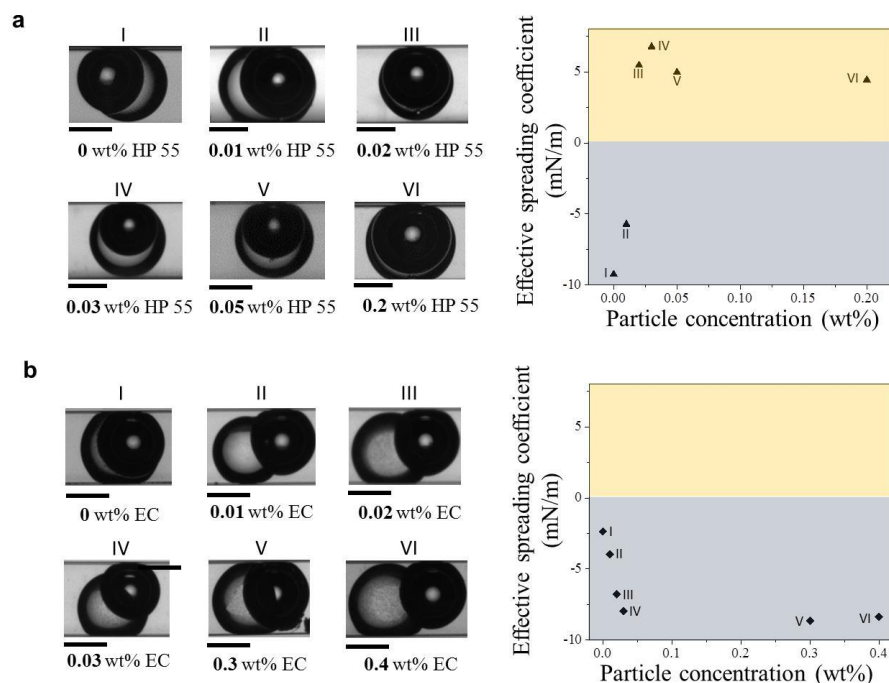


Figure 6.7 Wetting behaviors as a function of particle concentrations. (a) Wetting morphologies and corresponding effective spreading coefficients of air-hexadecane-water system by gradually changing concentrations of the HP 55 particles. (b) Wetting morphologies and corresponding effective spreading coefficients of air-TPGDA-water system by gradually changing concentrations of the EC particles. Scale bars are 500 μm .

6.3.6 Direct observation of the interfacially adsorbed particles

The hypothesis that particle adsorption at the fluid-fluid interfaces is indeed the cause for the observed modulation of the wetting configurations was further supported by confocal microscopy. The EC and HP 55 particles were labeled with Nile red. When the air bubble and hexadecane droplet were brought into contact in water containing 0.2 wt% Nile red labeled-HP 55 particles, we observed complete bubble engulfment (Figure 6.8a), the same wetting configuration found in the presence of label-free HP 55 particles. The confocal micrograph and the intensity profile (Figure 6.8d) indicate an accumulation of the HP 55 particles at the hexadecane-water interface. This particle adsorption reduces

the energetic penalty (tension) of the oil-water interface, thus promoting its expansion. When the air bubble and hexadecane droplet were brought into contact in water containing Nile red labeled-EC particles, we observed that the system retained the partial bubble engulfment, even when the particle concentration was doubled to 0.4 wt% (Figure 6.8b,c). Confocal images and the fluorescence intensity profiles suggest that EC particles accumulate at both the air-water and hexadecane-water interface (Figures 6.8b, c, e, f). Again, the particle adsorption in the hexadecane-water interface reduces the effective oil-water interfacial tension and raises the oil spreading coefficient, but in the case of EC particles the competing adsorption in the air-water interface (Figure 6.8b,e) is also strong and mitigates the increase in the oil spreading coefficient, keeping its final value below zero (Figure 6.4h). We note that the fluorescence intensity from particles at the air-water interface (Figure 6.8e) in fact exceeds the intensity recorded from the oil-water interface (Figure 6.8f), for which the particle-induced reduction of interfacial tension is nonetheless more pronounced (Figure 6.4e,h). To appreciate why these observations are not inconsistent, we point out that the fluorescence intensity does not lend itself for direct comparison of the particle concentrations in the two interfaces, because it also depends on the fluid environment, while that the reduction in interfacial tension depends not only on the interfacial particle concentration, but also on the particle contact angle with the interface.

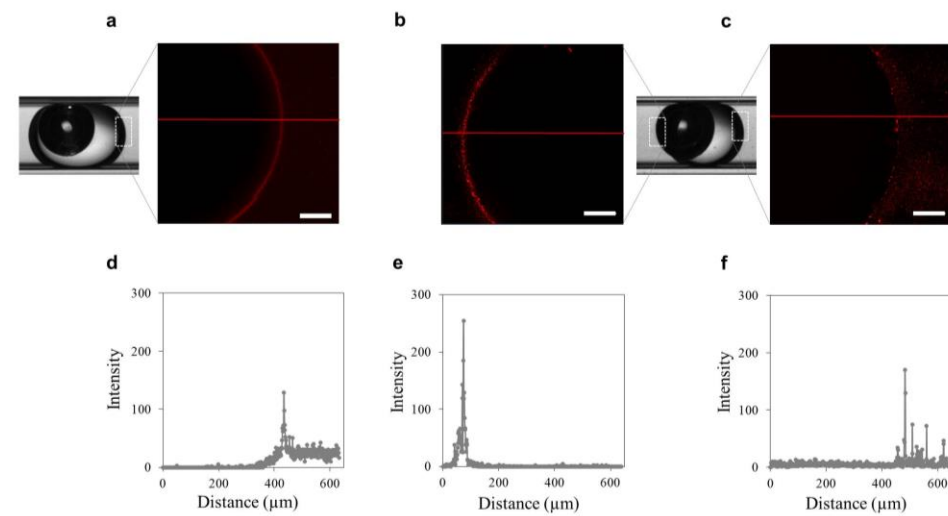


Figure 6.8 The adsorption of appropriate particles in the interfaces leads to the tuning of the wetting configuration. (a) Confocal microscope images of a close-up of hexadecane-water interface when an air bubble and a hexadecane droplet were brought into contact in a water medium containing 0.2 wt% Nile red-labeled HP 55 particles. Confocal microscope images of a close-up of (b) air-water interface and (c) hexadecane-water interface when an air bubble and a hexadecane droplet were brought into contact in a water medium containing 0.4 wt% Nile red-labeled EC particles. Scale bars are 100 μm . (d-f) The fluorescence intensity profiles along a line across the confocal images in parts a, b, and c, respectively.

6.3.7 In situ reconfiguration of pre-established wetting morphologies

In addition to tuning the wetting configuration through the selection of particles, we also studied the dynamic, in situ change of pre-formed wetting morphologies upon addition of particles to the system. An air bubble and an oil droplet, both suspended in the water phase, were brought into contact in a glass tube open at both ends. This tube was then placed into a particle dispersion containing either 0.4 wt% EC or 0.2 wt% HP 55 particles (Figure 6.9a). As HP 55 particles diffused into the tube, we observed that the wetting morphology changed from partial to complete wetting for the air-hexadecane-water three-phase system over the course of 15 minutes (Figure 6.9b). A substantial reduction of oil-bubble contact area was seen when exposing the air-TPGDA-water three-

phase system to the EC particle dispersion (Figure 6.9c). The final configurations observed here match the ones seen when the particles are present before the bubble and oil droplet are brought into contact (Figure 6.4 and 6.6). The experiments of Figure 6.9 show that the particles can be used to reconfigure an already established wetting state in situ. We expect that this novel capability of dynamically tuning the wetting morphology in colloidal multi-phase systems with particles will provide new impulses for the development of advanced materials.

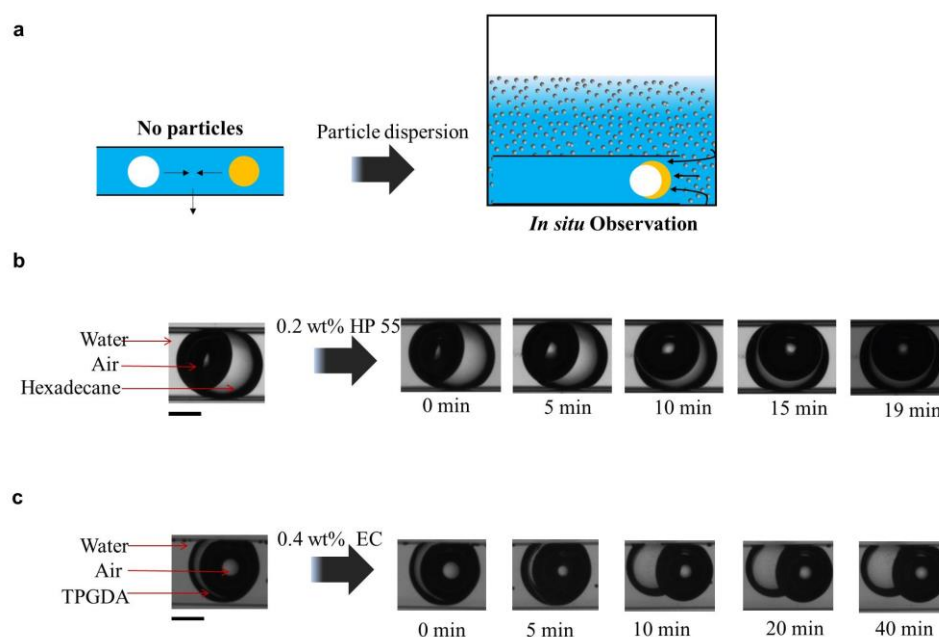


Figure 6.9 In-situ transition of the wetting morphology as particles diffuse to the interfaces. (a) Schematic illustration of the experimental procedure: an air bubble and an oil droplet are brought into contact in a particle-free water phase inside an open microfluidic glass channel, which is then placed in a particle suspension containing 0.4 wt% EC or 0.2 wt% HP 55 particles. (b) Wetting morphology transition for air-hexadecane-water system as HP 55 particles diffuse. (c) Wetting morphology transition for air-TPGDA-water system as EC particles diffuse. Scale bars are 500 μm .

6.3.8 Particle adsorption at different rates to air-water and oil-water interfaces leads to transient wetting behavior

We have demonstrated that particles can be used as wetting modifiers (Figures 6.4, 6.6, 6.7, and 6.9). Figure 6.4b indicated that the presence of 0.2 wt% of EC particles did not qualitatively change the equilibrium wetting behavior of air-hexadecane-water system, but dynamic interfacial tensiometry (Figure 6.4e) suggested an effective (dynamic) spreading coefficient (Figure 6.4h) that transiently assumes positive values before dropping back below zero. This suggests that particles may induce a transient wetting behavior, with a transition from partial to complete and back to partial bubble engulfment by the oil, and such behavior was indeed observed. To test whether this transient wetting can also be observed upon exposure of a pre-established, partially engulfed bubble to the particles, we carried out a dynamic reconfiguration experiment analogous to those described by Figure 6.9: An open glass tube with an inner diameter of 2 mm, filled with a an air bubble partially engulfed by hexadecane in particle-free water and held horizontally, was placed into a particle dispersion containing 0.2 wt% EC particles. As the particles diffused into the tube, we observed that the wetting morphology changed from partial to complete bubble engulfment within the first two minutes (Figure 6.10), and then back to partial engulfment over the course of three hours. To our knowledge, such slow and transient bubble or droplet wetting has never been observed in particle-free systems (with surfactants as wetting modifiers).

Both the tension of the air-water interface and of the hexadecane-water interface decrease with time as a result of interfacial particle adsorption (Figure 6.4e, and a close-up of the initial change in the supporting Figure 6.11). As the figure shows, the rate of

tension reduction is larger for the oil-water interface than for the air-water interface, which can be attributed to the faster rate of particle adsorption to the oil-water interface. It is well known that both bare oil-water and air-water interfaces tend to carry electric negative surface charge, most likely due to the adsorption of hydroxyl ions.⁵⁷⁻⁶⁴ EC particles in water are also negatively charged (with zeta potential of -50 mV at pH 6). Electric double layer interaction and image charge repulsion can result in an electrostatic barrier to particle adsorption to the interface, and one may expect the barrier to be higher at the interface with the larger drop in the dielectric permittivity, i.e. the air-water interface. We therefore speculate that faster particle adsorption to the oil-water interface may result from a weaker adsorption barrier in the oil-water interface. Similar dynamic tension effects were also found for negatively charged silica particles (with a zeta potential of -46.3 mV) adsorbing to air-water and hexadecane-water interfaces. In the transient wetting shown in Figure 6.10, the fast reduction of the effective interfacial tension at the hexadecane-water interface initially causes the effective oil spreading coefficient to become positive and triggers the complete bubble engulfment by the oil (Figure 6.4h, Figures 6.11b,d). Once the air-water interface has been completely replaced by the oil film, a new air-water interface (i.e. a hole in the engulfing oil film) first has to nucleate before that new interface can grow and be stabilized by adsorbing particles. The exact mechanism for this dewetting transition is unclear – nucleation may e.g. be facilitated by particle adsorption at the thinnest region of the oil layer – but it seems plausible that this nucleation and growth would take far longer than particle adsorption to a readily available interface. We also note that similar surfactant-induced transitions from complete to partial engulfment⁴ and even the inversion of complete engulfment

morphologies¹⁵ (but no transient wetting phenomena) have been reported in recent studies on systems of immiscible liquid droplets.

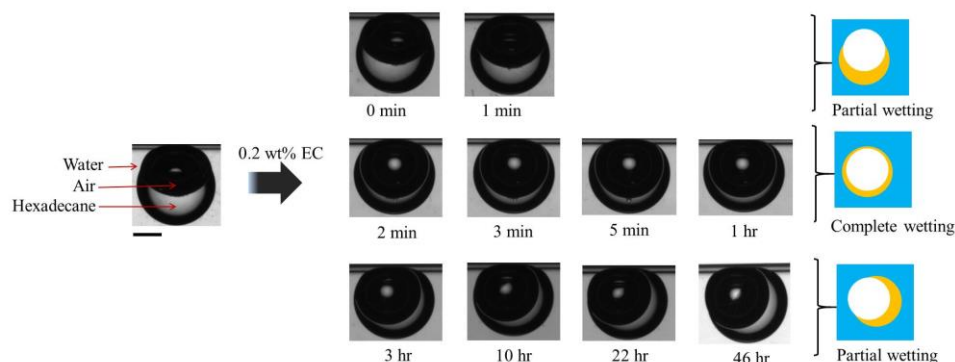


Figure 6.10 Transient wetting behavior. An air bubble and a hexadecane oil droplet were brought into contact in a particle-free water phase inside an open microfluidic glass channel, which was then placed in a particle suspension containing 0.2 wt% EC particles. Wetting morphology transition for air-hexadecane-water system as EC particles diffuse. Scale bar is 500 μm .

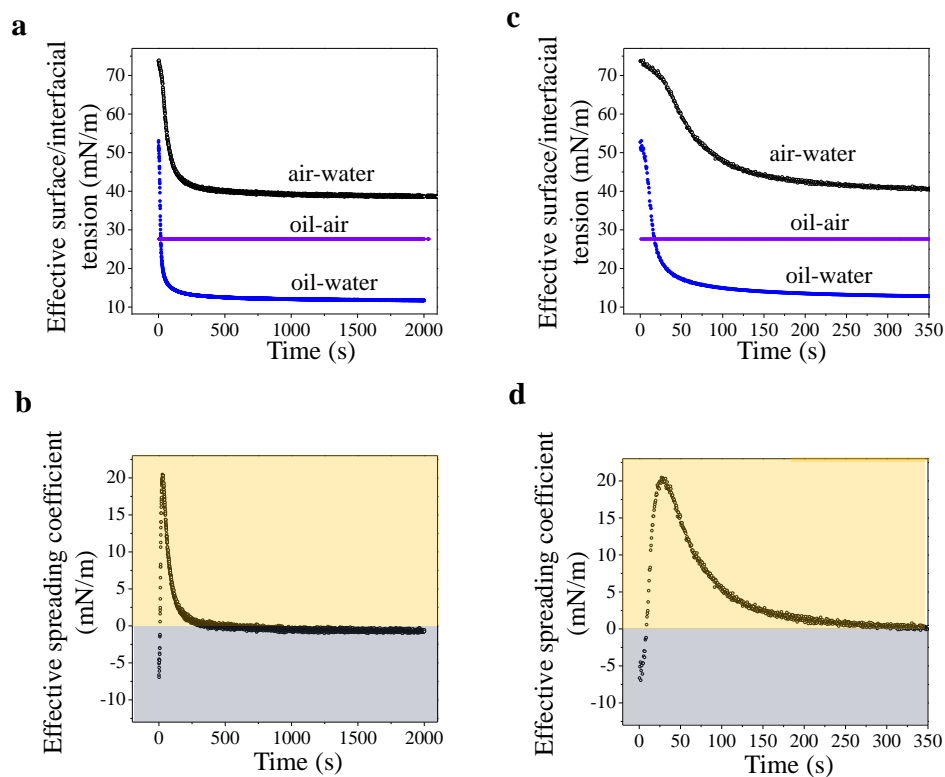


Figure 6.11 (a) The dynamic effective surface and interfacial tensions and (b) the corresponding dynamic effective spreading coefficient of an air-hexadecane-water

system in which the water phase contains 0.2 wt% EC particles. (c,d) Close-up of figures in (a) and (b) in the first 350 seconds, respectively.

6.3.9 Evidence that the particles do not introduce significant surface-active impurities

In this work, we have reported that tuning the wetting configuration from partial to complete or even complete to partial wetting can be achieved by using particles. Commercially available EC or HP 55 particles could contain impurities, such as molecular surfactant, which tends to be surface-active and may affect the wetting configuration. In order to purify the particle suspension used in the current study and remove any surface-active contaminants, the EC and HP 55 particle suspensions were passed three times through a C18-silica chromatographic column (Phenomenex) that had been preactivated with an acetonitrile-water (80:20) mixture and flushed several times with hot DI water.⁶⁵ In addition, we studied dynamic surface tensions of supernatants of EC and HP 55 particles by centrifuging their particle dispersions. These surface tension measurements show close agreement with the surface tension of ultrapure DI water (Figures 6.12a,b) and suggest that there are no surface-active contaminations or impurities in the EC and HP 55 particle suspension used in our study. Therefore, we can conclude that the particles are responsible for the reconfiguration of the wetting morphology, as opposed to surface contaminants.

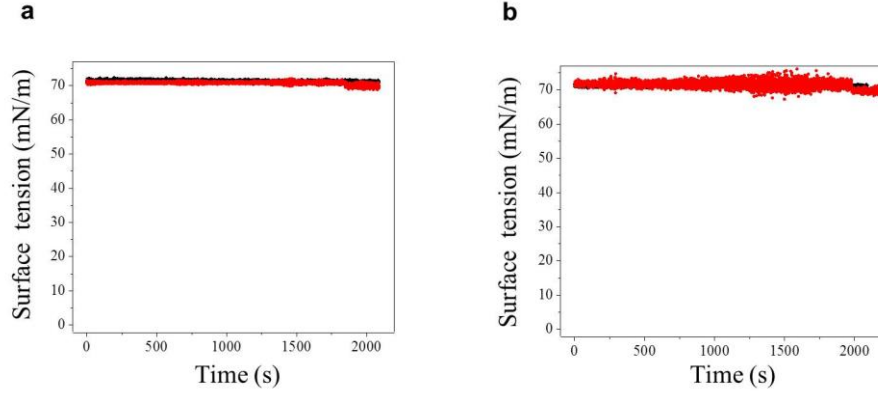


Figure 6.12 (a) Dynamic surface tension of supernatant of EC particles (red points) in comparison to the dynamic surface tension of ultrapure DI water (black points). (b) Dynamic surface tension of supernatant of HP 55 particles (red points) in comparison to the dynamic surface tension of ultrapure DI water (black points). 0.1 M hydrochloric acid was added before centrifugation to ensure the formation of particle aggregates and achieve good separation.

6.3.10 The influence of particles on the effective surface tension of the air-oil interface

The effective interfacial tension of the air-oil interface is assumed to be constant. The particles may adsorb on the oil-air interface and reduce the air-oil surface tension when an air bubble and an oil droplet is brought into contact in the water phase that contains particles. However, it is difficult to directly measure the dynamic surface tension of the oil-air interface in the presence of particles because the particles are delivered from the water phase. Here, the three-phase contact angle of particles at an air-oil interface was measured and used to quantify its influence on the effective surface tension, which is given by^{30,48}

$$\gamma'_{ao} = \gamma_{ao} (1 - \phi (1 - \cos \theta_{aop})^2) \quad (3)$$

where γ_{ao} is the surface tension of the air-oil interface without particles, ϕ is the packing density of particles at the interface, θ_{aop} is the contact angle of the particle at the air-oil

interface. As illustrated in Figure 6.13a, the particle contact angle can be correlated to the oil droplet contact angle on the flat surface.

A thin film of EC or HP 55 particles dissolved in acetone was cast on a clean glass surface. An oil droplet was placed on the coated glass surface in air, and a goniometer (Rame-hart, model-250) was used to measure the contact angle. The measured values are given in Figures 6.13b, c, d, and e. The contact angle of HP55 particle on the hexadecane- or TPDGA-air interface is below 10° (Figures 6.13c and e), which points to a low affinity for the interface, and a very small influence on the oil-air surface tension. The same procedure was used to estimate the affinity of the EC particle for the hexadecane-air interface. The experiments suggested that EC particles have the highest affinity for the TPDGA-air interface with a measured contact angle θ_{aop} of 44.5° , consistent with strong particle adsorption to the TPGDA-air interface and a significant reduction of its surface tension. From the measured contact angle, a measured TPGDA surface tension γ_{ao} of 36.9 mN/m, and assuming dense particle packing in the interface (area fraction ϕ of 91 % for 2D close packing), we obtained an estimate of 34.14 mN/m for the effective surface tension γ'_{ao} of TPDGA-air from Equation (3). With the calculated effective surface tension data, the effective spreading coefficient of fluid TPDGA can be calculated by

$$S'_o = \gamma'_{aw} - (\gamma'_{ao} + \gamma'_{ow}). \quad (4)$$

Although the calculation result shows that the effective spreading coefficient increases from -7.8 mN/m (assuming γ'_{ao} is constant) to -5.04 mN/m (considering the maximum possible influence of particles on γ'_{ao} in the case of dense packing), S'_o is still negative. As mentioned, the negative effective spreading coefficient indicates that oil engulfs the

bubble only partially. The predicted morphologies based on the current effective spreading coefficient matches the previously observed wetting configurations of partial wetting when the water phase contains EC particles (Figures 6.6b and 6.9c).

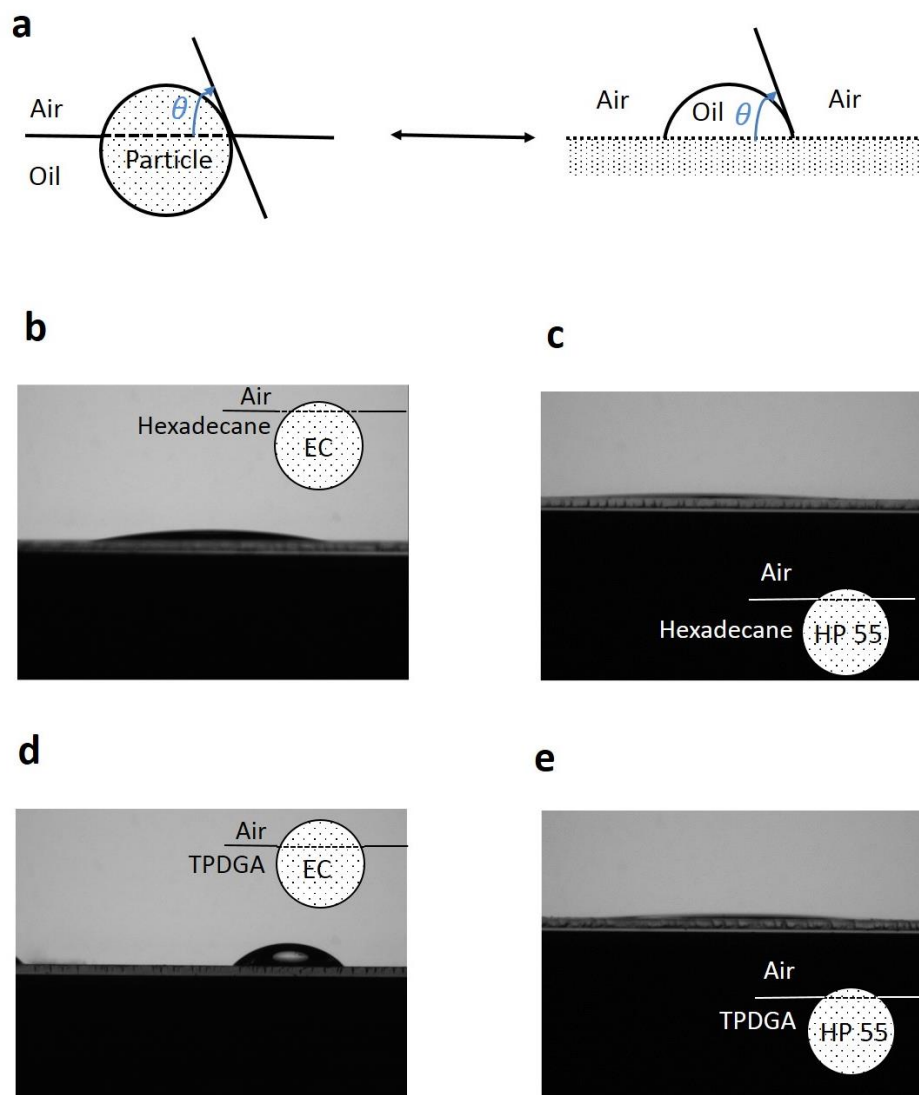


Figure 6.13 The Contact angle of a particle on the air-oil interface. (a) Graphical illustration that particle contact angle at the air-oil interface can be correlated to the oil droplet contact angle on a flat surface. Contact angles of hexadecane droplet on (b) EC-coated flat surface and (c) HP 55-coated flat surface, respectively. Contact angle of TPDGA droplet on (d) EC-coated flat surface and (e) HP 55-coated flat surface, respectively.

6.3.11 Confocal microscopy study of particles in the oil-air interface

The particles are not collected in the oil-air interface was further confirmed by confocal microscopy image. The air-hexadecane-water system in the presence of 0.4wt% EC particles was used as an example. The EC particles were labeled with Nile red. When an air bubble and a hexadecane droplet were brought into contact in water containing 0.4 wt% Nile red labeled-EC particles, we observed partial bubble engulfment (Figure 6.14a). Figure 6.14b is a confocal microscope image of a close-up of hexadecane-air interface which demonstrates that EC particles are not collected in the hexadecane-air interface.

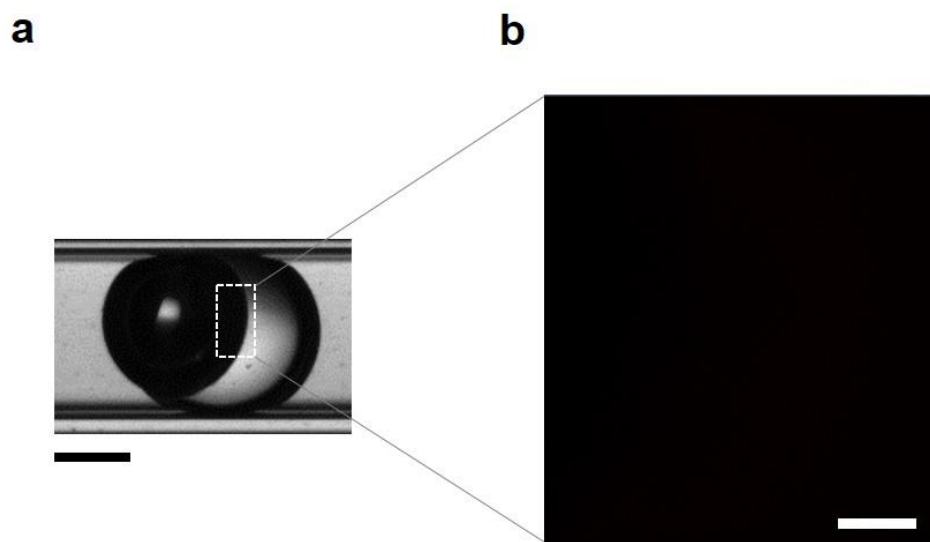


Figure 6.14 EC particles are not collected in the hexadecane-air interface. (a) Experimental observation of an air bubble and a hexadecane droplet brought into contact in a water phase containing 0.4 wt% Nile red labeled-EC particles. Scale bar is 500 μm . (b) Confocal microscope image of a close-up of hexadecane-air interface. Scale bar is 100 μm .

6.4 Conclusion

To summarize, in this chapter, we have reported a new strategy for tuning the wetting configuration of colloidal multiphase systems. Through the adsorption of cellulosic particles at fluid-fluid interfaces, a change of surface and interfacial tensions was achieved, as determined by dynamic pendant drop tensiometry. The wetting morphology predicted by the effective spreading coefficient, calculated from dynamic tensiometry data, agrees with the directly observed wetting configurations. In addition, particles can induce slow, transient wetting behavior. This study provides a new strategy for controlling and predicting the wetting configuration of an air bubble and an oil droplet in a water medium, which is relevant to a wide variety of materials research problems, industrial processes, and commercial products. We expect the tuning method presented here to be more general and applicable also to other types of particles and colloidal multiphase systems, such as complex emulsions of three or four immiscible liquids. Furthermore, the tunability of interfacial tensions via particle adsorption suggests that particles can also be useful as wetting modifiers in liquid-liquid-solid and liquid-vapor-solid systems.

6.5 References

1. Mayer, D.; Surfaces, I., Colloids: principles and applications. Wiley, New York: 1999.
2. Tian, Y.; Su, B.; Jiang, L., Interfacial material system exhibiting superwettability. *Adv Mater* 2014, 26 (40), 6872-6897.
3. Torza, S.; Mason, S., Three-phase interactions in shear and electrical fields. *J Colloid Interf Sci* 1970, 33 (1), 67-83.
4. Pannacci, N.; Bruus, H.; Bartolo, D.; Etchart, I.; Lockhart, T.; Hennequin, Y.; Willaime, H.; Tabeling, P., Equilibrium and nonequilibrium states in microfluidic double emulsions. *Phys Rev Lett* 2008, 101 (16), 164502- 164505.
5. Guzowski, J.; Korczyk, P. M.; Jakiela, S.; Garstecki, P., The structure and stability of multiple micro-droplets. *Soft Matter* 2012, 8 (27), 7269-7278.
6. Xu, J. H.; Chen, R.; Wang, Y. D.; Luo, G. S., Controllable gas/liquid/liquid double emulsions in a dual-coaxial microfluidic device. *Lab Chip* 2012, 12 (11), 2029-2036.
7. Tiarks, F.; Landfester, K.; Antonietti, M., Preparation of polymeric nanocapsules by miniemulsion polymerization. *Langmuir* 2001, 17 (3), 908-918.
8. Chu, L. Y.; Utada, A. S.; Shah, R. K.; Kim, J. W.; Weitz, D. A., Controllable monodisperse multiple emulsions. *Angew Chem Int Edit* 2007, 46 (47), 8970-8974.
9. Garrett, P., Defoaming: theory and industrial applications. CRC Press: 1992.
10. Walther, A.; Muller, A. H. E., Janus particles: synthesis, self-assembly, physical properties, and applications. *Chem Rev* 2013, 113 (7), 5194-5261.
11. Lone, S.; Cheong, I. W., Fabrication of polymeric Janus particles by droplet microfluidics. *Rsc Adv* 2014, 4 (26), 13322-13333.
12. Huang, X. P.; Qian, Q. P.; Wang, Y. P., Anisotropic particles from a one-pot double emulsion induced by partial wetting and their triggered release. *Small* 2014, 10 (7), 1412-1420.

13. Chen, D. L. L.; Li, L.; Reyes, S.; Adamson, D. N.; Ismagilov, R. F., Using three-phase flow of immiscible liquids to prevent coalescence of droplets in microfluidic channels: Criteria to identify the third liquid and validation with protein crystallization. *Langmuir* 2007, 23 (4), 2255-2260.
14. Evans, D. F.; Wennerstrom, H., *Colloidal domain*. Wiley-Vch: 1999.
15. Zarzar, L. D.; Sresht, V.; Sletten, E. M.; Kalow, J. A.; Blankschtein, D.; Swager, T. M., Dynamically reconfigurable complex emulsions via tunable interfacial tensions. *Nature* 2015, 518 (7540), 520-524.
16. Worthen, A. J.; Bagaria, H. G.; Chen, Y. S.; Bryant, S. L.; Huh, C.; Johnston, K. P., Nanoparticle-stabilized carbon dioxide-in-water foams with fine texture. *J Colloid Interf Sci* 2013, 391, 142-151.
17. Rosen, M. J.; Kunjappu, J. T., *Surfactants and interfacial phenomena*. John Wiley & Sons: 2012.
18. Crossley, S.; Faria, J.; Shen, M.; Resasco, D. E., Solid nanoparticles that catalyze biofuel upgrade reactions at the water/oil interface. *Science* 2010, 327 (5961), 68-72.
19. Wang, Z. P.; van Oers, M. C. M.; Rutjes, F. P. J. T.; van Hest, J. C. M., Polymersome colloidosomes for enzyme catalysis in a biphasic system. *Angew Chem Int Edit* 2012, 51 (43), 10746-10750.
20. Dickinson, E., Food emulsions and foams: Stabilization by particles. *Curr Opin Colloid In* 2010, 15 (1-2), 40-49.
21. Frelichowska, J.; Bolzinger, M. A.; Chevalier, Y., Pickering emulsions with bare silica. *Colloid Surface A* 2009, 343 (1-3), 70-74.
22. Binks, B. P., Particles as surfactants - similarities and differences. *Curr Opin Colloid In* 2002, 7 (1-2), 21-41.
23. Binks, B. P.; Horozov, T. S., *Colloidal particles at liquid interfaces*. Cambridge University Press: 2006.

24. Poulichet, V.; Garbin, V., Ultrafast desorption of colloidal particles from fluid interfaces. *P Natl Acad Sci USA* 2015, 112 (19), 5932-5937.
25. Ramsden, W., Separation of solids in the surface-layers of solutions and 'Suspensions' (Observations on surface-membranes, bubbles, emulsions, and mechanical coagulation). Preliminary Account. *P R Soc London* 1903, 72 (479), 156-164.
26. Pickering, S. U., Emulsions. *J Chem Soc* 1907, 91, 2001-2021.
27. Alargova, R. G.; Warhadpande, D. S.; Paunov, V. N.; Veleev, O. D., Foam superstabilization by polymer microrods. *Langmuir* 2004, 20 (24), 10371-10374.
28. Binks, B. P.; Horozov, T. S., Aqueous foams stabilized solely by silica nanoparticles. *Angew Chem Int Edit* 2005, 44 (24), 3722-3725.
29. Gonzenbach, U. T.; Studart, A. R.; Tervoort, E.; Gauckler, L. J., Ultrastable particle-stabilized foams. *Angew Chem Int Edit* 2006, 45 (21), 3526-3530.
30. Zhang, Y.; Wu, J.; Wang, H. Z.; Meredith, J. C.; Behrens, S. H., Stabilization of liquid foams through the synergistic action of particles and an immiscible liquid. *Angew Chem Int Edit* 2014, 53 (49), 13385-13389.
31. Li, Z. F.; Ming, T.; Wang, J. F.; Ngai, T., High internal phase emulsions stabilized solely by microgel particles. *Angew Chem Int Edit* 2009, 48 (45), 8490-8493.
32. Destribats, M.; Gineste, S.; Laurichesse, E.; Tanner, H.; Leal-Calderon, F.; Heroguez, V.; Schmitt, V., Pickering emulsions: what are the main parameters determining the emulsion type and interfacial properties? *Langmuir* 2014, 30 (31), 9313-9326.
33. Aussillous, P.; Quere, D., Liquid marbles. *Nature* 2001, 411 (6840), 924-927.
34. Binks, B. P.; Murakami, R., Phase inversion of particle-stabilized materials from foams to dry water. *Nat Mater* 2006, 5 (11), 865-869.

35. Dinsmore, A. D.; Hsu, M. F.; Nikolaides, M. G.; Marquez, M.; Bausch, A. R.; Weitz, D. A., Colloidosomes: Selectively permeable capsules composed of colloidal particles. *Science* 2002, 298 (5595), 1006-1009.
36. Miguel, A. S.; Behrens, S. H., Permeability control in stimulus-responsive colloidosomes. *Soft Matter* 2011, 7 (5), 1948-1956.
37. Herzig, E. M.; White, K. A.; Schofield, A. B.; Poon, W. C. K.; Clegg, P. S., Bicontinuous emulsions stabilized solely by colloidal particles. *Nat Mater* 2007, 6 (12), 966-971.
38. Xu, H.; Goedel, W. A., Particle-assisted wetting. *Langmuir* 2003, 19 (12), 4950-4952.
39. Xu, H.; Goedel, W. A., Mesoscopic rings by controlled wetting of particle imprinted templates. *Angew Chem Int Edit* 2003, 42 (38), 4696-4700.
40. Ding, A. L.; Binks, B. P.; Goedel, W. A., Influence of particle hydrophobicity on particle-assisted wetting. *Langmuir* 2005, 21 (4), 1371-1376.
41. Ding, A. L.; Goedel, W. A., Experimental investigation of particle-assisted wetting. *J Am Chem Soc* 2006, 128 (15), 4930-4931.
42. Jin, H. J.; Zhou, W. Z.; Cao, J.; Stoyanov, S. D.; Blijdenstein, T. B. J.; de Groot, P. W. N.; Arnaudov, L. N.; Pelan, E. G., Super stable foams stabilized by colloidal ethyl cellulose particles. *Soft Matter* 2012, 8 (7), 2194-2205.
43. Bizmark, N.; Ioannidis, M. A.; Henneke, D. E., Irreversible adsorption-driven assembly of nanoparticles at fluid interfaces revealed by a dynamic surface tension probe. *Langmuir* 2014, 30 (3), 710-717.
44. Chen, H. S.; Li, J.; Zhou, W. Z.; Pelan, E. G.; Stoyanov, S. D.; Arnaudov, L. N.; Stone, H. A., Sonication-microfluidics for fabrication of nanoparticle-stabilized microbubbles. *Langmuir* 2014, 30 (15), 4262-4266.
45. Xie, H.; She, Z. G.; Wang, S.; Sharma, G.; Smith, J. W., One-step fabrication of polymeric Janus nanoparticles for drug delivery. *Langmuir* 2012, 28 (9), 4459-4463.

46. Wege, H. A.; Kim, S.; Paunov, V. N.; Zhong, Q. X.; Velev, O. D., Long-term stabilization of foams and emulsions with in-situ formed microparticles from hydrophobic cellulose. *Langmuir* 2008, 24 (17), 9245-9253.
47. Stocco, A.; Drenckhan, W.; Rio, E.; Langevin, D.; Binks, B. P., Particle-stabilised foams: an interfacial study. *Soft Matter* 2009, 5 (11), 2215-2222.
48. Du, K.; Glogowski, E.; Emrick, T.; Russell, T. P.; Dinsmore, A. D., Adsorption energy of nano- and microparticles at liquid-liquid interfaces. *Langmuir* 2010, 26 (15), 12518-12522.
49. Garbin, V., Colloidal particles: Surfactants with a difference. *Phys Today* 2013, 66 (10), 68-69.
50. Isa, L.; Amstad, E.; Schwenke, K.; Del Gado, E.; Ilg, P.; Kroger, M.; Reimhult, E., Adsorption of core-shell nanoparticles at liquid-liquid interfaces. *Soft Matter* 2011, 7 (17), 7663-7675.
51. Foster, L. M.; Worthen, A. J.; Foster, E. L.; Dong, J. N.; Roach, C. M.; Metaxas, A. E.; Hardy, C. D.; Larsen, E. S.; Bollinger, J. A.; Truskett, T. M.; Bielawski, C. W.; Johnston, K. P., High interfacial activity of polymers "grafted through" functionalized iron oxide nanoparticle clusters. *Langmuir* 2014, 30 (34), 10188-10196.
52. Nelson, A.; Wang, D. P.; Koynov, K.; Isa, L., A multiscale approach to the adsorption of core-shell nanoparticles at fluid interfaces. *Soft Matter* 2015, 11 (1), 118-129.
53. Keller, A. A.; Chen, M. J., Effect of spreading coefficient on three-phase relative permeability of nonaqueous phase liquids. *Water Resour Res* 2003, 39 (10).
54. Lam, S.; Blanco, E.; Smoukov, S. K.; Velikov, K. P.; Velev, O. D., Magnetically responsive Pickering foams. *J Am Chem Soc* 2011, 133 (35), 13856-13859.
55. Blanco, E.; Lam, S.; Smoukov, S. K.; Velikov, K. P.; Khan, S. A.; Velev, O. D., Stability and viscoelasticity of magneto-Pickering foams. *Langmuir* 2013, 29 (32), 10019-10027.

56. Lam, S.; Velikov, K. P.; Velev, O. D., Pickering stabilization of foams and emulsions with particles of biological origin. *Curr Opin Colloid In* 2014, 19 (5), 490-500.
57. Graciaa, A.; Morel, G.; Saulner, P.; Lachaise, J.; Schechter, R. S., The Zeta-potential of gas-bubbles. *J Colloid Interf Sci* 1995, 172 (1), 131-136.
58. Marinova, K. G.; Alargova, R. G.; Denkov, N. D.; Velev, O. D.; Petsev, D. N.; Ivanov, I. B.; Borwankar, R. P., Charging of oil-water interfaces due to spontaneous adsorption of hydroxyl ions. *Langmuir* 1996, 12 (8), 2045-2051.
59. Stachurski, J.; Michalek, M., The effect of the zeta potential on the stability of a non-polar oil-in-water emulsion. *J Colloid Interf Sci* 1996, 184 (2), 433-436.
60. Yang, C.; Dabros, T.; Li, D. Q.; Czarnecki, J.; Masliyah, J. H., Measurement of the zeta potential of gas bubbles in aqueous solutions by microelectrophoresis method. *J Colloid Interf Sci* 2001, 243 (1), 128-135.
61. Elmallidy, A. M.; Mirnezami, M.; Finch, J. A., Zeta potential of air bubbles in presence of frothers. *Int J Miner Process* 2008, 89 (1-4), 40-43.
62. Oliveira, C.; Rubio, J., Zeta potential of single and polymer-coated microbubbles using an adapted microelectrophoresis technique. *Int J Miner Process* 2011, 98 (1-2), 118-123.
63. Jia, W. H.; Ren, S. L.; Hu, B., Effect of water chemistry on Zeta potential of air bubbles. *Int J Electrochem Sc* 2013, 8 (4), 5828-5837.
64. Wang, H. Z.; Singh, V.; Behrens, S. H., Image charge effects on the formation of Pickering emulsions. *J Phys Chem Lett* 2012, 3 (20), 2986-2990.
65. Cayre, O. J.; Paunov, V. N., Contact angles of colloid silica and gold particles at air-water and oil-water interfaces determined with the gel trapping technique. *Langmuir* 2004, 20 (22), 9594-9599.

CHAPTER 7

INTERFACIAL ACTIVITIES OF ISOTROPIC PARTICLES AT FLUID-FLUID INTERFACES

7.1 Introduction

Surfactants are organic compounds that contain both hydrophilic groups (water soluble heads) and hydrophobic groups (water insoluble tails). Because of this amphiphilicity, they tend to adsorb in fluid-fluid interfaces and lower the interfacial tension. The interfacial adsorption of surfactants can also provide a steric or electrostatic barrier to the coalescence of liquid droplets or of gas bubbles. In addition to stabilizing emulsions and foams, they act as wetting modifiers (wetting agents) in many products such as detergents for laundry and dish washing, coatings, or pharmaceutical formulations.¹ Like surfactants, particles with appropriate wettability can adsorb to fluid-fluid interfaces; in fact they typically adsorb more strongly.^{2,3} The adsorption of particles tends to lower interfacial energy so significantly that the particle attachment is practically irreversible.^{2,3} The reduction energy of particle adsorption (the free energy change upon particle adsorption to the interface) is given by:^{4,5}

$$\Delta G_{ad,ij} = -\pi R^2 \gamma_{ij} \left(1 - \left|\cos \theta_{ij}\right|\right)^2$$

where γ_{ij} denotes the surface (interfacial) tension, θ_{ij} is the contact angle of a single particle at the interface, and R is the particle radius.

As a result of their strong attachment to the interface, adsorbed particles inhibit bubble or droplet coalescence and coarsening through providing a mechanical barrier. Since the pioneering work of Ramsden and Pickering in the early 20th century,^{6,7}

numerous studies on using particles as stabilizers in the interface have been conducted. Particle-stabilized foams⁸ and emulsions⁹⁻¹¹ have been studied in a variety of fields ranging from materials science to catalysis, and from food science to biomedicine and the use of chemical sensors. In addition to dispersed droplets or bubbles, new classes of soft materials-such as bijels,¹² colloidosomes,¹³ liquid marbles,^{14,15} and capillary foams^{16,17} have also been prepared using particles as stabilizers.

Despite many studies about the adsorption of particles in the interface, there appears to be no general consensus on whether isotropic particles adsorbed at an interface will reduce the interfacial tension. Some studies show that often particles do not¹⁸⁻²⁴ but other studies suggest that they can do so.²⁵⁻²⁹ Vignati et al. demonstrated that the adsorption of silanized silica particles at the water- isooctane oil interface did not lead to appreciable changes in droplet interfacial tension.¹⁹ Fernandez-Rodriguez et al. reported that functionalized silica particles and homogeneous poly(methyl methacrylate) particles did not show a strong effect on reducing the water-decane interfacial tension.²⁰ Moghadamis et al. demonstrated that the presence of ZnO had no effect on the n-decane-water interfacial tension.²¹ Pichot et al. showed that the presence of hydrophilic silica particles had no effect on the vegetable oil–water interfacial tension.²² Drelich et al. demonstrated that no interfacial tension reduction was observed at the paraffin oil-water interface in the presence of hydrophobic silica particles.²³ Manga et al. found that charge stabilized particles had little or no influence on the interfacial tensions.²⁴ Other studies demonstrated that particles can lower the interfacial tensions.²⁵⁻²⁹ Dong et al. showed that the surface tension of charge-stabilized titania suspensions first decreased significantly and then increased to a plateau with the increase of particle concentration.²⁵ Navid

Bizmark et al. reported that the adsorption of ethyl cellulose particles dramatically lowered the surface tension of air-water interface from 72.30 to 38.9 mN/m.²⁶ Antonio Stocco et al. demonstrated that partially hydrophobic fumed silica particles could reduce the air-water surface tension value from 72.8 to around 50 mN/m.²⁷ Du et al. showed that the adsorption of particles to the oil-water interface slightly lowered the interfacial tension.²⁸ Powell et al. reported that carboxyl-terminated carbon black (CB) particles could decrease the n-dodecene-water interfacial tension from 30 to 8.5 mN/m.²⁹ When significant interfacial tension reduction is observed, the effect is generally explained by large adsorption energy of particles at the interface. When no change in interfacial tension is observed, the results are often declared “not surface active” despite adsorption taking place.³⁰

In this chapter, we present a systematic study of interfacial tension effects caused by isotropic silica particles with different hydrophobicity. Our results suggest that isotropic particles can change the interfacial tensions as long as they do adsorb and have strong affinity to the interface. A simple thermodynamic model is seen to predict reasonably well the effective interfacial tension due to the adsorption of particles in the fluid-fluid interfaces. Finally, this study provides a convenient and accurate way to assess the packing density of particles in fluid-fluid interfaces by combining dynamic interfacial tension measurements with information about the particles’ wetting properties.

7.2 Materials and Methods

7.2.1 Materials

Wacker-Chemie AG provided fumed silica particles in powder form with different degrees of hydrophobicity: HDK N20 (unmodified, 100% SiOH coverage) and

MM038-5 (68% methylsilyl capped, 32% SiOH). Methylsilyl modification was performed by the manufacturer through reaction with dichlorodimethylsilane.³¹ Direct measurement of particle contact angle, for example, by gel trapping method,³² freeze-fracture shadow-casting cryo-scanning electron microscopy (FreSCa cryo-SEM),³³ or digital holography,³⁴ is a challenging issue for fumed silica particles with a few hundred nanometers and nonspherical shapes. The wettability of silica particles was characterized by measuring the contact angle of a water drop in air on a pressed tablet of silica particles. Particle hydrodynamic radius in water of silica particles was measured by dynamic light scattering using a Malvern Zetasizer Nano ZS90. The hydrodynamic radius and wettability of silica particles are shown in Table 7.1. Trimethylolpropane trimethacrylate (TMPTMA) and n-hexadecane were bought from Sigma-Aldrich. TMPTMA was treated with Al₂O₃ to remove inhibitor, and enriched with 6 wt % of the photoinitiator benzoin isobutyl for experiments requiring polymerization. The n-hexadecane was purified by mixing it with basic alumina and silica gel, allowing it to stand overnight, and then separating it through centrifugation. Ultrapure water with a resistivity of 18.2 MΩ•cm (Barnstead) was used. Since the partially hydrophobic silica particles (32% SiOH) do not disperse easily in DI water, aqueous dispersions were prepared by first dispersing the particles in acetone and then transferring them to the DI water using repeated centrifugation and replacement of the supernatant.

Table 7.1 Hydrodynamic radius and wettability of silica particles coated with various extends of methylsilyl groups. Contact angle data of 100% SiOH silica particles were obtained from reference 35.

Particle	Coating	Psarticle hydrodynamic radius (nm) in water	Contact angle at air-water interface (°)
100%	Bare	251.73±18.86	20.42±5.21
32%	68% methylsilyl	239.17±21.70	114.06±9.41

7.2.2 EC nanoparticle synthesis and characterization

Ethyl cellulose (EC) particles were synthesized by following the reported method.³⁶ Briefly, 1 wt% solution of EC (Sigma-Aldrich, product code: 247499-100G) in acetone was prepared using a magnetic stirrer at 1100 rpm and 45 °C until EC particles were dissolved. An equal volume of ultrapure DI water was then quickly poured into the EC solution while stirring it at 1100 rpm, after which the solution became turbid as a result of EC nanoparticle nucleation and growth. Then the acetone and part of the water was removed by evaporation, and the EC particle suspension was purified by passing it three times through a C18–silica chromatographic column (Phenomenex) that had been preactivated with an acetonitrile–water (80:20) mixture and flushed several times with hot DI water. The hydrodynamic radius of the EC particles was measured through dynamic light scattering using a Malvern Zetasizer Nano ZS90. The diameter inferred from the z-average diffusion coefficient of the EC particles is 102.3 nm, and the corresponding coefficient of variation is 13%.

7.2.3 Tensiometry

The dynamic interfacial tension was measured via axisymmetric drop shape analysis with a Ramé-hart goniometer (model-250). This method has been widely used for determining the evolution of the interfacial tension due to the adsorption of particles to the interface. Briefly, a pendant droplet was created by a syringe with a steel needle, and a high speed CCD camera was programmed to capture the variation of drop shape over time. The interfacial tension was obtained by analyzing the contour shape resulting from the balance of gravitational forces and tension forces. All experiments were performed at a room temperature of 21°C. The dynamic and equilibrium interfacial tensions for air-water and oil-water in the absence and presence of particles were measured at different particle concentrations.

7.2.4 Contact angle

The contact angle of EC particles in the TMPTMA-water interface was investigated using a Ramé-Hart goniometer and a TMPTMA droplet in water on a proxy surface mimicking the EC particles. An EC-coated substrate was prepared from particles dissolved in acetone using spin coating (1000 rpm, 60 s). The measurements were carried out in a quartz cell filled with water. The substrate was submerged in the quartz-cell and suspended by a holder. A drop of TMPTMA, which is slightly denser than water, was then deposited on the substrate with a 22 gauge needle. The TMPTMA and water phase were mutually saturated prior to the experiment by vigorously mixing equal liquid volumes for overnight and separating them with centrifugation awaiting phase separation.

7.2.5 Packing density

The packing density (ϕ) of EC particles in the TMPTMA-water interface was measured by analyzing scanning electron microscopy (SEM) images of particles trapped in a polymerized TMPTMA droplet. Briefly, a droplet of TMPTMA immersed in an EC particles suspension was created by a syringe with a steel needle. After the EC particles were adsorbed to the interface (at $t=1800$ s), the TMPTMA droplet was polymerized using a UV lamp. The cured TMPTMA droplets with EC particles in the interface were sputter-coated with a thin layer of gold, and SEM images were taken using a Zeiss Ultra60 field emission scanning electron microscope (FE-SEM; Carl Zeiss Microscopy, LLC North America, Peabody, MA).

7.3 Results and Discussion

7.3.1 Effect of silica particles on water surface tension

To study the influence of isotropic particles on the surface tension of water, the surface tension of 1 wt% hydrophilic silica particle (100% SiOH) suspension was measured by pendant drop shape analysis using a Rame-hart tensiometer. Figure 7.1a shows that the surface tension remains unchanged over time. In addition, we determined the dependence of the surface tension (taken at $t=1800$ s) on particle concentrations ranging from 0.25 wt% to 2 wt%. Figure 7.1b shows some scatter in the surface tension measured for different particle concentrations, but in general, the surface tension of hydrophilic silica particle suspensions remained within ± 1 mN/m of the value for particle-free deionized water. Figure 7.1b demonstrates that hydrophilic silica particles do not have surface activities in the air-water interface. This is because 100% SiOH silica particles are too hydrophilic to collect, or adsorb, at the air-water interface (air-water

contact angle is $20.42 \pm 5.21^\circ$).³⁷ Okubo et al. tested the effects of colloidal particles on the equilibrium air-water surface tension and also found that hydrophilic colloidal silica can increase or decrease the equilibrium surface tension at the air-water interface only slightly.³⁸

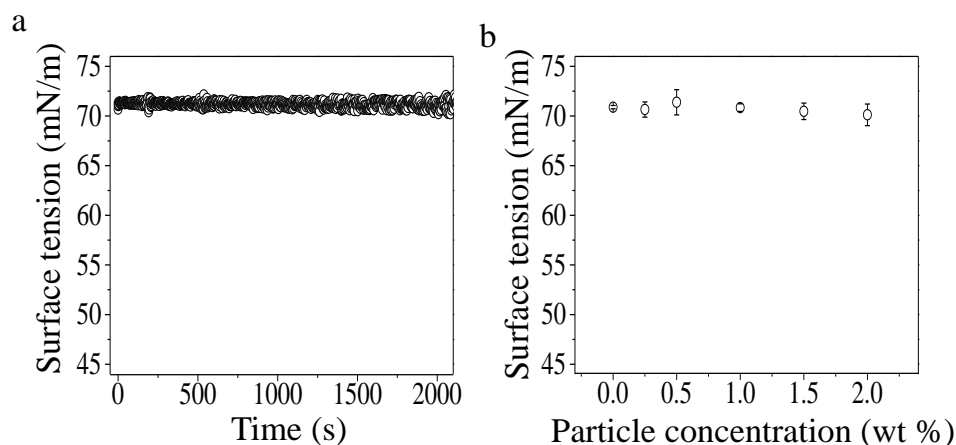


Figure 7.1 Interfacial activity of hydrophilic silica particles (100% SiOH) in the air-water interface. (a) Surface tension over time for 1 wt% hydrophilic silica particles in the air-water interface. (b) Steady state surface tension obtained at $t=1800$ s for various particle concentrations. Water was used as the drop phase in which silica particles were dispersed.

Expecting that hydrophobically modified silica particles with a strong affinity to the air-water interface can substantially reduce the surface tension, we turn to a system in which hydrophilic particles were replaced by the more hydrophobic silica particles (32% SiOH), which can strongly adsorb on the air-water interface and are known to be good stabilizers for aqueous foams.³⁹ We measured the dynamic surface tension of 1 wt% particle dispersion over time as particle adsorption at the interface (Figure 7.2a). We also investigated the steady state surface tension (taken at $t=1800$ s) of the same hydrophobic silica particles with various concentrations ranging from 0.25 wt% to 2 wt% (Figure 7.2b). Figure 7.2b shows that the hydrophobic silica particles slightly decrease the surface tension. We propose that the interfacial activity of hydrophobic silica particles,

which have strong affinity to the air-water interface, may be limited by an energy barrier to particle adsorption. It is well known that both silica particles in water and a bare air-water interface tend to carry an electric surface charge due to dissociable surface groups and to the adsorption of ions.⁴⁰⁻⁴² This can result in an electrostatic barrier that hinders the particle adsorption and can cause a failure of particles to reach the interface.⁴³⁻⁴⁵ In addition, in the case of air-water interfaces, repulsive London-van der Waals interaction further contributes to the particle repulsion from the interface.⁴⁶ The interaction between particles and the air-water interface can be screened by salt ions. To test our hypothesis, we measured the dynamic surface tension of a 1wt% dispersion of same hydrophobic silica particles (32% SiOH) containing 50 mM NaCl. Figure 7.2c clearly shows that the surface tension decreases with time and reaches a lower steady state value than in the absence of salt. We also studied the dependence of steady state surface tension on the particle concentration. Figure 7.2d shows that the equilibrium surface tension first decreases significantly with an increase in the particle concentration and then reaches a plateau with a further increase of particle concentration. We did not study the surface tension in the presence of even higher particle concentration (larger than 2 wt%) because the particle suspension becomes viscous at a higher particle concentration in the presence of salt.

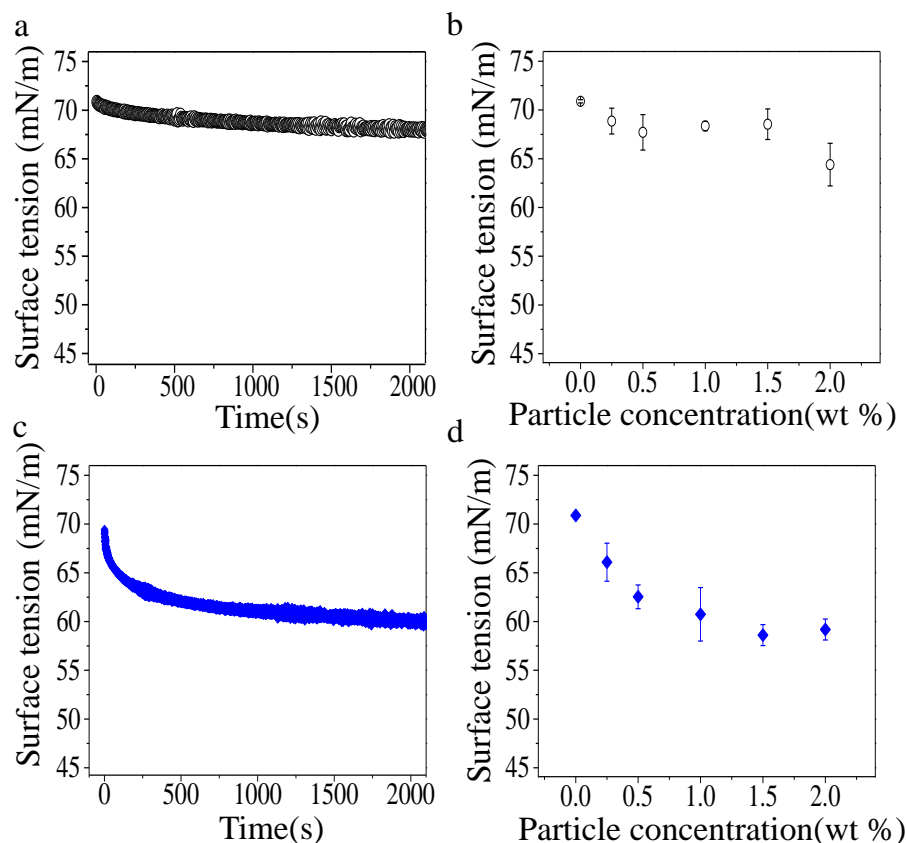


Figure 7.2 Interfacial activity of hydrophobic silica particles (32% SiOH) in the air-water interface. (a) Surface tension over time for 1 wt% hydrophobic silica particles at the air-water interface. (b) Steady state surface tension obtained at $t=1800$ s for hydrophobic silica particles with various particle concentrations. (c) Surface tension over time for 1 wt% hydrophobic silica particles at the air-water interface in the presence of 50 mM NaCl. (d) Steady state surface tension obtained at $t=1800$ s for hydrophobic silica particles with various particle concentrations in the presence of 50 mM NaCl. Water was used as the drop phase in which silica particles were dispersed.

In the control experiment with particle-free 1 M NaCl solution (at a concentration 40 times greater than its concentration used in the measurement), the surface tension as a function of time remains constant at 70.4 mN/m (Figure 7.3a). Another battery of control experiments was carried out to confirm that the large reduction in surface tension was due to particle adsorption at the air-water interface and not due to the adsorption of water-soluble impurities in the originating with the silica particles or the residual acetone. The

dynamic surface tension of the supernatant of hydrophobic silica particles was measured and shows close agreement with the surface tension of ultrapure DI water (Figure 7.3b), which suggests that there are no significant surface-active contaminations or impurities in the particle suspension used in our study. The results of these control experiments verify that the change of the surface tension of the particle dispersion is caused by the particles adsorption and not by the salt or by impurities in the starting materials.

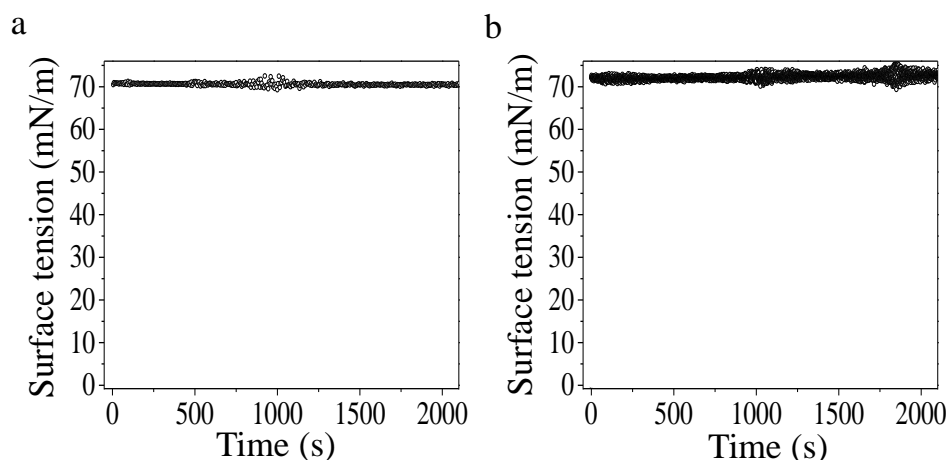


Figure 7.3 Evidence that salt and particles do not introduce significant surface-active impurities. (a) Dynamic surface tension of 1 M NaCl. (b) Dynamic surface tension of supernatant of 32% SiOH silica.

7.3.2 Effect of particles on the tension of hexadecane-water interfaces

We also investigated the effect of particles on the equilibrium oil-water interfacial tension. For the tension of a hexadecane-water interface, with hydrophilic silica particles (100% SiOH) dispersed in the water phase was measured. Figure 7.4a show the effective interfacial tensions (taken at $t=1800$ s) of the alkane with aqueous suspensions of the hydrophilic silica particles for particle concentrations ranging from 0 wt% to 2 wt%. Figure 7.4a demonstrates that 100% SiOH silica particles only slightly decrease the interfacial tension at the hexadecane–water interface. These results are expected from the

weak affinity of very hydrophilic particles to the hexadecane-water interface. Figure 7.4b shows the effective interfacial tension (at $t=1800$ s) of hexadecane with relatively hydrophobic silica particle (32% SiOH) suspensions in a particle concentration range from 0.25 wt% to 2 wt%. Figure 7.4b demonstrates that the effective interfacial tension first decreases with increasing particle concentrations and then reaches plateau. The hydrophobically modified silica particles (32% SiOH) produce a larger reduction in equilibrium interfacial tension than the very hydrophilic silica particles (100% SiOH). We also studied the influence of added salt on the reduction of hexadecane-water interfacial tension for dispersions of both particle types. Figures 7.4a,b show that the equilibrium hexadecane-water interfacial tension in the presence of 50 mM NaCl closely resembles the values obtained without added salt, suggesting that neither particle type experiences a significant barrier to adsorption at the oil-water interface. In the case of air-water interfaces, London-van der Waals interaction is repulsive, whereas for oil-water interfaces that interaction is attractive, which might contribute the weak adsorption barrier in the oil-water interface.

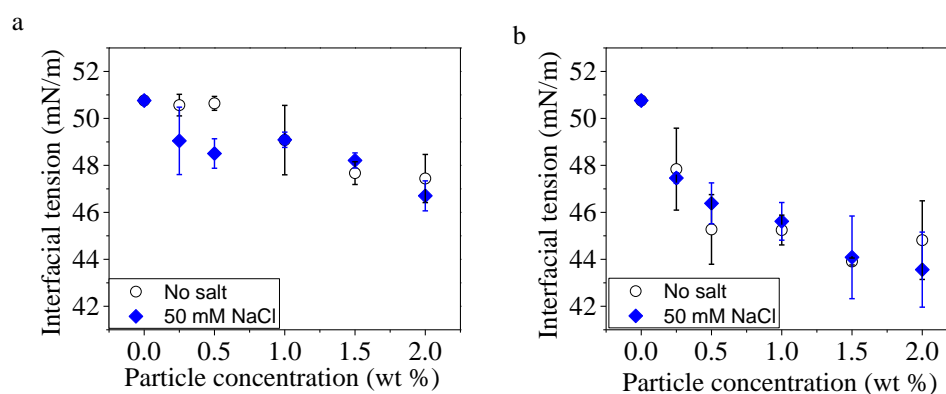


Figure 7.4 Interfacial activity of silica particles in the hexadecane oil-water interface. (a) Steady state hexadecane-water interfacial tension obtained at $t=1800$ s for hydrophilic silica particles (100% SiOH) with various particle concentrations.

(b) Steady state hexadecane-water interfacial tension obtained at t=1800 s for hydrophobic silica particles (32% SiOH) with various particle concentrations.

7.3.3 Theoretical estimate of effective interfacial tension

We have seen that particles can change interfacial tensions if they are adsorbed and have strong affinity to the interface. Next we examine whether the observed particle effect on interfacial tension can be predicted theoretically. If particle-particle interactions are neglected (a common but potentially problematic approximation,³⁰ then the effective interfacial energy takes the form:²⁸

$$E' = \gamma_o A + N_s \Delta E_{ad} \quad (2)$$

where γ_o is the tension of bare interface, A is the interfacial area, N_s is the number of adsorbed particles in the interface, and ΔE_{ad} is the energy benefit per particle adsorbed from the water phase, given by^{2,4,5}

$$\Delta E_{ad} = -\pi R^2 \gamma_o (1 - \cos \theta)^2 \quad (3)$$

where R is the radius of the particle and θ is the particle's equilibrium contact angle with the fluid-fluid interface, measured through the water phase by convention.

From the thermodynamic definition of surface tension as the change in free energy per unit surface area, we can write an expression for the effective interfacial tension of the particle covered interface

$$\gamma' = E' / A = \gamma_o + N_s \Delta E_{ad} / A \quad (4)$$

Combining Eqs. 3 and 4 yields the effective interfacial tension γ'_{ij} of the interface between two fluids i and j in the presence of particles as

$$\gamma'_{ij} = \gamma_{ij} \left(1 - \phi \left(1 - \cos \theta_{ijp} \right)^2 \right) \quad (5)$$

where $\phi = N_s \pi R^2 / A$ is the packing density (area fraction) of the particles adsorbed in the interface.

7.3.4 Comparison between theoretically predicted and experimentally measured effective interfacial tension

According to Equation 5, an estimate of the effective interfacial tension in the presence of particles, γ'_{ij} , can be obtained from independently measured values of γ_{ij} , θ_{ijp} and ϕ . The interfacial tension γ_{ij} can be measured by a variety of methods, including axisymmetric drop shape analysis, as shown in our study. The three-phase particle contact angle (θ_{ijp}) can be determined using following methods:⁴⁷ indirect measurement (drop shape techniques, capillary rise methods, and surface pressure–area isotherms), direct measurement of multiple particles by the gel trapping method³² or freeze–fracture shadow-casting cryo-scanning electron microscopy,³³ and by direct measurements of single particles using digital holography.³⁴ As for the particle packing density, it can sometimes be inferred from direct microscopic observation; alternatively, it is possible to measure the average center-to-center distance between neighboring particles by use of in situ small-angle X-ray scattering.⁴⁸ An obvious question is how predictions for the effective interfacial tension γ'_{ij} in the presence of adsorbing particles from Equation 5 with measured values of γ_{ij} , θ_{ijp} and ϕ compare to direct measurements of γ'_{ij} . To address this question we examined the steady state interfacial tension of TMPTMA and water in the presence of 0.2 wt% EC particles as an example. The effective

interfacial tension of an EC particle-laden TMPTMA-water interface was obtained through Equation 5 and independent measurements of γ_{ij} , θ_{ijp} and ϕ . A tension of 19.22 ± 0.05 mN/m was obtained axisymmetric drop shape analysis. The contact angle of EC particles in the TMPTMA-water interface is estimated as $89.86 \pm 4.30^\circ$ from the contact angle of five TMPTMA drops under water on an EC coated substrate (Figure 7.5a). TMPTMA is photopolymerizable and recent studies indicate that the polymerization process does not change its interfacial properties.⁴⁹⁻⁵¹ Consequently, polymerizing a particle-laden TMPTMA droplet (Figure 7.5b) yield a solid version of the particle-decorated oil interface that facilitates the observation of the embedded particles. We examined two polymerized TMPTMA droplets by SEM and analyzed the area fraction of particles in the twenty-two different locations of interfaces. Figures 7.5c, d, e, and f are four representative SEM images of particles in different places of a polymerized TMPTMA droplet. From these images, we calculated the corresponding packing density of particles in the interface (as shown in Table 7.2). With the measured γ_{ij} , θ_{ijp} and ϕ , the calculated the effective interfacial tension of TMPTMA-water interface in the presence of 0.2 wt% EC particles is 7.74 ± 2.23 mN/m (Figure 7.6, Table 7.3). The large uncertainty of calculated effective interfacial tension might be attributed to the challenge of obtaining accurate packing density and contact angle of nanoparticles with a wide distributions of sizes and shapes in the fluid-fluid interfaces.

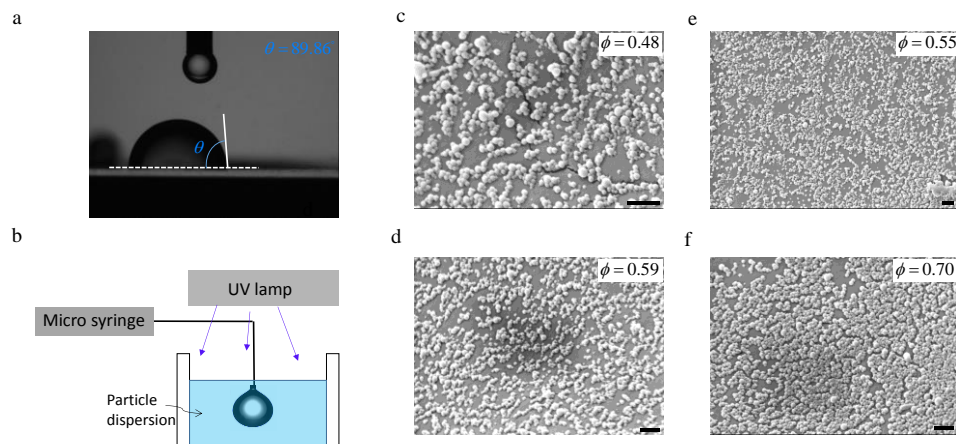


Figure 7.5 Measurements of contact angle and packing density of particles in fluid-fluid interfaces. (a) Image of a TMPTMA drop on a flat EC particle thin film placed inside the water medium. (b) Experimental setup for the measurement of the particle packing density in the TMPTMA-water interface. (c, d, e, f) SEM images of trapped EC particles at different locations on a polymerized TMPTMA droplet. Scale bars are 200 nm.

Table 7.2. Packing density and contact angle of EC particles in the TMPTMA-water interfaces.

												Average	STD
Φ	0.52	0.48	0.52	0.56	0.58	0.49	0.68	0.55	0.69	0.60	0.48	0.60	0.07
	0.71	0.59	0.62	0.70	0.59	0.70	0.62	0.63	0.62	0.57	0.68		
θ	86.2	85.4	89.5	95.6	92.6							89.86	4.30

The effective interfacial tension of the TMPTMA-water interface in the presence of 0.2 wt% EC particles was also experimentally obtained by pendant drop tensiometry. The effective TMPTMA-water interfacial tension initially decreases and then reaches an equilibrium value of 8.04 ± 0.06 mN/m, which agrees reasonably well the calculated effective interfacial tension of 7.74 ± 2.23 based on Equation 5. As a further test of Equation 5, the adsorption of EC particles in the air-water was studied (Table 7.3). Since the direct measurement of packing density of EC particles with a few hundred

nanometers and a wide distribution of sizes requires special instruments and sample preparation, the interface was assumed as close-packed ($\phi = 0.91$). We accomplished this by increasing the bulk density of EC until the equilibrium effective surface tensions no longer changed.²⁸ For the adsorption of EC particles in the air-water interface, the measured effective surface tension value of 39.64 ± 0.23 mN/m, using pendant drop tensiometer, matches reasonable well with the calculated effective surface tension of 39.23 ± 1.69 mN/m based on Equation 5. In 2011, Dinsmore et al.²⁸ measured the adsorption energy of polystyrene particles functionalized with amidine by monitoring the reduction of effective interfacial tension in the fluorohexane–water interface and assuming a closed-packed monolayer. Using the contact angle, interfacial tension of bare interface, and effective interfacial tension due to the adsorption of particles from this study, and assuming a hexagonal close packing of particles in the interface, the value of the predicted effective interfacial tension of 23.2 ± 0.10 mN/m matches well with the experimentally measured effective interfacial tensions of 23.2 ± 0.10 mN/m (Table 7.3). These comparisons suggest that Equation 5 provides a reasonable well estimate of the effective interfacial tension with particles adsorbed in fluid-fluid interfaces.

Table 7.3. Theoretically predicted and experimentally measured effective interfacial tension of particles in fluid-fluid interfaces.

Particles	Interfaces	Packing density	Contact angle (°)	Interfacial tension (mN/m)	Predicted effective interfacial tension (mN/m)	Measured effective interfacial tension (mN/m)
Ethyl cellulose	TMPTMA and water	0.6 ± 0.07	89.86 ± 4.30	19.22 ± 0.05	7.74 ± 2.23	8.04 ± 0.06
Ethyl cellulose	Air and water	0.91	72.57 ± 1.12	70.88 ± 0.17	39.23 ± 1.69	39.64 ± 0.23
Polystyrene	fluorohexane and water	0.91	36.9	24.1 ± 0.10	23.2 ± 0.10	23.2 ± 0.10

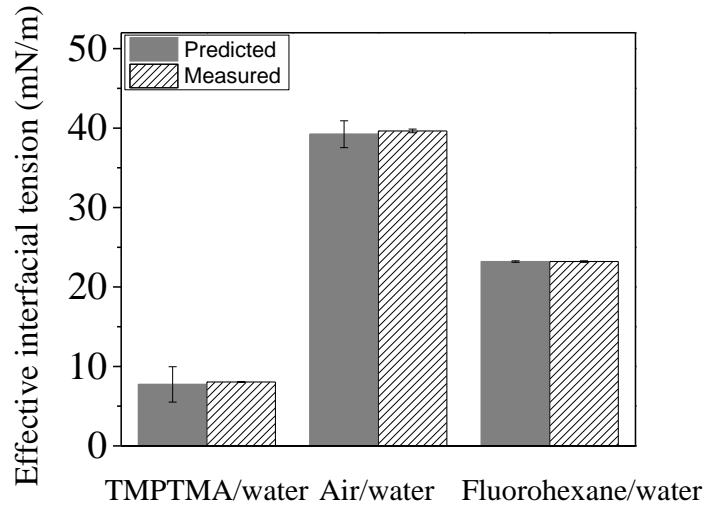


Figure 7.6 Comparison between theoretically predicted and experimentally measured effective interfacial tension.

7.3.5 Packing density can be obtained through dynamic surface tension measurement

The concentration of colloidal particles adsorbed to a fluid-fluid interface, which can be quantified as particle packing density or area fraction, plays a central role in many scientific problems and practical applications, for example, in the stabilization of foams

and emulsions, food processing, and in the colloidal assembly of functional microcapsules for pharmaceutical, agrochemical, or cosmetic formulations. Predicting the packing density of interfacially adsorbed particles can be difficult, because it is strongly influenced, in ways that are not well understood, by the interaction between particles adsorbed in the interface and the distributions of particle sizes and shapes. Similarly it can be challenging to determine the packing density experimentally, especially for small particles or nanoparticles with a wide distribution of sizes or shapes. Clearly, an appropriate average may be more useful than a local value. Small-angle X-ray scattering (SAXS) and small-angle neutron scattering (SANS) provide such an average, but require special instruments and sample preparation. Equation 5 implies that dynamic surface tension measurements (γ_{ij}' and γ_{ij}), when combined with information about the particles' wetting properties (θ_{ijp}), provide a convenient and accurate way to assess the packing density of particles in fluid-fluid interfaces. Table 7.4 shows predicted packing densities obtained from Equation 5 with measure tensions and contact angles. The predicted packing density of 0.58 ± 0.09 for EC particles in the TMPTMA/water interface agrees well with the experimentally obtained local value of 0.60 ± 0.07 (Table 7.4, Figure 7.7). For the adsorption of EC particles in the air-water interface, the predicted packing density of 0.90 ± 0.05 shows close agreement with the assumption of hexagonal close packing density of 0.91 (Table 7.4, Figure 7.7). For the adsorption of polystyrene particles in the fluorohexane-water interface, although a large uncertainty for predicted packing density is observed, the predicted packing density of 0.93 ± 0.14 shows reasonable close to a hexagonal close packing density value of 0.91. Figure 7.7 suggests that the

proposed method will be useful for studying the adsorption behavior of particles at fluid-fluid interfaces, and help in the directed assembly of particles for various applications.

Table 7.4. Theoretically predicted and experimentally measured packing density of particles in fluid-fluid interfaces.

Particles	Interfaces	Contact angle (°)	Interfacial tension (mN/m)	Effective interfacial tension (mN/m)	Predicted packing density	Measured/close packing density
Ethyl cellulose	TMPTMA and water	89.86±4.30	19.22±0.05	8.04±0.06	0.58±0.09	0.60±0.07
Ethyl cellulose	Air and water	72.57±1.12	70.88±0.17	39.64±0.23	0.90±0.05	0.91
Polystyrene	fluorohexane and water	36.9	24.1±0.1	23.2±0.1	0.93±0.14	0.91

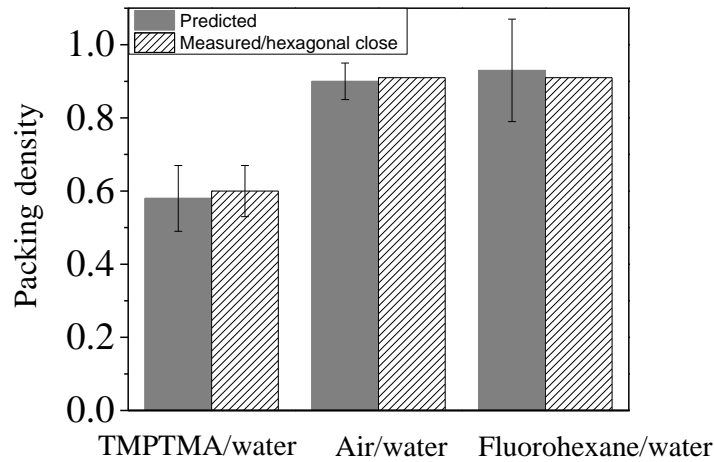


Figure 7.7 Comparison between theoretically predicted and experimentally measured packing density.

7.4 Conclusion

In summary, we have measured the interfacial activity of silica nanoparticles for air-water and hexadecane-water interfaces by using pendant drop tensiometry. Our measurements show that isotropic particles can be used to change interfacial tensions as long as they are adsorbed to the interface and have strong affinity to the interface, which can be characterized by the contact angle; it is maximal for angles close to 90° . In addition, a simple thermodynamic model was used to estimate the effective interfacial tensions of a particle-laden interface, which matches the experimentally measured effective interfacial tensions by using pendant drop tensiometer. Finally, this study offers a simple and efficient way to estimate the average packing density of particles adsorbed to the fluid-fluid interface. The results and the method will be useful for controlling the assembly of nanoparticles at liquid interfaces.

7.5 References

1. Rosen, M. J.; Kunjappu, J. T., Surfactants and interfacial phenomena. John Wiley & Sons: 2012.
2. Binks, B. P., Colloidal particles at liquid interfaces. *Phys Chem Chem Phys* 2007, 9 (48), 6298-6299.
3. Wege, H. A.; Kim, S.; Paunov, V. N.; Zhong, Q. X.; Velev, O. D., Long-term stabilization of foams and emulsions with in-situ formed microparticles from hydrophobic cellulose. *Langmuir* 2008, 24 (17), 9245-9253.
4. Pieranski, P., Two-Dimensional Interfacial Colloidal Crystals. *Phys Rev Lett* 1980, 45 (7), 569-572.
5. Binks, B. P.; Lumsdon, S. O., Influence of particle wettability on the type and stability of surfactant-free emulsions. *Langmuir* 2000, 16 (23), 8622-8631.
6. Ramsden, W., Separation of solids in the surface-layers of solutions and 'Suspensions' (Observations on surface-membranes, bubbles, emulsions, and mechanical coagulation). Preliminary Account. *P R Soc London* 1903, 72 (479), 156-164.
7. Pickering, S. U., Emulsions. *J Chem Soc* 1907, 91, 2001-2021.
8. Gonzenbach, U. T.; Studart, A. R.; Tervoort, E.; Gauckler, L. J., Ultrastable particle-stabilized foams. *Angew Chem Int Edit* 2006, 45 (21), 3526-3530.
9. Levine, S.; Bowen, B. D.; Partridge, S. J., Stabilization of emulsions by fine particles .1. partitioning of particles between continuous phase and oil-water interface. *Colloid Surface* 1989, 38 (4), 325-343.
10. Aveyard, R.; Binks, B. P.; Clint, J. H., Emulsions stabilised solely by colloidal particles. *Advances in Colloid and Interface Science* 2003, 100, 503-546.
11. Lee, D.; Weitz, D. A., Double emulsion-templated nanoparticle colloidosomes with selective permeability. *Adv Mater* 2008, 20 (18), 3498-3503.

12. Cates, M. E.; Clegg, P. S., *Bijels: a new class of soft materials*. *Soft Matter* 2008, 4 (11), 2132-2138.
13. Dinsmore, A. D.; Hsu, M. F.; Nikolaides, M. G.; Marquez, M.; Bausch, A. R.; Weitz, D. A., *Colloidosomes: Selectively permeable capsules composed of colloidal particles*. *Science* 2002, 298 (5595), 1006-1009.
14. Aussillous, P.; Quere, D., *Liquid marbles*. *Nature* 2001, 411 (6840), 924-927.
15. Dupin, D.; Armes, S. P.; Fujii, S., *Stimulus-responsive liquid marbles*. *J Am Chem Soc* 2009, 131 (15), 5386-5387.
16. Zhang, Y.; Wu, J.; Wang, H. Z.; Meredith, J. C.; Behrens, S. H., *Stabilization of liquid foams through the synergistic action of particles and an immiscible liquid*. *Angew Chem Int Edit* 2014, 53 (49), 13385-13389.
17. Zhang, Y.; Allen, M. C.; Zhao, R. Y.; Deheyn, D. D.; Behrens, S. H.; Meredith, J. C., *Capillary foams: Stabilization and functionalization of porous liquids and solids*. *Langmuir* 2015, 31 (9), 2669-2676.
18. Chevalier, Y.; Bolzinger, M. A., *Emulsions stabilized with solid nanoparticles: Pickering emulsions*. *Colloid Surface A* 2013, 439, 23-34.
19. Vignati, E.; Piazza, R.; Lockhart, T. P., *Pickering emulsions: Interfacial tension, colloidal layer morphology, and trapped-particle motion*. *Langmuir* 2003, 19 (17), 6650-6656.
20. Fernandez-Rodriguez, M. A.; Ramos, J.; Isa, L.; Rodriguez-Valverde, M. A.; Cabrerizo-Vilchez, M. A.; Hidalgo-Alvarez, R., *Interfacial activity and contact angle of homogeneous, functionalized, and Janus nanoparticles at the water/decane interface*. *Langmuir* 2015, 31 (32), 8818-8823.
21. Moghadam, T. F.; Azizian, S., *Effect of ZnO nanoparticle and hexadecyltrimethylammonium bromide on the dynamic and equilibrium oil-water interfacial tension*. *J Phys Chem B* 2014, 118 (6), 1527-1534.
22. Pichot, R.; Spyropoulos, F.; Norton, I. T., *Competitive adsorption of surfactants and hydrophilic silica particles at the oil-water interface: Interfacial tension and contact angle studies*. *J Colloid Interf Sci* 2012, 377, 396-405.

23. Drelich, A.; Gomez, F.; Clausse, D.; Pezron, I., Evolution of water-in-oil emulsions stabilized with solid particles: influence of added emulsifier. *Colloid Surface A* 2010, 365 (1-3), 171-177.
24. Manga, M. S.; Hunter, T. N.; Cayre, O. J.; York, D.; Reichert, M. D.; Anna, S. L.; Walker, L. M.; Williams, R. A.; Biggs, S. R., Measurements of sub-micron particle adsorption and particle film elasticity at oil-water interfaces. *Langmuir* 2016 DOI: 10.1021/acs.langmuir.5b04586.
25. Dong, L. C.; Johnson, D., Surface tension of charge-stabilized colloidal suspensions at the water-air interface. *Langmuir* 2003, 19 (24), 10205-10209.
26. Bizmark, N.; Ioannidis, M. A.; Henneke, D. E., Irreversible adsorption-driven assembly of nanoparticles at fluid interfaces revealed by a dynamic surface tension probe. *Langmuir* 2014, 30 (3), 710-717.
27. Stocco, A.; Drenckhan, W.; Rio, E.; Langevin, D.; Binks, B. P., Particle-stabilised foams: an interfacial study. *Soft Matter* 2009, 5 (11), 2215-2222.
28. Du, K.; Glogowski, E.; Emrick, T.; Russell, T. P.; Dinsmore, A. D., Adsorption energy of nano- and microparticles at liquid-liquid interfaces. *Langmuir* 2010, 26 (15), 12518-12522.
29. Powell, K. C.; Chauhan, A., Interfacial tension and surface elasticity of carbon black (CB) covered oil-water interface. *Langmuir* 2014, 30 (41), 12287-12296.
30. Fan, H.; Striolo, A., Nanoparticle effects on the water-oil interfacial tension. *Phys Rev E* 2012, 86 (5), 051610.
31. Worthen, A. J.; Bagaria, H. G.; Chen, Y. S.; Bryant, S. L.; Huh, C.; Johnston, K. P., Nanoparticle-stabilized carbon dioxide-in-water foams with fine texture. *J Colloid Interf Sci* 2013, 391, 142-151.
32. Paunov, V. N., Novel method for determining the three-phase contact angle of colloid particles adsorbed at air-water and oil-water interfaces. *Langmuir* 2003, 19 (19), 7970-7976.

33. Isa, L.; Lucas, F.; Wepf, R.; Reimhult, E., Measuring single-nanoparticle wetting properties by freeze-fracture shadow-casting cryo-scanning electron microscopy. *Nat Commun* 2011, 2.
34. Kaz, D. M.; McGorty, R.; Mani, M.; Brenner, M. P.; Manoharan, V. N., Physical ageing of the contact line on colloidal particles at liquid interfaces. *Nat Mater* 2012, 11 (2), 138-142.
35. Kostakis, T.; Ettelaie, R.; Murray, B. S., Effect of high salt concentrations on the stabilization of bubbles by silica particles. *Langmuir* 2006, 22 (3), 1273-1280.
36. Jin, H. J.; Zhou, W. Z.; Cao, J.; Stoyanov, S. D.; Blijdenstein, T. B. J.; de Groot, P. W. N.; Arnaudov, L. N.; Pelan, E. G., Super stable foams stabilized by colloidal ethyl cellulose particles. *Soft Matter* 2012, 8 (7), 2194-2205.
37. Binks, B. P.; Murakami, R., Phase inversion of particle-stabilized materials from foams to dry water. *Nat Mater* 2006, 5 (11), 865-869.
38. Okubo, T., Surface-tension of structured colloidal suspensions of polystyrene and silica spheres at the air-water-interface. *J Colloid Interf Sci* 1995, 171 (1), 55-62.
39. Binks, B. P.; Horozov, T. S., Aqueous foams stabilized solely by silica nanoparticles. *Angew Chem Int Edit* 2005, 44 (24), 3722-3725.
40. Bueno-Tokunaga, A.; Perez-Garibay, R.; Martinez-Carrillo, D., Zeta potential of air bubbles conditioned with typical froth flotation reagents. *Int J Miner Process* 2015, 140, 50-57.
41. Elmallidy, A. M.; Mirnezami, M.; Finch, J. A., Zeta potential of air bubbles in presence of frothers. *Int J Miner Process* 2008, 89 (1-4), 40-43.
42. Oliveira, C.; Rubio, J., Zeta potential of single and polymer-coated microbubbles using an adapted microelectrophoresis technique. *Int J Miner Process* 2011, 98 (1-2), 118-123.
43. Wang, H. Z.; Singh, V.; Behrens, S. H., Image charge effects on the formation of Pickering emulsions. *J Phys Chem Lett* 2012, 3 (20), 2986-2990.

44. Kutuzov, S.; He, J.; Tangirala, R.; Emrick, T.; Russell, T. P.; Boker, A., On the kinetics of nanoparticle self-assembly at liquid/liquid interfaces. *Phys Chem Chem Phys* 2007, 9 (48), 6351-6358.
45. Dugyala, V. R.; Muthukuru, J. S.; Mani, E.; Basavaraj, M. G., Role of electrostatic interactions in the adsorption kinetics of nanoparticles at fluid-fluid interfaces. *Phys Chem Chem Phys* 2016, 18 (7), 5499-5508.
46. Tabor, R. F.; Manica, R.; Chan, D. Y. C.; Grieser, F.; Dagastine, R. R., Repulsive van der Waals forces in soft matter: why bubbles do not stick to walls. *Phys Rev Lett* 2011, 106 (6), 064501.
47. Snoeyink, C.; Barman, S.; Christopher, G. F., Contact angle distribution of particles at fluid interfaces. *Langmuir* 2015, 31 (3), 891-897.
48. Lin, Y.; Boker, A.; Skaff, H.; Cookson, D.; Dinsmore, A. D.; Emrick, T.; Russell, T. P., Nanoparticle assembly at fluid interfaces: Structure and dynamics. *Langmuir* 2005, 21 (1), 191-194.
49. Xu, H.; Goedel, W. A., Particle-assisted wetting. *Langmuir* 2003, 19 (12), 4950-4952.
50. Ding, A. L. PhD. Dissertation, Chemnitz University of Technology, 2007.
51. Ding, A. L.; Goedel, W. A., Experimental investigation of particle-assisted wetting. *J Am Chem Soc* 2006, 128 (15), 4930-4931.

CHAPTER 8

CONCLUSIONS AND FUTURE WORK

8.1 Conclusions

Common colloidal systems are simply fine dispersions of one phase into another. More complex systems containing multiple dispersed fluids also occur naturally and play increasingly important roles in industrial applications. Their various applications depend on both their stability and their intrinsic wetting morphology. Surfactants traditionally serve as stabilizers and wetting modifiers. However, surfactants suffer from drawbacks such as chemical degradation under harsh application conditions, potential environmental pollution, and recovery difficulty. The aim of the work in this thesis is to use particles as stabilizers and wetting modifiers in colloidal multiphase systems.

We are interested in particles as novel stabilizers in aqueous foams. Specifically, we discovered a long-term stable foam material, capillary foams, which are obtained by frothing a suspension of colloidal particles in the presence of a small amount (less than 1 wt%) of oil. We investigated the stabilization mechanism and explained the huge difference that a small amount of oil can make in these foams. We also studied the formation stages of capillary foams and reported that particle networks are the first to form, and then air bubbles are entrapped in the entire system, forming the capillary foams. In addition, we systematically investigated the influence of process parameters on the preparation of capillary foams and showed that capillary foams can be prepared alternatively by either introducing air or oil simultaneously to a particle suspension by frothing a capillary suspension or by mixing oil into a Pickering foam. Finally, to

illustrate some potential applications, we demonstrate the preparation of intensely colored foams that are notoriously difficult to achieve with traditional methods and the preparation of load-bearing porous solids.

In addition to serving as co-stabilizers, we found that colloidal particles can be used as efficient wetting modifiers. We used the wetting configuration of an air bubble produced by an oil droplet in a water medium as a model system because it is used in a wide variety of industrial processes. We demonstrated that particles can be used both to promote “bubble wetting” and to induce complete bubble engulfment by an oil drop or to trigger progressive “bubble de-wetting,” that is, to substantially reduce the oil-bubble contact area. In addition, particle can induce slow, transient wetting behavior. A mechanistic understanding of this reconfiguration process was obtained by measuring the effective dynamic surface and interfacial tensions obtained by axisymmetric drop shape analysis. The tunability of the wetting configuration is attributed to changes in interfacial energy caused by the adsorption of particles at fluid-fluid interfaces.

Finally, the interfacial activity of isotropic silica nanoparticles was analyzed through pendant drop tensiometry for air-water and hexadecane-water interfaces. We demonstrated that isotropic particles can change interfacial tensions as long as they are delivered and have strong affinity to the interface. A thermodynamic model was used for estimating the effective interfacial tensions in the presence of particles. The results of the model match the results of experiments. This study offers a simple and efficient way to estimate the average packing density of particles adsorbed to the fluid-fluid interface. The results and the method will be useful for controlling the assembly of nanoparticles at liquid interfaces.

8.2 Future work

8.2.1 Capillary emulsions

We have demonstrated the formation of a new class of colloidal four-phase system, capillary foams.¹ The air bubbles in our capillary foams could be replaced by oil droplets. Accordingly, we hypothesize that these mixtures of solid colloidal particles and three mutually immiscible *liquids* (e.g., perfluorohexane, hexane, and water²) with appropriate wetting properties will robustly and predictably assemble, upon agitation, into systems with an intricate multi-scale structure. The generated systems might be called “capillary emulsions” by analogy. Just like capillary foams, capillary emulsions have two features: (a) the formation of a gel-like network of bridged particles held together by the capillary forces associated with their liquid bridges, and (b) the engulfment of droplets in the bridging phase facilitated by the particles (Figure 8.1). The investigation of capillary emulsions is highly recommended for the future work. From a practical viewpoint, the presence of so many phases and their interfaces in capillary emulsions offer a wealth of processing opportunities (e.g., drying, hardening of liquid phases, interfacial polymerization, and chemical functionalization) for the development of new materials with well-defined chemical or mechanical properties and transport characteristics.

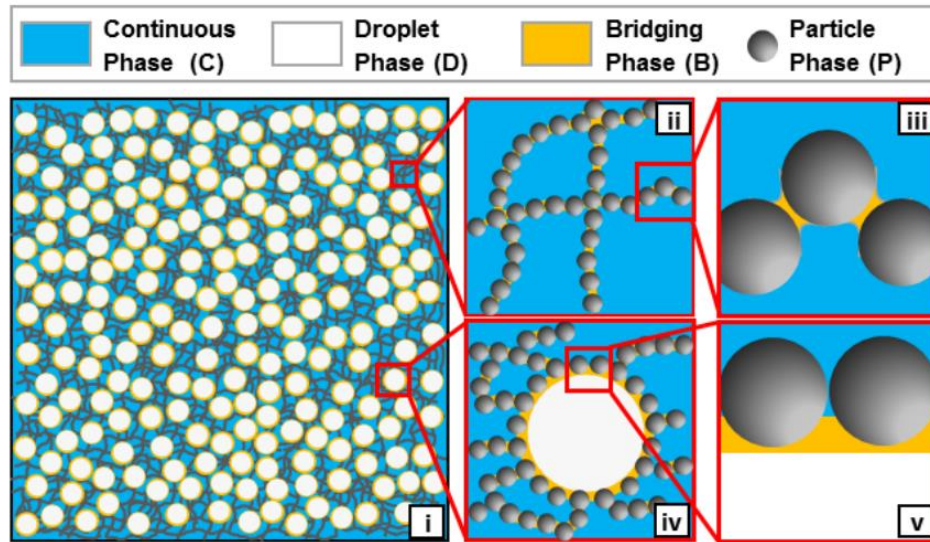


Figure 8.1 Capillary emulsions. The system contains a continuous water phase, an oil phase, another immiscible oil phase, as well as particles. The agitation of the mixture results in a space-spanning network of particles in water (ii) connected by bridges of oil phase (iii), with another immiscible oil droplets embedded in the network (iv) via a joint adsorption of particles and a thin oil film.

8.2.2 Capillary foam-enhanced oil recovery

One of the major applications of foams is in enhanced oil recovery (EOR). On average, only about 35% of the crude oil can be recovered from subsurface reservoirs through natural depletion and water flooding.³ A common practice is then to inject gas, solvent, or chemicals into the reservoir to extract oils. The injected gas can swell the oil and thus reduce the viscosity of oil phase. A large fraction of remaining oil can be recovered by gas-enhanced oil recovery.³ However, the main problem associated with gas injection is that the gas has high mobility and low density compared with reservoir fluid, leading to poor sweep efficiency and low recovery.³⁻⁵ The foaming of injected gas, a potential solution to this problem, has been widely used in the oil recovery process.³⁻⁵ Foams can improve the sweep efficiency of gas-enhanced oil recovery by overcoming gravity override, viscous fingering, and channeling.³⁻⁵ A major problem of foam-assisted

oil recovery is foam stability in the presence of oil.⁶⁻⁸ Foams should be stable in the presence of oil to achieve high recovery efficiency.⁶⁻⁸ Although surfactant-stabilized foams have been used in the enhanced oil recovery process, they lack stability in the presence of oil, which limits their applications. Our preliminary results show that capillary foams show a highly oil-tolerant property in the presence of crude oil. Further investigation in understanding the capillary foam-crude oil interaction is recommended, including the rheology and flow of capillary foams in a porous environment.

8.3 References

1. Zhang, Y.; Wu, J.; Wang, H. Z.; Meredith, J. C.; Behrens, S. H., Stabilization of liquid foams through the synergistic action of particles and an immiscible liquid. *Angew Chem Int Edit* 2014, 53 (49), 13385-13389.
2. Zarzar, L. D.; Sresht, V.; Sletten, E. M.; Kalow, J. A.; Blankschtein, D.; Swager, T. M., Dynamically reconfigurable complex emulsions via tunable interfacial tensions. *Nature* 2015, 518 (7540), 520-524.
3. Andrianov, A.; Farajzadeh, R.; Nick, M. M.; Talanana, M.; Zitha, P. L. J., Immiscible foam for enhancing oil recovery: bulk and porous media experiments. *Ind Eng Chem Res* 2012, 51 (5), 2214-2226.
4. Gauglitz, P. A.; Friedmann, F.; Kam, S. I.; Rossen, W. R., Foam generation in homogeneous porous media. *Chem Eng Sci* 2002, 57 (19), 4037-4052.
5. Conn, C. A.; Ma, K.; Hirasaki, G. J.; Biswal, S. L., Visualizing oil displacement with foam in a microfluidic device with permeability contrast. *Lab Chip* 2014, 14 (20), 3968-3977.
6. Duan, X. G.; Hou, J. R.; Cheng, T. T.; Li, S.; Ma, Y. F., Evaluation of oil-tolerant foam for enhanced oil recovery: Laboratory study of a system of oil-tolerant foaming agents. *J Petrol Sci Eng* 2014, 122, 428-438.
7. Farajzadeh, R.; Andrianov, A.; Krastev, R.; Hirasaki, G. J.; Rossen, W. R., Foam-oil interaction in porous media: Implications for foam assisted enhanced oil recovery. *Advances in Colloid and Interface Science* 2012, 183, 1-13.
8. Simjoo, M.; Rezaei, T.; Andrianov, A.; Zitha, P. L. J., Foam stability in the presence of oil: Effect of surfactant concentration and oil type. *Colloid Surface A* 2013, 438, 148-158.